# Induction Machines Handbook

THIRD EDITION

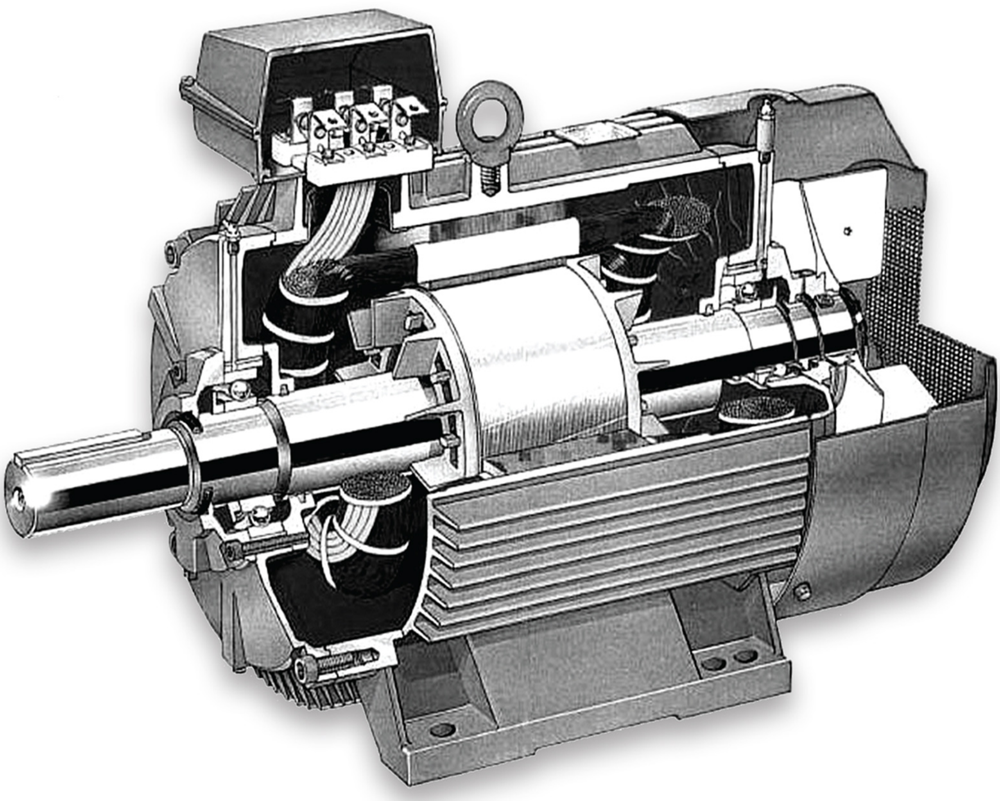

Ion Boldea

CRC Press
Taylor & Francis Group

# Induction Machines Handbook

THIRD EDITION

## Steady State Modeling and Performance

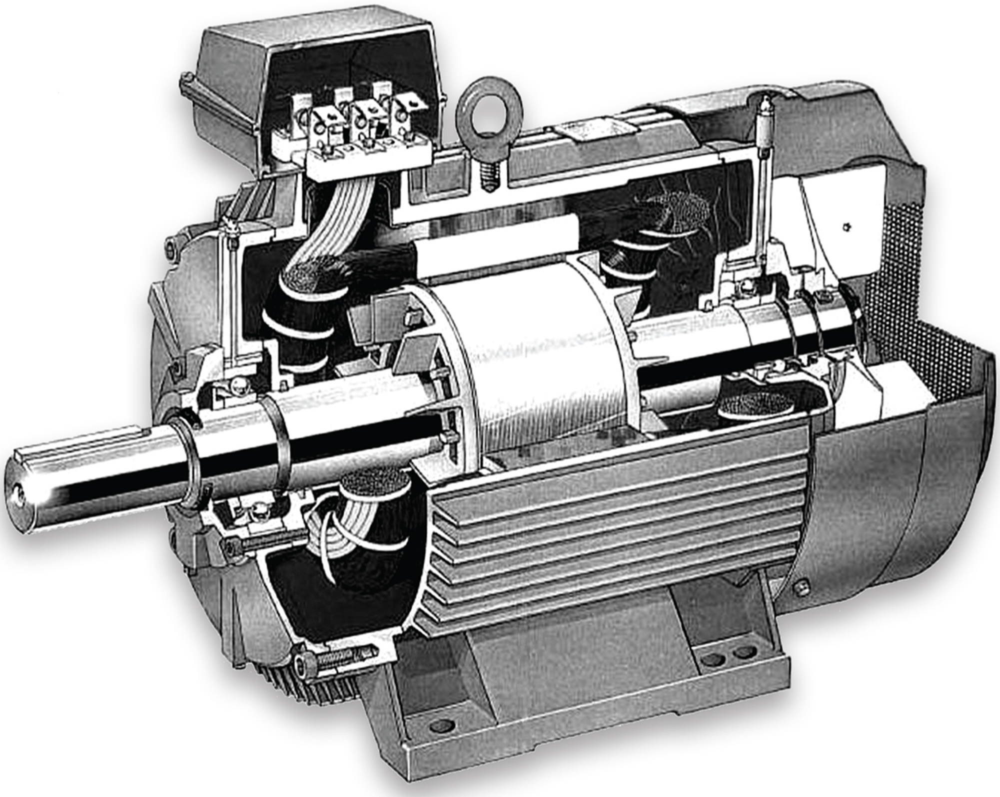

Ion Boldea

CRC Press
Taylor & Francis Group

# Induction Machines Handbook

# Electric Power Engineering Series

*Series Editor:*
Leonard L. Grigsby

Electromechanical Systems, Electric Machines, and Applied Mechatronics
*Sergey E. Lyshevski*

Power Quality
*C. Sankaran*

Power System Operations and Electricity Markets
*Fred I. Denny and David E. Dismukes*

Electric Machines
*Charles A. Gross*

Electric Energy Systems
Analysis and Operation
*Antonio Gomez-Exposito, Antonio J. Conejo, and Claudio Canizares*

The Induction Machines Design Handbook, Second Edition
*Ion Boldea and Syed A. Nasar*

Linear Synchronous Motors
Transportation and Automation Systems, Second Edition
*Jacek F. Gieras, Zbigniew J. Piech, and Bronislaw Tomczuk*

Electric Power Generation, Transmission, and Distribution, Third Edition
*Leonard L. Grigsby*

Computational Methods for Electric Power Systems, Third Edition
*Mariesa L. Crow*

Electric Energy Systems
Analysis and Operation, Second Edition
*Antonio Gomez-Exposito, Antonio J. Conejo, and Claudio Canizares*

Induction Machines Handbook, Third Edition (Two-Volume Set)
*Ion Boldea*

Induction Machines Handbook, Third Edition
Steady State Modeling and Performance
*Ion Boldea*

Induction Machines Handbook, Third Edition
Transients, Control Principles, Design and Testing
*Ion Boldea*

For more information about this series, please visit: https://www.crcpress.com/Electric-Power-Engineering-Series/book-series/CRCELEPOWENG

# Induction Machines Handbook

## Steady State Modeling and Performance

Third Edition

Ion Boldea

CRC Press
Taylor & Francis Group
Boca Raton London New York

CRC Press is an imprint of the
Taylor & Francis Group, an **informa** business

Third edition published 2020
by CRC Press
6000 Broken Sound Parkway NW, Suite 300, Boca Raton, FL 33487-2742

and by CRC Press
2 Park Square, Milton Park, Abingdon, Oxon, OX14 4RN



First edition published by CRC Press 2001
Second edition published by CRC Press 2009

CRC Press is an imprint of Taylor & Francis Group, LLC



*Library of Congress Cataloging-in-Publication Data*
Names: Boldea, I., author.
Title: Induction machines handbook: steady state modeling and performance / Ion Boldea.
Description: Third edition. | Boca Raton: CRC Press, 2020. |
Series: Electric power engineering | Includes bibliographical references and index. |
Contents: v. 1. Induction machines handbook: steady stat — v.
2. Induction machines handbook: transients
Identifiers: LCCN 2020000304 (print) | LCCN 2020000305 (ebook) |
ISBN 9780367466121 (v. 1 ; hbk) | ISBN 9780367466183 (v. 2 ; hbk) |
ISBN 9781003033417 (v. 1 ; ebk) | ISBN 9781003033424 (v. 2 ; ebk)
Subjects: LCSH: Electric machinery, Induction—Handbooks, manuals, etc.
Classification: LCC TK2711 .B65 2020 (print) | LCC TK2711 (ebook) |
DDC 621.34—dc23
LC record available at https://lccn.loc.gov/2020000304
LC ebook record available at https://lccn.loc.gov/2020000305

ISBN: 978-0-367-46612-1 (hbk)
ISBN: 978-1-003-03341-7 (ebk)

Typeset in Times
by codeMantra

*A humble, late, tribute to:*

*Nikola Tesla*

*Galileo Ferraris*

*Dolivo-Dobrovolski*

# Contents

# Preface

## MOTIVATION

The 2010–2020 decade has seen notable progress in induction machines (IMs) technology such as

- Extension of analytical and finite element modelling (FEM) for better precision and performance
- Advanced FEM-assisted optimal design methodologies with multi-physics character
- Introduction of upgraded premium efficiency IM international standards
- Development and fabrication of copper cage rotor IM drives for traction on electric vehicles
- Extension of wound rotor induction generators (WRIG or DFIG) with partial rating A.C.–D.C.–A.C. converters in wind energy conversion and to pump storage reversible power plants (up to 400 MVA/unit)
- Extension of cage rotor induction generators with full power pulse width modulation (PWM) converters for wind energy conversion (up to 5 MVA/unit)
- Development of cage (or nested cage) rotor dual stator winding induction generators/motors with partial rating power electronics for wind energy and vehicular technologies (autonomous operation)
- Development of line-start premium efficiency IMs with cage rotor, provided with PMs and/or magnetic saliency for self-synchronisation and operation at synchronism (three phase and one phase), for residential applications, etc.
- Introduction of multiphase ($m > 3$) IMs for higher torque density and more fault-tolerant electric drives.

All the above, reflected in a strong increase of line-start IMs and variable speed IM motor and generator drives markets, have prompted us to prepare a new (third) edition of the book.

## VOLUME 1: *INDUCTION MACHINE: STEADY STATE MODELING AND PERFORMANCE*, THIRD EDITION/437 PP.

### Short Description

In essence, as a compromise between not confusing the readers of the second edition, but bringing new knowledge in too, it was decided to introduce the new knowledge towards the end of each chapter mainly, but not only, as new paragraphs.

Also the text, equations, figures, and numbers in the numerical examples have been checked carefully with local corrections/improvements/additions wherever necessary.

Finally, new/recent representative references have been added and assessed in the text (sometimes in the existing paragraphs) of each chapter.

The new paragraphs are

Chapter 4/4.14 – Multiphase and multilayer tooth-wound coil windings
Chapter 6/6.14 – The brushless doubly fed induction machine (BDFIM)
Chapter 7/7.19 – Equivalent circuits for brushless doubly fed IMs
Chapter 8/8.6 – Control basics of DFIMs
Chapter 9/9.9 – Magnetic saturation effects or current/slip and torque/slip curves
Chapter 9/9.10 – Rotor slot leakage reactance saturation effects
Chapter 9/9.11 – Closed slot IM saturation effects

Chapter 10/10.11 – The origin of electromagnetic vibration: by practical experience
Chapter 13/13.10 – PM-assisted split-phase cage-rotor IMs.

All efforts have been made to keep the mathematics extension under control **but introduce ready-to-use expressions of industry parameters and performance computation**. In compensation, numerical examples have been generously spread all over the book to facilitate a strong feeling of magnitudes which is, in our view, indispensable in engineering.

There are in total 14 chapters (1–14) in Volume I, which totalise about 437 pages.

## Contents

As already mentioned, Volume I refers to steady-state modelling and performance of induction machines, covering 14 chapters. Here is a short presentation of the 14 chapters by content.

*Chapter 1*: "Induction Machines: An Introduction"/16 pages.

Induction machines (IMs) are related to mechanical into electrical energy conversion via magnetic energy storage in an ensemble of coupled electric and magnetic circuits. Energy is paramount to prosperity, while electric energy conversion in electric power plants and in motion digital control by power electronics is the key to higher industrial productivity with reasonable impact on the environment. A historical touch is followed by IMs' application examples in a myriad of industries, with IM not only the workhorse but also one important racehorse of the industry (at variable speed).

*Chapter 2*: "Construction Aspects and Operation Principles"/18 pages.

This chapter introduces the main parts of IMs and the principles of electromagnetic induction (Faraday law) in producing electromagnetic force (torque) on the rotor (mover) made of a cage or two- (three-) phase A.C. winding (coil) placed in a slotted laminated silicon-iron core. The principles explained this way apply to both linear motion and rotary electric machines (where the torque concept replaces the tangential force concept).

The recent premium IMs with PM and magnetic saliency added beneath the rotor cage are also referred to.

*Chapter 3*: "Magnetic, Electric, and Insulation Materials for IM"/16 pages.

Main active materials – magnetic, electric, and insulation types – used in the IM fabrication are presented with their characteristic performance, with additional data on recently developed such materials (and pertinent source literature). Core loss basic formulae have been derived starting from Maxwell equations, and tables illustrate core losses/kg of silicon steel at various flux densities and a few frequencies of interest.

*Chapter 4*: "Induction Machine Windings and Their mmfs"/40 pages.

The fundamental concept of magnetomotive force (mmf) as the source of a travelling magnetic field in the airgap of IMs is introduced, first produced with three-phase alternative current (A.C.) windings (coils), then with two-phase A.C. windings (for single-phase A.C. source supplies), and finally (new) with multiphase (5, 7, 2 × 3, 3 × 3 phases) A.C. windings, introduced recently. The placement of A.C. windings in slots is discussed in detail. The winding factor's three components for distributed windings (integer or fractionary slot/pole/phase, $q \geq 1$) are derived both for the fundamental component (average torque producing) and for the m.m.f. space harmonics. Finally, the "skewing" m.m.f. concept is introduced, only to be, later in this book, used to prove the axially non-uniform magnetic saturation of the stator core, especially at high currents (above 2–3 p.u.; p.u. means relative values to rated current).

*Chapter 5*: "The Magnetisation Curve and Inductance"/32 pages.

The magnetisation curve (magnetisation fundamental airgap) flux linkage $\Psi_{m1}$ versus stator fundamental phase current $i_{m10}$ (with zero rotor current and/or the magnetisation inductance $L_m = \Psi_{m1}/i_{m10}$) are crucial to IM performance and are calculated first analytically by a simplified and then by analytical iterative model (AIM) both accounting for magnetic saturation and for the slotting influences, with results proved experimentally. The magnetic saturation airgap, teeth, and back-iron flux density harmonics are illustrated as a basis to calculate iron losses in a later chapter.

The electromagnetic force (emf) induced in an A.C. winding is calculated illustrating the same three components of the winding factors already derived for mmfs and the emf time harmonics, produced essentially by the mmf and magnetic saturation-caused space harmonics.

Finally, finite element modelling (FEM) – numerical – computation of airgap flux density for zero rotor currents (ideal no-load currents: at ideal (synchronous) no-load speed $n_1$ of mmf wave fundamental: $n_1 = f_1/p_1$; $f_1$ – A.C. stator currents frequency, $p_1$ – number of pole pairs (periods) of travelling field along one revolution) is performed to illustrate the space fundamental and harmonics produced by the slotting (and magnetic saturation). A numerical detailed example for the magnetisation curve calculation gives a stronger feeling of magnitudes for its components in air and iron cores.

*Chapter 6*: "Leakage Inductances and Resistances"/25 pages.

The part of the magnetic field that does not embrace both stator and rotor windings, called generically leakage field, being mostly in air, is decomposed in differential (space harmonics), slot (distinct for different practical slot geometries), zig-zag – airgap and end – connection components to give rise to respective leakage inductance components in the stator and in the rotor ($L_{sl}$ and $L_{rl}$). This important aspect of IM technology is presented quantitatively in ample detail. Numerical examples illustrate the magnitudes, and very recent refined calculation methodologies of leakage inductances – with FEM validation – are synthesised (**new**). The stator- and rotor-phase resistances ($R_s$ and $R_r$) are calculated too.

*Chapter 7*: "Steady-State Equivalent Circuit and Performance"/47 pages.

Based on the main phase circuit parameters, extracted from magnetic field distribution (fluxes, energy), – $L_m$, $L_{sl}$, $L_{rl}$, $R_s$, $R_r$ – the standard phase equivalent circuit of the IM with three phases is introduced and then, particularised for: ideal no-load speed ($n_0 = n_1 = n$; $S_{0i} = (n_1 - n)/n_1 = 0$), no-load motoring ($n = n_0$, $S_0 = (n_1 - n_0)/n_1$; $S_0 > S_{0i}$), on load ($S = (n_1 - n)/n_1 > s_0$) but in the interval of 0.05–0.005, with increasing power, generator to the grid, capacitor (self-excited) autonomous generator, mechanical characteristic, efficiency, power factor, unbalanced stator or rotor operation, voltage sags, swells, and time harmonics, with numerical examples. Finally, the steady-state equivalent circuit of nested-cage dual stator winding IM and of cascaded – dual stator winding IM are presented in view of their recent proposition for wind energy conversion (**new**).

*Chapter 8*: "Starting and Speed Control Methods"/31 pages.

Starting and close loop control of IMs is an art of itself – electric drives – but the principles of it have to be derived first by a deep knowledge of IM operation modes. This chapter presents first the starting and speed control methods of line-start (constant stator frequency) cage and wound rotor IMs. Then the two main categories of close loop speed control: V/f control (with stabilizing loops recently) and field-oriented control (FOC), illustrated by exemplary mechanical characteristics and block (structural) control diagrams are unfolded and complimented by self-explanatory numerical examples.

*Chapter 9*: "Skin and On-Load Saturation Effects"/51 pages.

Skin (frequency) and on-load magnetic saturation influence on IM resistances, inductances, characteristics, and performance are investigated in detail in this chapter as they are key issues in optimal design of IMs for various applications from industrial drives to wind generators, electric vehicle propulsion, or deep underground (or underwater) fluid pump motors, etc., or home appliance split-phase motors.

Both these phenomena are presented quantitatively, with practical methodologies of industrial value. A comprehensive analytical non-linear approach for linkage saturation and skin effect in IMs is unfolded to shed light on its various aspects, with experimental validation.

Finally, FEM is illustrated as a suitable approach to calculate skin effects in slots with multiple conductors. New paragraphs deal with such subtle phenomena in very recent treatments (torque/slip curves as influenced by saturation harmonics eddy currents in high-speed IM closed slot (saturation effects)).

*Chapter 10*: "Airgap Field Space Harmonics Parasitic Torques, Radial Forces, and Noise Basics"/32 pages.

The airgap field space harmonics produced by mmf space harmonics, airgap magnetic permeance harmonics, and magnetic saturation give rise to parasitic torques (time pulsations in the torque), strong local variations in time of radial forces, and thus, additional vibration and more.

These phenomena are all treated quantitatively for uniform airgap and for the influence of static and dynamic eccentricity, via many numerical examples. The main result is founding a way to choose proper combinations of stator and rotor slot numbers for various number of pole pairs, which is crucial in a good industrial IM design.

A **new** section (10.11) dealing with the origin of electromagnetic vibration by practical experience is introduced.

*Chapter 11*: "Losses in Induction Machines"/41 pages.

Losses defined as the difference between input and output power of IM have many components. There is, however, a notable difference between the losses measured under direct load and the ones calculated from the separation of losses methods (in no-load and short-circuit tests). This difference is called stray load losses, and they vary from 0.5% to 2.5% of full power; they occur even on motor no-load operation.

This chapter attempts a rather exhaustive approach to calculate the additional (stray load) losses produced by the magnetic field space harmonics in the presence of slotting and finally of current (and magnetic flux) time harmonics so common in variable speed drives fed from PWM static power converters. Numerical results illustrate the concepts step by step and offer a strong feeling of magnitudes. Loss computation by FEM, which lumps in all aspects is also illustrated at the end of this chapter. A comparison between sinusoidal source and PWM source inverter IM losses via an experimental case study is added as **new**.

*Chapter 12*: "Thermal Modelling and Cooling"/24 pages.

A highly non-linear system, the thermal model of IM may be approached by a lump equivalent circuit method or by FEM.

This chapter develops such an equivalent thermal circuit with expressions for its parameters, to calculate steady-state temperatures in a few points (nodes). It also develops on temperature variation in time (thermal transients) and on FEM computation of temperatures in the machine with lumped thermal parameter estimation. As this subject represents an art of itself, recent/representative literature is added for the diligent reader to explore it further on his own.

*Chapter 13*: "Single-Phase Induction Machines: The Basics"/22 pages.

Single-phase A.C. sources are common in residential/building supply power technologies.

Line-start split-phase IMs have been developed for worldwide spread applications; so efficiency is paramount.

A classification of them is offered, with the shaded-pole IM also added. The principle of operation with two A.C. windings at start (at least) to create a strong forward travelling field is described together with the symmetrical components' general model and its complex-variable steady-state equivalent circuit. The d-q model is introduced as a tool to investigate more complex topologies (Steinmetz connection) and transients.

The **new** section (13.10) describes the model of the split-phase IM when PMs and (or) a magnetic saliency are added to the cage rotor, to improve efficiency.

*Chapter 14*: "Single-Phase Induction Motors: Steady State"/41 pages.

This chapter starts with steady-state operation with open auxiliary winding: equivalent circuits, mechanical characteristics, efficiency, and power factor, via a numerical example.

The split-phase capacitor IM steady state is then investigated by the complex equivalent circuit defined in the previous chapter via another numerical example. Then, the symmetrisation simetrization conditions, starting torque and current inquires, typical motor characteristics, non-orthogonal winding modelling, via extended numerical graphical delta from a dedicated

MATLAB® computer code, mmf space harmonics parasitic torques, interbar rotor currents, voltage harmonics effects, the doubly tapped winding capacitor IM, a 2/4 pole split-phase capacitor motor are all subjects treated quantitatively as issues of industrial importance (new).

*Timisoara, 2019*

MATLAB® is a registered trademark of The MathWorks, Inc. For product information, please contact:

The MathWorks, Inc.
3 Apple Hill Drive
Natick, MA 01760-2098 USA
Tel: 508-647-7000
Fax: 508-647-7001
E-mail: info@mathworks.com
Web: www.mathworks.com

# Author

**Ion Boldea,** IEEE Life Fellow and Professor Emeritus at University Politehnica Timisoara, Romania, has taught, did research, and published extensively papers and books (monographs and textbooks) over more than 45 years, related to rotary and linear electric motor/generator variable speed drives, and maglevs. He was a visiting professor in the USA and UK for more than 5 years since 1973 to present.

He was granted four IEEE Best Paper Awards, has been a member of IEEE IAS, IE MEC, and IDC since 1992, was the guest editor of numerous special sections in IEEE Trans, vol. IE, IA, delivered keynote addresses at quite a few IEEE-sponsored International Conferences, participated in IEEE Conference tutorials, and is an IEEE IAS distinguished lecturer since 2008 (with lecture in the USA, Brasil, South Korea, Denmark, Italy, etc.). He held periodic intensive graduate courses for Academia and Industry in the USA and Denmark in the last 20 years.

He was a general chair of ten biannual IEEE-sponsored OPTIM International Conferences (www.info-optim.ro) and is the founding and current chief editor, since 2000, of the Internet-only *Journal of Electrical Engineering*, "www.jee.ro".

As a full member of Romanian Academy, he received the IEEE-2015 "Nikola Tesla Award" for his contributions to the development of rotary and linear electric motor/generator drives and maglevs modelling, design, testing, and control in industrial applications.

# 1 Induction Machines
## *An Introduction*

### 1.1 ELECTRIC ENERGY AND INDUCTION MOTORS

The level of prosperity of a community is related to its capability to produce goods and services. However, producing goods and services is strongly related to the use of energy in an intelligent way.

Motion and temperature (heat) control are paramount in energy usage. Energy comes into use in a few forms such as thermal, mechanical, and electrical.

Electrical energy, measured in kWh, represents more than 30% of all used energy, and it is on the rise. Part of electrical energy is used directly to produce heat or light (in electrolysis, metallurgical arch furnaces, industrial space heating, lighting, etc.).

The larger part of electrical energy is converted into mechanical energy in electric motors. Amongst electric motors, induction motors are most used both for home appliances and in various industries [1–11].

This is so because they have been traditionally fed directly from the three-phase A.C. electric power grid through electromagnetic power switches with adequate protection. It is so convenient.

Small-power induction motors, in most home appliances, are fed from the local single-phase A.C. power grids. Induction motors are rugged and have moderate costs, explaining their popularity.

In developed countries today, there are more than 3 kW of electric motors per person and most of them are induction motors.

While most induction motors are still fed from the three- or single-phase power grids, some are supplied through frequency changers (or power electronics converters) to provide variable speeds.

In developed countries, already 20% of all induction motor power is converted in variable speed drive applications. The annual growth rate of variable speed drives has been 9% in the past decade, while the electric motor markets showed an average annual growth rate of 4% in the same time.

Variable speed drives with induction motors are used in transportation, pumps, compressors, ventilators, machine tools, robotics, hybrid or electric vehicles, washing machines, etc.

The forecast is that in the next decade, up to 50% of all electric motors will be fed through power electronics with induction motors covering 60%–70% of these new markets.

The ratings of induction motors vary from a few tens of watts to 33,120 kW (45,000 HP). The distribution of ratings in variable speed drives is shown in Table 1.1 [1].

Intelligent use of energy means higher productivity with lower active energy and lower losses at moderate costs. Reducing losses leads to lower environmental impact where the motor works and lower thermal and chemical impacts at an electric power plant that produces the required electrical energy.

Variable speed through variable frequency is paramount in achieving such goals. As a side effect, the use of variable speed drives leads to current harmonics pollution in the power grid and

**TABLE 1.1**
**Variable Speed A.C. Drives Ratings**

| Power (kW) | 1–4 | 5–40 | 40–200 | 200–600 | >600 |
|---|---|---|---|---|---|
| Percentage | 21 | 26 | 26 | 16 | 11 |

electromagnetic interference (EMI) with the environment. So power quality and EMI have become new constraints on electric induction motor drives.

Digital control is now standard in variable speed drives, while autonomous intelligent drives to be controlled and repaired via the Internet are on the horizon. And new application opportunities abound: from digital appliances to hybrid and electric vehicles and more electric aircraft.

So much on the future, let us now go back to the first two invented induction motors.

## 1.2 A HISTORICAL TOUCH

Faraday discovered the electromagnetic induction law around 1831, and Maxwell formulated the laws of electricity (or Maxwell's equations) around 1860. The knowledge was ripe for the invention of the induction machine (IM) which has two fathers: Galileo Ferraris (1885) and Nikola Tesla (1886). Their IMs are shown in Figures 1.1 and 1.2.

Both motors have been supplied from a two-phase A.C. power source and thus contained two-phase concentrated coil windings 1-1′ and 2-2′ on the ferromagnetic stator core.

In Ferrari's patent, the rotor was made of a copper cylinder, while in Tesla's patent, the rotor was made of a ferromagnetic cylinder provided with a short-circuited winding.

Though the contemporary induction motors have more elaborated topologies (Figure 1.3) and their performance is much better, the principle has remained basically the same.

That is, a multiphase A.C. stator winding produces a travelling field that induces voltages that produce currents in the short-circuited (or closed) windings of the rotor. The interaction between the stator-produced field and the rotor-induced currents produces torque and thus operates the induction motor. As the torque at zero rotor speed is nonzero, the induction motor is self-starting. The three-phase A.C. power grid capable of delivering energy at a distance to induction motors and other consumers has been put forward by Dolivo-Dobrovolsky around 1880.

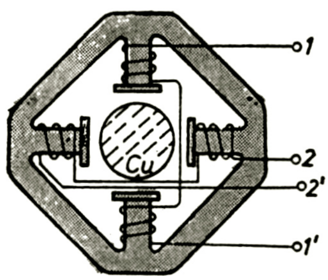


**FIGURE 1.1** Ferrari's induction motor (1885).

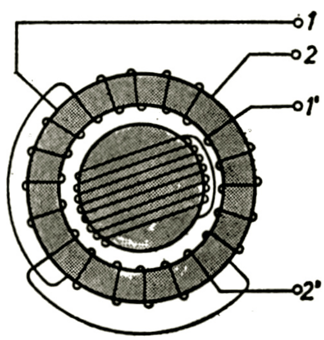


**FIGURE 1.2** Tesla's induction motor (1886).

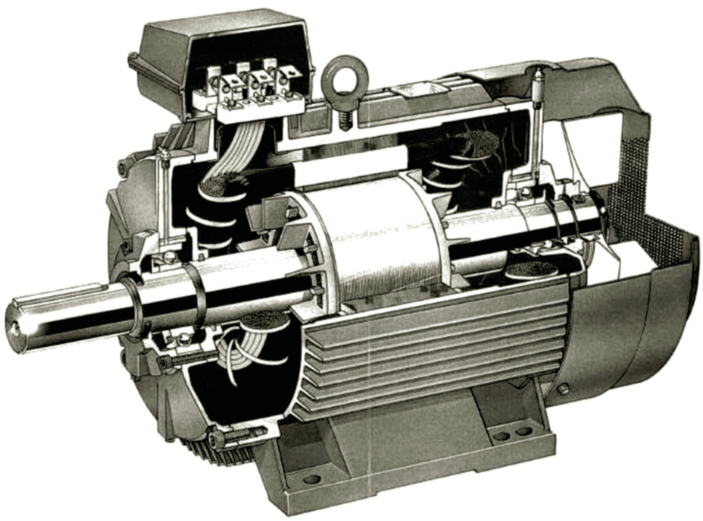


**FIGURE 1.3** A state-of-the-art three-phase induction motor. (Source: ABB motors.)

In 1889, Dolivo-Dobrovolsky invented the three-phase induction motor with the wound rotor and subsequently the cage rotor in a topology very similar to that used today. He also, apparently, invented the double-cage rotor.

Thus, around 1900, the induction motor was ready for wide industrial use. No wonder that before 1910, in Europe, locomotives provided with induction motor propulsion were capable of delivering 200 km/h.

However, at least for transportation, the D.C. motor took over all markets until around 1985 when the insulated gate bipolar transistor pulse width modulation (IGBT PWM) inverter has provided for efficient frequency changers. This promoted the induction motor spectacular comeback in variable speed drives with applications in all industries.

Mainly due to power electronics and digital control, the induction motor may add to its old nickname of "the workhorse of industry" and the label of "the racehorse of high-tech".

A more complete list of events that marked the induction motor history follows:

- Better and better analytical models for steady-state and design purposes
- The orthogonal (circuit) and space phasor models for transients
- Better and better magnetic and insulation materials and cooling systems
- Design optimisation deterministic and stochastic methods
- IGBT PWM frequency changers with low losses and high power density (kW/m$^3$) for moderate costs
- Finite element modellings (FEMs) for field distribution analysis and coupled circuit-FEM models for comprehensive exploration of IMs with critical (high) magnetic and electric loading
- Development of induction motors for super-high speeds and high powers
- A parallel history of linear induction motors with applications in linear motion control has unfolded
- New and better methods of manufacturing and testing for IMs
- Integral induction motors: induction motors with the PWM converter integrated into one piece.

## 1.3 INDUCTION MACHINES IN APPLICATIONS

Induction motors are, in general, supplied from single- or three-phase A.C. power grids.

Single-phase supply motors, which have two-phase stator windings to provide self-starting, are used mainly for home applications (fans, washing machines, etc.): up to 2.2–3 kW. A typical contemporary single-phase induction motor with dual (start and run) capacitor in the auxiliary phase is shown in Figure 1.4.

Three-phase induction motors are sometimes built with aluminium frames for general-purpose applications below 55 kW (Figure 1.5).

Standard efficiency (IE1), high efficiency (IE2), premium efficiency (IE3 and NEMA premium), and super-premium efficiency (IE4) have been defined in the second edition of the IEC 60034-30. Standard induction motors have been introduced to promote further energy savings both at constant and variable speeds (Figure 1.6). For IE4 (IE5), line-start permanent magnet motors have been considered (Table 1.2), but too large starting/rated current, the lower peak, rated and starting/rated torque, size, and cost are issues to be dealt with (notice the cost of line start synchronous permanent motor (LSPM) is 230% of IM cost in Table 1.2). However, even at this high cost, the payback time of LSPM, for 6000 hours/year, is less than 3 years.

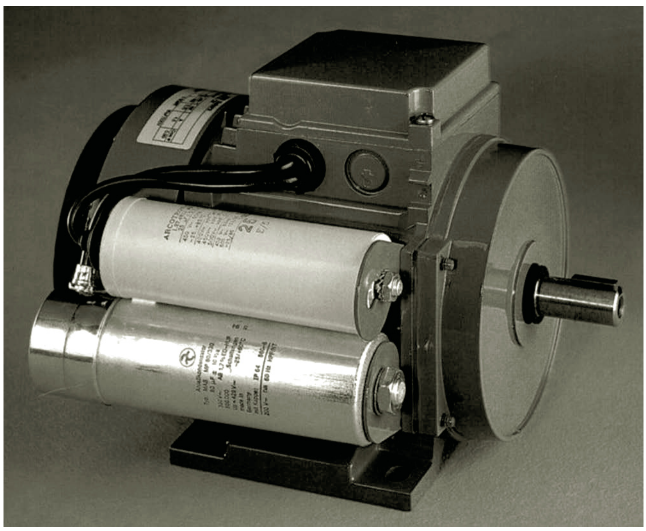

**FIGURE 1.4** Start-run capacitor single-phase induction motor. (Source: ABB.)

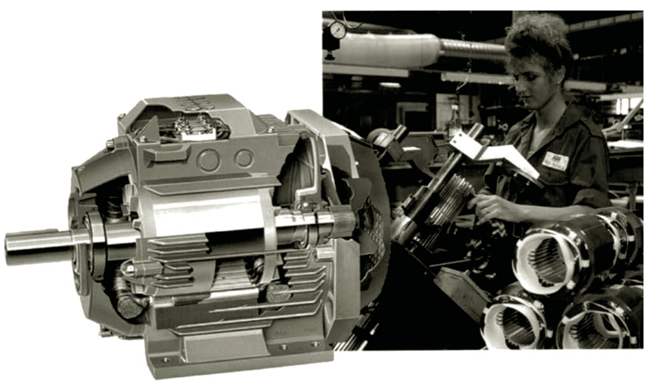

**FIGURE 1.5** Aluminium frame induction motor. (Source: ABB.)

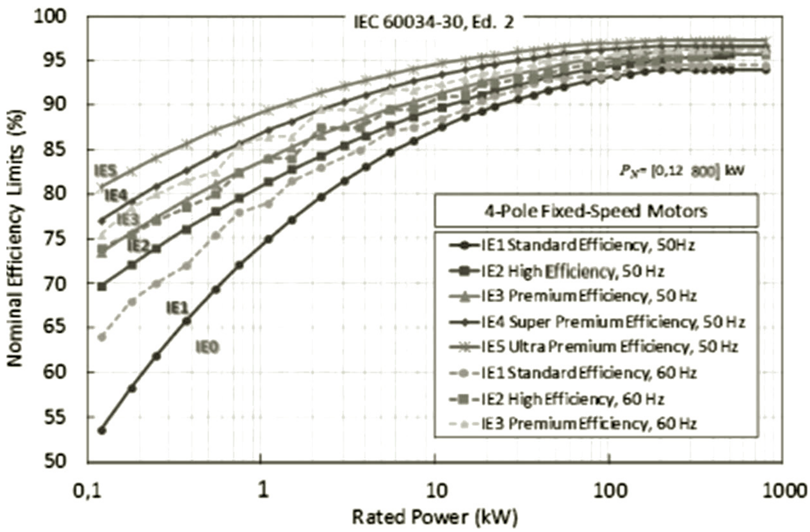


**FIGURE 1.6** Rated efficiency class limits proposed in IEC60034-30 for four-pole motors (0.12–800 kW) [12].

**TABLE 1.2**
**Commercial IE-2, IE-3, IE-4 Class 7.5 kW Four-Pole Motors [12]**

| Standard and the Year Published | State |
|---|---|
| **IEC 60034-1**, Ed. 12, 2010, Rating and performance. | Active. |
| Application: Rotating electrical machines. | |
| IEC 60034-2-1, Ed. 1, 2007, Standard method for determining losses and efficiency from tests (excluding machines for traction vehicles). Establishes methods of determining efficiencies from tests and also specifies methods of obtaining specific losses. | Active but under revision. |
| Application: D.C. machines and A.C. synchronous and IMs of all sizes within the scope of 1EC 60034-1. | |
| IEC 60034-2-2, Ed. 1, 2010, Specific methods for determining separate losses of large machines from tests – supplement to IFC60034-2-I. Establishes additional methods of determining separate losses and to define an efficiency supplementing IEC 60034-2-1. These methods apply when full-load testing is not practical and result in a greater uncertainty. | Active. |
| Application: Special and large rotating electrical machines. | |
| **IEC 60034-2-3**, Ed. 1, 2011, Specific test methods for determining losses and efficiency of convener-fed A.C. motors. | Not active. Draft. |
| Application: Convener-fed motors. | |
| **IEC 60034-30**, Ed. 1, 2008, Efficiency classes of single-speed, three-phase, cage induction motors (IEC code). | Active but under revision. |
| Application: 0.75–375 kW, 2,4, and 6 poles, 50 and 60 Hz. | |
| **IEC60034-31**, Ed. 1, 2010, Selection of energy-efficient motors including variable speed applications – application guide. | Active. |
| Provides a guideline of technical aspects for the application of energy – efficient, three-phase, electric motors. It not only applies to motor manufacturers, original equipment manufacturers, end users, regulators, and legislators but also to all other interested parties. | |
| Application: Motors covered by IEC 60034-30 and variable frequency/speed drives. | |
| **IEC 60034-17**, Ed 4, 2006, Cage induction motors when fed from conveners – application guide. | Active. |
| Deals with the steady-state operation of cage induction motors within the scope of IEC 60034-12, when fed from converters. Covers the operation over the whole speed setting range but does not deal with starting or transient phenomena. | |
| Application: Cage induction motors fed from converters. | |

Cast iron finned frame efficient motors up to 2000 kW are built today with axial exterior air cooling. The stator and the rotor have laminated single stacks.

Typical values of efficiency and sound pressure for such motors built for voltages of 3800–11,500 V and 50–60 Hz are shown in Table 1.3 (source: ABB). For large starting torque, dual-cage rotor induction motors are built (Figure 1.7).

There are applications (such as overhead cranes) where for safety reasons, the induction motor should be braked quickly when the motor is turned off. Such an induction motor with an integrated brake is shown in Figure 1.8.

Induction motors used in pulp and paper industry need to be kept clean from excess pulp fibres. Rated to IP55 protection class, such induction motors prevent the influence of ingress, dust, dirt, and damp (Figure 1.9).

Aluminium frames offer special corrosion protection. Bearing grease relief allows for greasing the motor while it is running.

IMs are extensively used for wind turbines up to 2000 kW per unit and more [13]. A typical dual winding (speed) such induction generator with cage rotor is shown in Figure 1.10.

Wind power conversion to electricity has shown a steady growth since 1985 [2].

50 GW of wind power were in operation, with 25% wind power penetration in Denmark, in 2005 and 180 GW were predicted for 2010 (source Windforce10). About 600 GW were expected to be installed worldwide by 2019.

**TABLE 1.3**
**Typical Values of Efficiency and Sound Pressure for High-Voltage Induction Machines**

| **Output** | **Efficiency (%)** | | |
|---|---|---|---|
| | **Typical Values of High-Voltage Four-Pole Machines** | | |
| kW | 4/4 load | 3/4 load | 1/2 load |
| 500 | 96.7 | 96.7 | 96.1 |
| 630 | 97.0 | 97.0 | 96.4 |
| 710 | 97.1 | 97.1 | 96.5 |
| 800 | 97.3 | 97.2 | 96.8 |
| 900 | 97.4 | 97.4 | 96.9 |
| 1000 | 97.4 | 97.4 | 97.1 |
| 1250 | 97.6 | 97.7 | 97.5 |
| 1400 | 97.8 | 97.8 | 97.5 |
| 2000 | 97.9 | 97.8 | 97.5 |

| **Frame/rpm** | **3000** | **1500** | **1000** | **≤750** |
|---|---|---|---|---|
| | **Typical Sound Pressure Levels in dB (A) at 1 m Distance** | | | |
| 315 | 79 | 78 | 76 | – |
| 355 | 79 | 78 | 76 | – |
| 400 | 79 | 78 | 76 | 75 |
| 450 | 80 | 78 | 76 | 75 |
| 500 | 80 | 78 | 76 | 75 |
| 560 | 80 | 78 | 76 | 75 |

The variation and measuring tolerance of the figures is 3 dB (A).

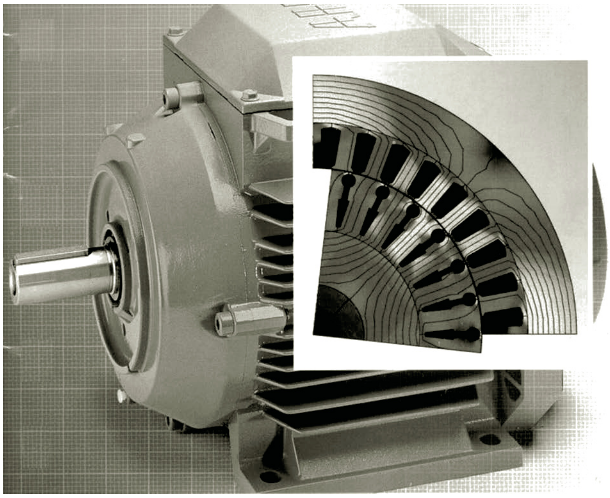

**FIGURE 1.7** Dual-cage rotor induction motors for large starting torque. (Source: ABB.)

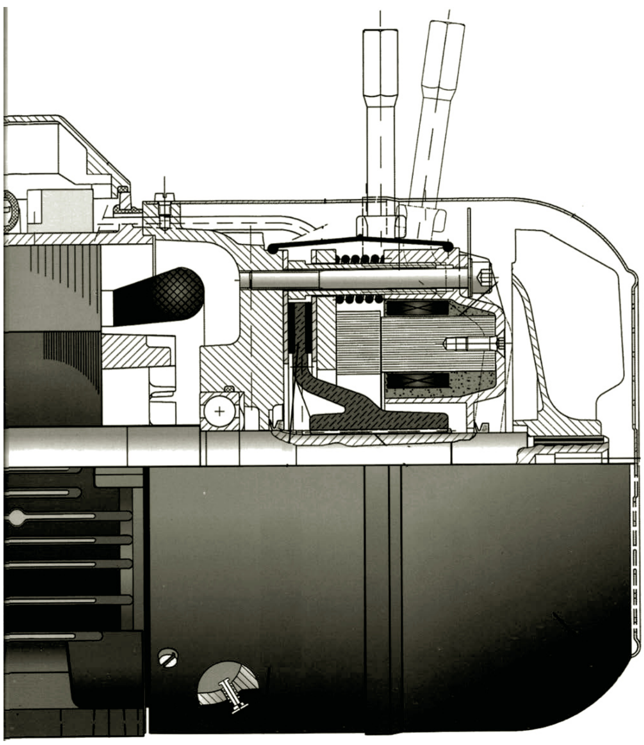

**FIGURE 1.8** Induction motor with integrated electromagnetic brake. (Source: ABB.)

The environmentally clean solutions to energy conversion are likely to grow in the near future. A 10% coverage of electrical energy needs in many countries of the world seems within reach in the next 20 years. Also, small power hydropower plants with induction generators may produce twice as much that amount.

Induction motors are used more and more for variable speed applications in association with PWM converters.

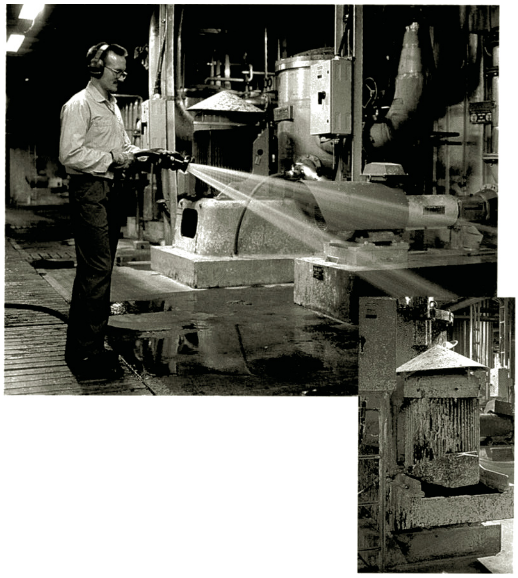

**FIGURE 1.9** Induction motor in pulp and paper industries. (Source: ABB.)

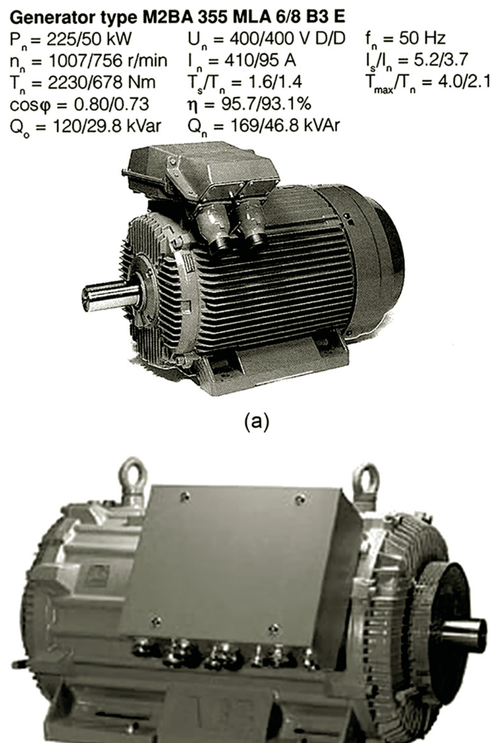


**FIGURE 1.10** (a) Dual-stator winding induction generator for wind turbines. (b) Wound rotor induction generator. (Source: ABB.) 750/200 kW, cast iron frame, liquid-cooled generator. Output power: kW and MW range; shaft height: 280–560. Features: air or liquid cooled; cast iron or steel housing. Single, two-speed, doubly-fed design or full variable speed generator.

Up to 5000 kW at 690 V (line voltage, RMS), PWM voltage-source IGBT converters are used to produce variable speed drives with induction motors. A typical frequency converter with a special induction motor series is shown in Figure 1.11.

Constant ventilator speed cooling by integrated forced ventilation independent of motor speed provides high continuous torque capability at low speed in servo drive applications (machine tools, etc.).

Roller tables use several low-speed ($2p_1 = 6$–$12$ poles) induction motors with or without mechanical gears, supplied from one or more frequency converters for variable speeds.

The high torque load and high ambient temperature, humidity, and dust may cause damage to induction motors unless they are properly designed and built.

Totally enclosed induction motors are fit for such demanding applications (Figure 1.12). Mining applications (hoists, trains, conveyors, etc.) are somewhat similar.

Induction motors are extensively used in marine environments for pumps, fans, compressors, etc. for power up to 700 kW or more. Due to the aggressive environment, they are totally enclosed and may have aluminium (at low power), steel, or cast iron frames (Figure 1.13).

Aboard ship, energy consumption reduction is essential, especially money-wise, as electric energy on board is produced through a diesel engine electrical generator system.

Suppose that electric motors aboard a ship amount to 2000 kW running 8000 hours/year. With an energy cost of US$0.15/kWh, the energy bill difference per year between two induction motor supplies with a 2% difference in motor efficiency is: $0.02 \times 2000 \times 8000$ hours $\times 0.15 =$ US$55,200 per year.

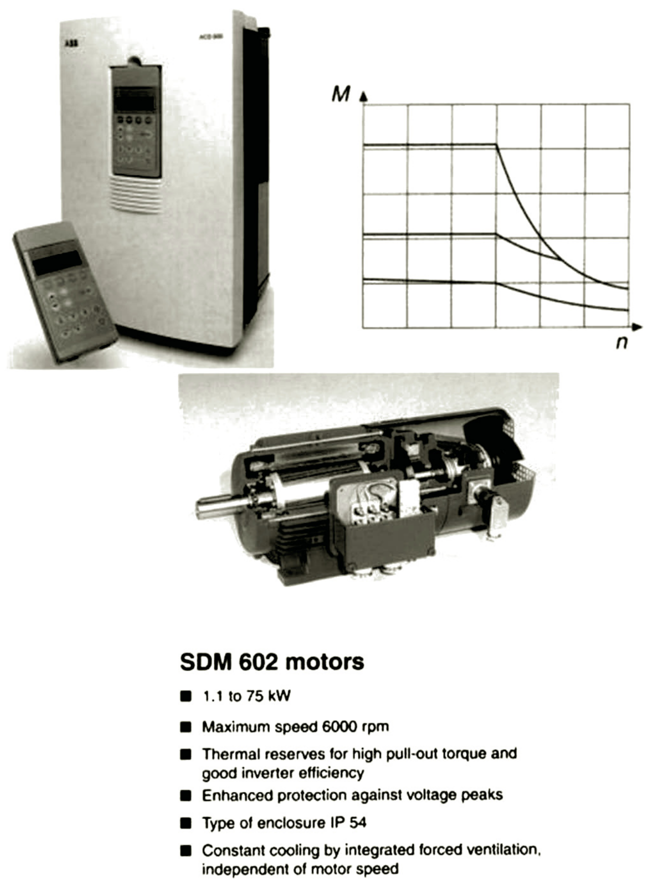


**FIGURE 1.11** Frequency converter with induction motor for variable speed applications. (Source: ABB.)

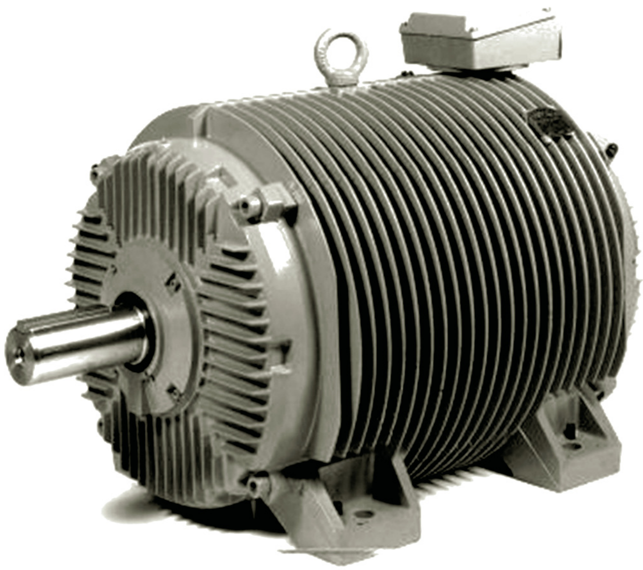

Roller table motor,
frame size 355 SB, 35 kW

(a)

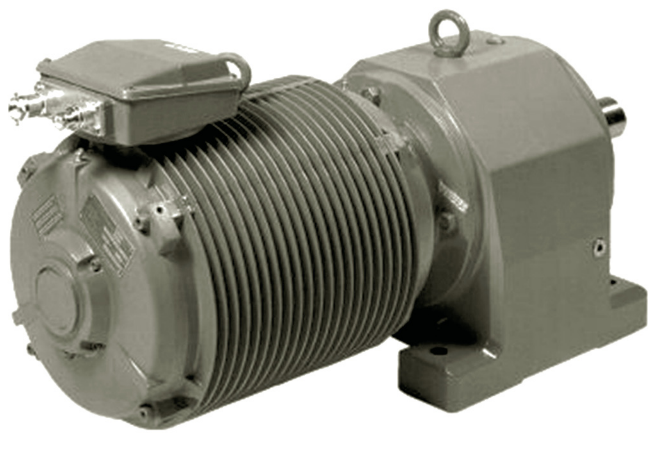

Roller table motor with a gear,
frame size 200 LB, 9.5 kW

(b)

**FIGURE 1.12** Roller table induction motors without (a) and with (b) a gear. (Source: ABB.)

Electric trains, light rail people movers in or around town, or trolleybuses of the last generation are propelled by variable speed induction motor drives.

Most pumps, fans, conveyors, or compressors in various industries are driven by constant or variable speed induction motor drives.

The rotor of a 2500 kW, 3 kV, 400 Hz, two-pole (24,000 rpm) induction motor in different stages of production as shown in Figure 1.14 proves the suitability of induction motors to high-speed and high-power applications.

Figure 1.15a shows a 3.68 kW (5 HP), 3200 Hz (62,000 rpm) induction motor, with direct water stator cooling, which weighs only 2.268 Kg (5 Pds). A high-speed gyroscope dual IM with high

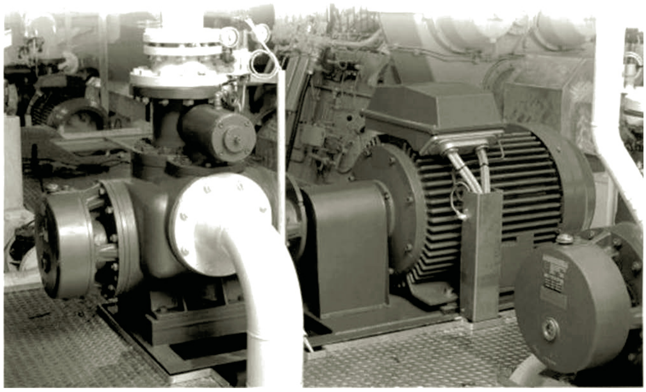

**FIGURE 1.13** Induction motor driving a pump aboard a ship. (Source: ABB.)

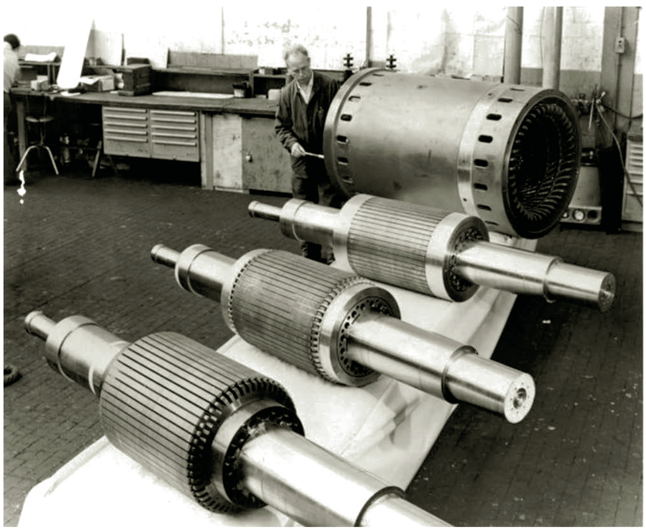

**FIGURE 1.14** A 2500 kW, 3 kV, 24,000 rpm induction motor. (Source: ABB.)

inertia external rotor is shown in Figure 1.15b. This is to show that it is rather the torque than the power that determines the electric motor size.

Copper-cage induction motor drives have been introduced to electric vehicles (Figure 1.16) due to their ruggedness and simpler control: the copper in the rotor cage leads to a better efficiency at high starting/accelerating torques and cruising speed.

At the other end of the applications scale, four- or two-pole changing IMs have been investigated for better efficiency line-start small refrigerator compressor drives (Figure 1.17).

It starts and operates mostly on four-pole configuration (with permanent magnets (PMs) under the rotor cage for an 88% efficiency at 50 W, 1500 rpm), but for short duty, it switches to two-pole operation (with a single-phase winding) for special compressor operation conditions.

In parallel with the development of rotary induction motor, power electronics driven linear motion induction motors have witnessed intense studies with quite a few applications [9,10,15]. Amongst them, Figure 1.18 shows the UTDC-built linear induction motor people mover (BC transit) in Vancouver now in use for more than two decades.

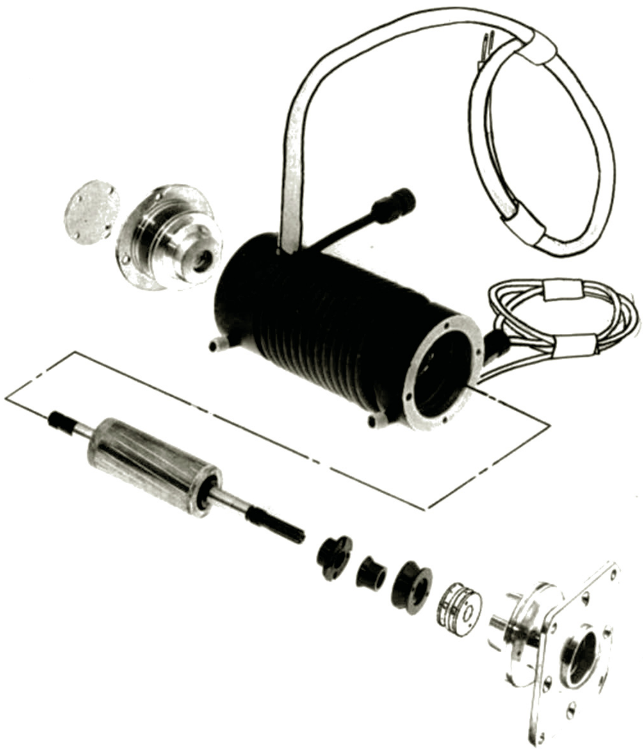

(a)

(b)

**FIGURE 1.15** A 3.68 kW (5 HP), 3200 Hz (62,000 rpm) induction motor with forced liquid cooling (a); high-speed gyroscope dual IM with outer rotor (b).

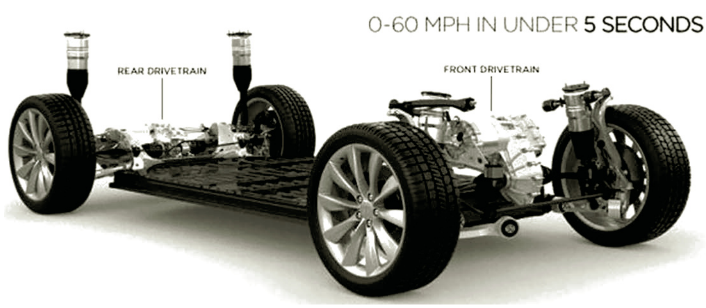


**FIGURE 1.16** Electric power train of "Tesla" electric vehicle, with copper cage rotor induction motor drives. (www.pinterest.com/pin/270145677620776613/).

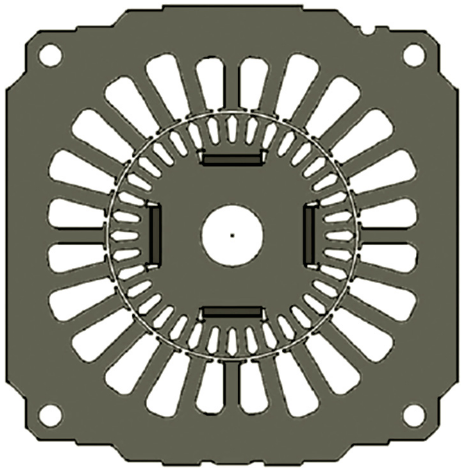

**FIGURE 1.17** Four- or two-pole changing split phase capacitor IM for small compressor drives [14].

**FIGURE 1.18** The BC transit system in Vancouver: with linear motion induction motor propulsion. (Source: UTDC.)

The panoramic view of induction motor applications sketched above is only to demonstrate the extraordinary breadth of IM speed and power ratings and of its applications both for constant and variable speeds.

## 1.4 CONCLUSION

After 1885, more than one century from its invention, the induction motor steps into the 21st century with a vigour hardly paralleled by any other motor.

Power electronics, digital control, computer-aided design, and new and better materials have earned the induction motor the new sobriquet of “the racehorse of industry” in addition to the earlier one of “the workhorse of industry”.

Present in all industries and in-home appliances in constant and variable speed applications, the induction motor seems now ready to make the X by wire and even the electric starter/generator systems aboard of the hybrid electric vehicles of the near future [16].

The new challenges in modelling, optimisation design in the era of FEMs, its control as a motor and generator for even better performance when supplied from PWM converters, and its enormous application potential hopefully justify this rather comprehensive book on IMs at the beginning of the 21st century.

## REFERENCES

1. R. J. Kerkman, G. L. Skibinski, D. W. Schlegel, AC drives; Year 2000 and beyond, *Record of IEEE – APEC* '99, March, 1999.
2. P. Gipe, *Wind Energy Comes of Age*, Wiley & Sons Inc., New York, 1995.
3. H. Sequenz, *The Windings of Electric Machines*, *Vol. 3: A.C. Machines*, Springer Verlag, Vienna, 1950 (in German).
4. R. Richter, *Electric Machines-Vol. 4-Induction Machines*, Verlag Birkhauser, Bassel/Stuttgart, 1954 (in German).
5. Ph. Alger, *The Nature of Induction Machines*, 2nd edition, Gordon & Breach, New York, 1970.
6. C. Veinott, *Theory and Design of Small Induction Motors*, McGraw-Hill, New York, 1959.
7. J. Stepina, *Single Phase Induction Motors*, Springer Verlag, Vienna, 1981 (in German).
8. B. Heller, V. Hamata, *Harmonic Field Effects in Induction Machines*, Elsevier Scientific Publishing Company, Amsterdam, 1977.
9. E. Laithwaite, *Induction Machines for Special Purposes*, Newness, London, UK, 1966.
10. I. Boldea, S. A. Nasar, *Linear Motion Electromagnetic Systems*, Wiley Interscience, London, UK, 1985.
11. EURODEEM by European Commission on Internet: http://iamest.jrc.it/projects/eem/eurodeem.htm
12. T. De Almeida, F.J.T.E. Ferreira, A. Q. Duarte, Technical and economical considerations on superhigh – Efficiency three phase motors, *IEEE Transactions on Industry Applications*, Vol. IA-50, No. 2, 2014, pp. 1274–1275.
13. I. Boldea, *Electric Generators, Part 2 Variable Speed Generators*, CRC Press, Taylor and Francis, New York, 2005.
14. F. J. Kalluf, L. N. Tutelea, I. Boldea, A. Espindola, 2/4-pole split-phase capacitor motor for small compressors: A comprehensive motor characterization, *IEEE Transactions on Industry Applications*, Vol. IA-50, No. 1, 2014, pp. 356–363.
15. I. Boldea, S. A. Nasar, *Linear Motion Electromagnetic Devices*, Taylor and Francis, New York, 2001.
16. M. Ehsani, Y. Gao, S. E. Gay, A. Emadi, *Modern Electric, Hybrid Electric, and Fuel Cell Vehicles*, CRC Press, Taylor & Francis, New York, 2004.

# 2 Construction Aspects and Operation Principles

The induction machine (IM) is basically an A.C. polyphase machine connected to an A.C. power grid, either in the stator or in the rotor. The A.C. power source is, in general, three phase, but it may also be single phase. In both cases, the winding arrangement on the part of the machine – the primary – connected to the grid (the stator in general) should produce a travelling field in the machine airgap. This travelling field will induce voltages in conductors on the part of the machine not connected to the grid (the rotor or the mover in general) – the secondary. If the windings on the secondary (rotor) are closed, A.C. currents occur in the rotor.

The interaction between primary field and secondary currents produces torque from zero rotor speed onwards. The rotor speed at which the rotor currents are zero is called the ideal no-load (or synchronous) speed. The rotor winding may be multiphase (wound rotors) or made of bars short-circuited by end rings (cage rotors).

All the windings on primary and secondary are placed in uniform slots stamped into thin silicon steel sheets called laminations.

The IM has a rather uniform airgap of 0.2–3 mm. The largest values correspond to large powers, 1 MW or more. The secondary windings may be short-circuited or connected to an external impedance or to a power source of variable voltage and frequency. In the latter case, the IM works, however, as a synchronous machine as it is doubly fed and both stator and rotor slip frequencies are imposed (the latter is speed dependent).

Though historically double-stator and double-rotor machines have also been proposed to produce variable speed more conveniently, they did not make it to the markets. Today's power electronics seem to move such solutions even further into forgetfulness.

In this chapter, we discuss construction aspects and operation principles of IMs. A classification is implicit.

The main parts of any IM are as follows:

- The stator slotted magnetic core
- The stator electric winding
- The rotor slotted magnetic core
- The rotor electric winding
- The rotor shaft
- The stator frame with bearings
- The cooling system
- The terminal box.

The IMs may be classified in many ways. Here are some of them.

- With rotary or linear motion
- Three-phase or single-phase supply
- With wound or cage rotor.

In very rare cases, the internal primary is the mover and the external secondary is at standstill. In most rotary IMs, the primary is the stator and the secondary is the rotor. It is not so for linear IMs. Practically all IMs have a cylindrical rotor, and thus, a radial airgap between stator and rotor, though, in principle, axial airgap IMs with disk-shaped rotor may be built to reduce volume and weight in special applications.

First, we discuss construction aspects of the abovementioned types of IMs and then essentials of operation principles and modes.

## 2.1 CONSTRUCTION ASPECTS OF ROTARY IMS

Let us start with the laminated cores.

### 2.1.1 The Magnetic Cores

The stator and rotor magnetic cores are made of thin silicon steel laminations with unoriented grain to reduce hysteresis and eddy current losses. The stator and rotor laminations are packed into a single (Figure 2.1) or multiple stacks (Figure 2.2). The latter has radial channels (5–15 mm wide) between elementary stacks (50–150 mm long) for radial ventilation.

Single stacks are adequate for axial ventilation.

Single-stack IMs have been traditionally used below 100 kW, but recently, they have been introduced up to 2 MW as axial ventilation has been improved drastically. The multistack concept is, however, necessary for large power (torque) with long stacks.

The multiple stacks lead to additional winding losses, up to 10%, in the stator and rotor as the coils (bars) lead through the radial channels without producing torque. Also, the electromagnetic field energy produced by the coil (bar) currents in the channels translates into additional leakage inductances which tend to reduce the breakdown torque and the power factor. They also reduce the starting current and torque. Typical multistack IMs are shown in Figure 2.2.

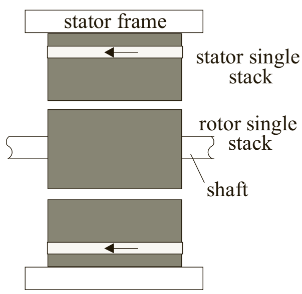


**FIGURE 2.1** Single-stack magnetic core.

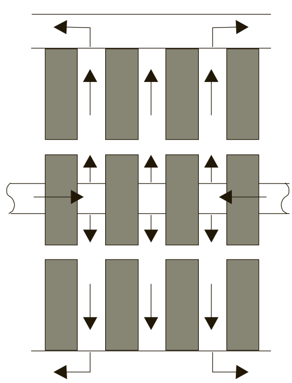

**FIGURE 2.2** Multiple-stack IM.

For IMs of fundamental frequency up to 300 Hz, 0.5 mm thick silicon steel laminations lead to reasonable core losses 2–4 W/Kg at 1 T and 50 Hz.

For higher fundamental frequency, thinner laminations are required. Alternatively, anisotropic magnetic powder materials may be used to cut down the core losses at high fundamental frequencies, above 500 Hz, at lower power factor, however (see Chapter 3 on magnetic materials).

### 2.1.2 Slot Geometry

The airgap, or the air space between the stator and the rotor, has to be travelled by the magnetic field produced by the stator. This in turn will induce voltages and produce currents in the rotor windings. Magnetising air requires large magnetomotive forces (mmfs) or ampere-turns. The smaller the air (nonmagnetic) gap, the smaller the magnetisation mmf. The lower limit of airgap g is determined by mechanical constraints and by the ratio of the stator and rotor slot openings $b_{os}$ and $b_{or}$ to airgap g in order to keep surface core and tooth flux pulsation additional losses within limits. The tooth is the lamination radial sector between two neighbouring slots.

Putting the windings (coils) in slots has the main merit of reducing the magnetisation current. Second, the winding manufacturing and placing in slots becomes easier. Third, the winding in slots is better off in terms of mechanical rigidity and heat transmission (to the cores). Finally, the total mmf per unit length of periphery (the coil height) could be increased, and thus, large power IMs could be built efficiently. What is lost is the possibility to build windings (coils) that can produce purely sinusoidal distribution ampere-turns (mmfs) along the periphery of the machine airgap. But this is a small price to pay for the incumbent benefits.

The slot geometry depends mainly on IM power (torque) level and thus on the type of magnetic wire – with round or rectangular cross section – from which the coils of windings are made. With round wire (random wound) coils for small power IMs (below 100 kW in general), the coils may be introduced in slots wire by wire, and thus, the slot openings may be small (Figure 2.3a). For preformed coils (in large IMs), made, in general, of rectangular cross-section wire, open or semiopen slots are used (Figure 2.3b and c).

In general, the slots may be rectangular, straight trapezoidal, or rounded trapezoidal. Open and semiopen slots tend to be rectangular (Figure 2.3b and c) in shape and the semiclosed ones are trapezoidal or rounded trapezoidal (Figure 2.3a).

In an IM, only slots on one side are open, while on the other side, they are semiclosed or semiopen.

The reason is that a large slot opening, $b_{os}$, per gap, g, ratio ($b_{os}/g > 6$) leads to lower average flux density, for given stator mmf and to large flux pulsation in the rotor tooth, whose pulsations (harmonics) will produce large additional core losses. In the airgap, flux density harmonics lead to parasitic torques, noise, and vibration as presented in subsequent, dedicated chapters. For semiopen and semiclosed slots, $b_{os}/g \cong (4–6)$ in general. For the same reasons, the rotor slot opening per airgap $b_{or}/g \cong 3–4$ wherever possible. Too a small slot opening per gap ratio leads to a higher magnetic field in the slot neck (Figure 2.3) and thus to a higher slot leakage inductance, which causes lower starting torque and current and lower breakdown torque.

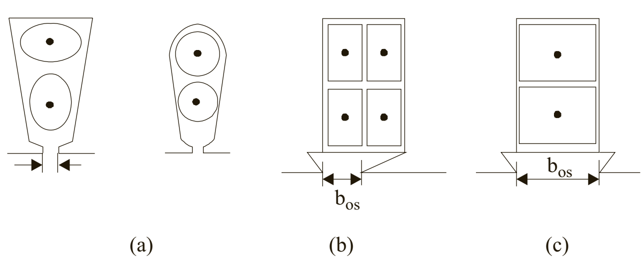


**FIGURE 2.3** Slot geometrics to locate coil windings (a) semiclosed, (b) semiopen, and (c) open.

Slots as in Figure 2.3 are used both for stator and wound rotors. Rotor slot geometry for cage rotors is much more diversified depending upon

- Starting and rated load constraints (specifications)
- Constant voltage/frequency (V/f) or variable voltage/frequency supply operation
- Torque range.

Less than rated starting torque, high-efficiency IMs for low power at constant V/f or for variable V/f may use round semiclosed slots (Figure 2.4a). Rounded trapezoidal slots with rectangular teeth are typical for medium starting torque (around rated value) in small power IMs (Figure 2.4b).

Closed rotor slots may be used to reduce noise and torque pulsations for low power circulating fluid pumps for homes at the expense of large rotor leakage inductance: that is, lower breakdown torque. In essence, the iron bridge (0.5–1 mm thick), above the closed rotor slot, already saturates at 10%–15% of rated current at a relative permeability of 50 or less that drops further to 15–20 for starting conditions (zero speed, full voltage).

For high starting torque, high rated slip (lower rated speed with respect to ideal no-load speed), rectangular deep-bar rotor slots are used (Figure 2.5a). Inverse trapezoidal or double-cage slots are used for low starting current and moderate and large starting torque (Figure 2.5b and c). In all these cases, the rotor slot leakage inductance increases, and thus, the breakdown torque is reduced to as low as 150%–200% rated torque.

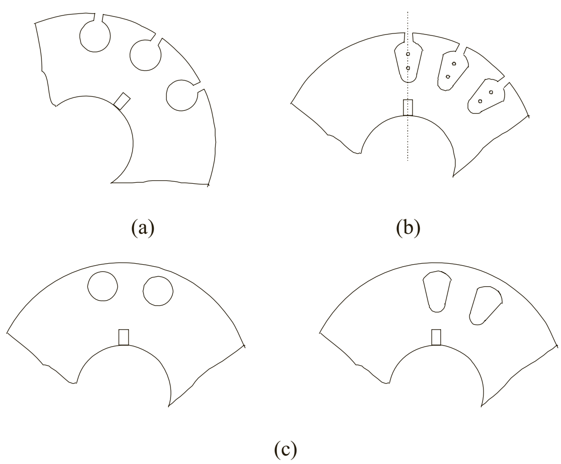


**FIGURE 2.4** Rotor slots for cage rotors: (a) semiclosed and round, (b) semiclosed and round trapezoidal, and (c) closed slots.

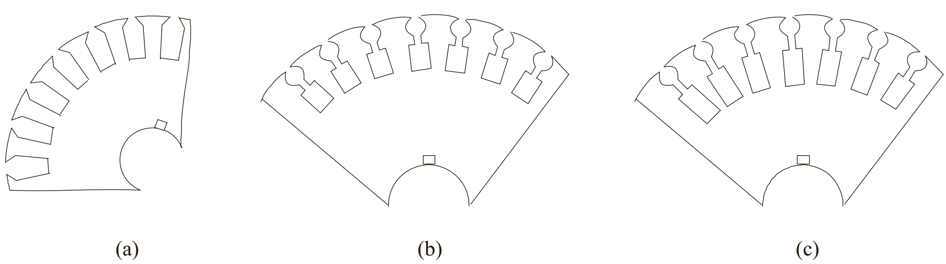


**FIGURE 2.5** Rotor slots for low starting current IMs: (a) high slip, high starting torque and (b) moderate starting torque, and (c) very high.

More general, optimal shape cage rotor slots may today be generated through direct FEM optimisation techniques to meet the desired performance constraints for special applications. In general, low stator current and moderate and high starting torque rely on the rotor slip frequency effect on rotor resistance and leakage inductance.

At the start, the frequency of rotor currents is equal to stator (power grid) frequency $f_1$, while at full load, $f_{sr} = S_n f_1$; $S_n$, the rated slip, is below 0.08 and less than 0.01 in large IMs:

$$S = \frac{f_1 - np_1}{f_1}; \quad \text{n-speed in rps} \tag{2.1}$$

$p_1$ is the number of spatial periods of airgap travelling field wave per revolution produced by the stator windings:

$$B_{g0}(x,t) = B_{gm0}\cos\left(p_1\theta_1 - \omega_1 t\right) \tag{2.2}$$

$\theta_1$ – mechanical position angle; $\omega_1 = 2\pi f_1$.

Remember that, for variable voltage and frequency supply (variable speed), the starting torque and current constraints are eliminated as the rotor slip frequency $Sf_1$ is always kept below that corresponding to breakdown torque.

Very important in variable speed drives is efficiency, power factor, breakdown torque, and motor initial or total costs (with capitalised loss costs included).

### 2.1.3 IM Windings

The IM is provided with windings both on the stator and on the rotor. Stator and rotor windings are treated in detail in Chapter 4.

Here we refer only to a primitive stator winding with six slots for two poles (Figure 2.6).

Each phase is made of a single coil whose pitch spans half of the rotor periphery. The three phases (coils) are space shifted by 120°. For our case, there are 120 mechanical degrees between phase axes as $p_1 = 1$ pole pair. For $p_1 = 2, 3, 4, 5, 6$, there will be $120°/p_1$ mechanical degrees between phase axes.

The airgap field produced by each phase has its maximum in the middle of the phase coil (Figure 2.6), and with the slot opening eliminated, it has a rectangular spatial distribution whose fundamental varies sinusoidally in time with frequency $f_1$ (Figure 2.7).

It is evident from Figure 2.7 that when the time angle $\theta_t$ electrically varies by $\pi/6$, so does the fundamental maximum of airgap flux density with space harmonics neglected, and a travelling wave field in the airgap is produced. Its direction of motion is from phase a to phase b axis, if the current in phase a leads (in time) the current in phase b and phase b leads phase c. The angular speed of this field is simply $\omega_1$, in electrical terms, or $\omega_1/p_1$ in mechanical terms (see also Equation (2.2)).

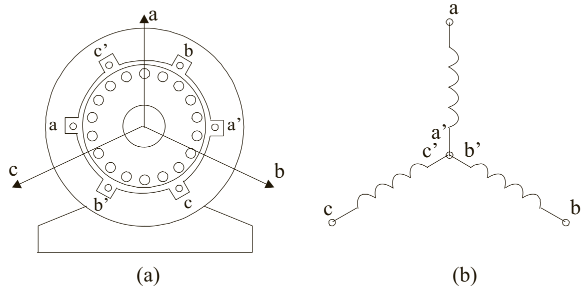


**FIGURE 2.6** Primitive IM with (a) six stator slots and (b) phase connection.

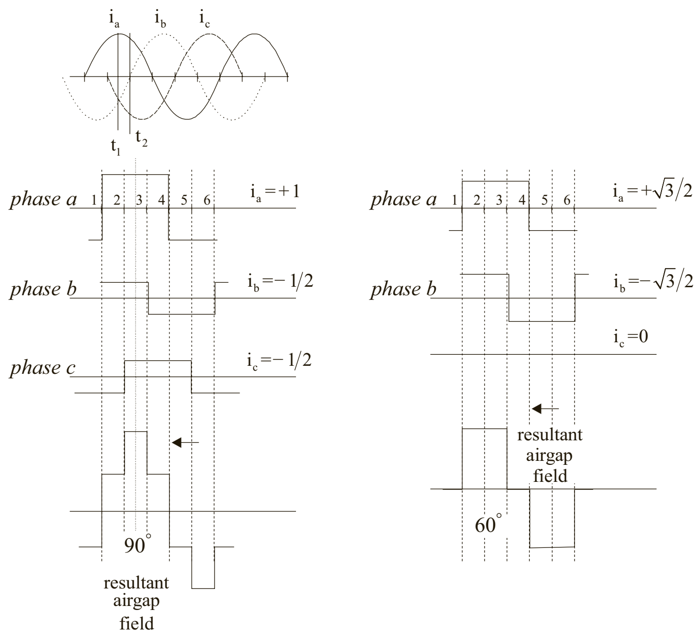


**FIGURE 2.7** Stator currents and airgap field at times $t_1$ and $t_2$.

$$\Omega_1 = 2\pi n_1 = \omega_1 / p_1 \tag{2.3}$$

So $n_1$, the travelling field speed in rps (rotations per second), is

$$n_1 = f_1 / p_1 \tag{2.4}$$

This is how for 50(60) Hz, the no-load ideal speed is 3000/3600 rpm for $p_1 = 1$, 1500/1800 rpm for $p_1 = 2$, and so on.

As the rated slip $S_n$ is small (less than 8% for most IMs), the rated speed is only slightly lower than a submultiple of $f_1$ in rps. The crude configuration in Figure 2.7 may be improved by increasing the number of slots and by using two layers of coils in each slot. This way the harmonic content of airgap flux density diminishes, approaching a better pure travelling field, despite the inherently discontinuous placement of conductors in slots.

A wound stator is shown in Figure 2.8. The three phases may be star or delta connected. Sometimes, during starting, the connection is changed from star to delta (for delta-designed IMs) to reduce starting currents in weak local power grids.

Wound rotors are built in a similar way (Figure 2.9). The slip rings are visible to the right. The stator-placed brush system is not visible. Single-phase-supply IMs have, on the other hand, in general, two windings on the stator.

The main winding (m) and the auxiliary (or starting) one (a) are used to produce a travelling field in the airgap. Similar to the case of three phases, the two windings are spatially phase shifted by 90° (electrical) in general. Also to phase shift the current in the auxiliary winding, a capacitor is used.

In reversible motion applications, the two windings are identical. The capacitor is switched from one phase to the other to change the direction of travelling field.

When auxiliary winding works continuously, each of the two windings uses half the number of slots. Only the number of turns and the cross section of wire differ.

The presence of auxiliary winding with capacitance increases the torque, efficiency, and power factor. In capacitor-start low-power (below 250 W) IMs, the main winding occupies 2/3 of stator slots

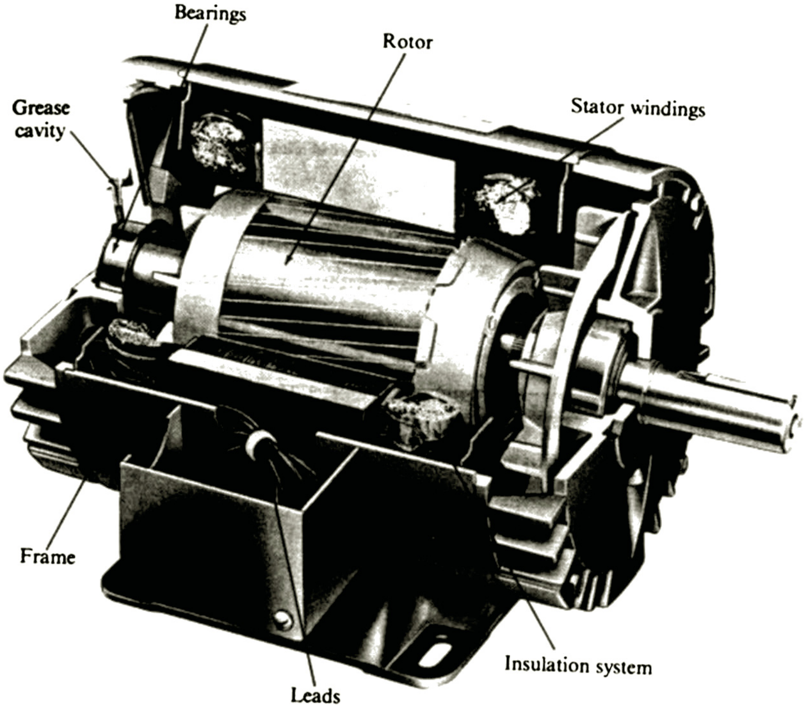


**FIGURE 2.8** IM wound three-phase stator winding with cage rotor.

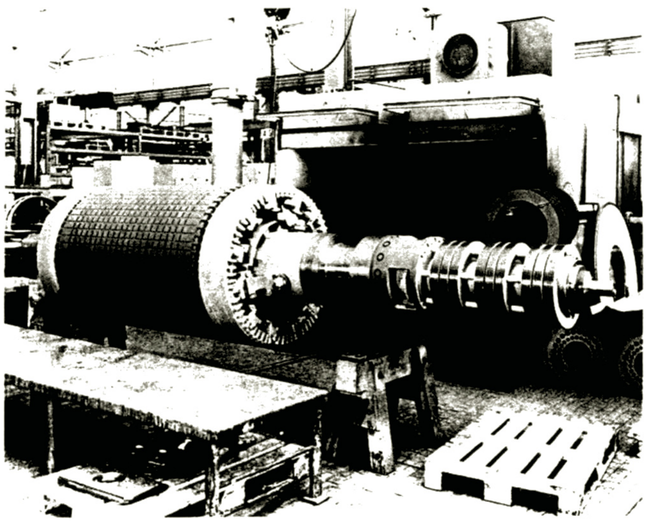

**FIGURE 2.9** Three-phase wound rotor.

and the auxiliary (starting) winding only 1/3. The capacitor winding is turned off in such motors by a centrifugal or time relay at a certain speed (time) during starting. In all cases, a cage winding is used in the rotor (Figure 2.10). For very low power levels (below 100 W in general), the capacitor may be replaced by a resistance to cut cost at the expense of lower efficiency and power factor.

Finally, it is possible to produce travelling field with a single-phase concentrated coil winding with shaded poles (Figure 2.11). The short-circuiting ring is retarding the magnetic flux of the stator in the shaded pole area with respect to the unshaded pole area.

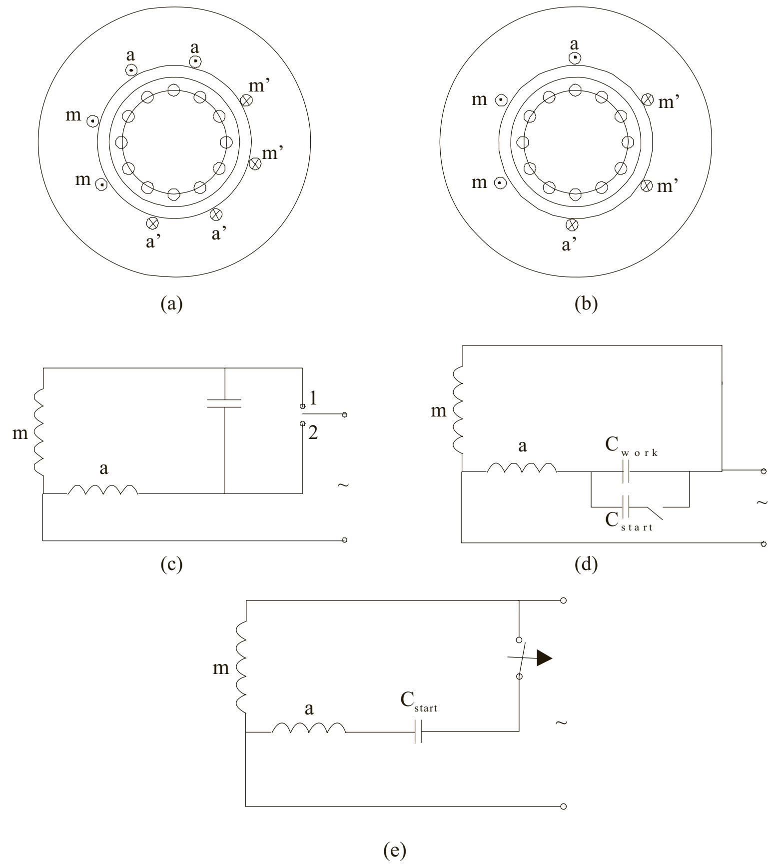


**FIGURE 2.10** Single-phase supply capacitor IMs: (a) primitive configuration with equally strong windings, (b) primitive configuration with 2/3, 1/3 occupancy windings, (c) reversible motor, (d) dual capacitor connection, and (e) capacitor start-only connection.

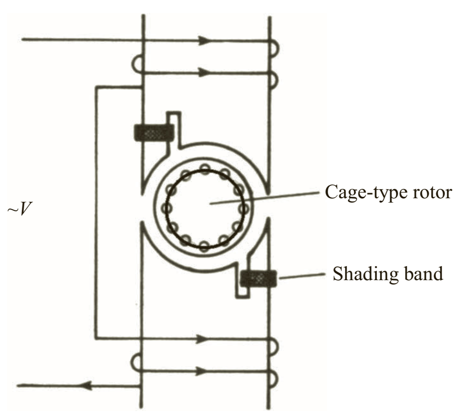


**FIGURE 2.11** Single-phase (shaded pole) IM.

The airgap field has a travelling component and the motor starts rotating from the unshaded to the shaded pole zone. The rotor has a cage winding. The low cost and superior ruggedness of shaded pole single-phase IM is paid for by lower efficiency and power factor. This motor is more of historical importance and it is seldom used, mostly below 100 W, where cost is the prime concern.

### 2.1.4 Cage Rotor Windings

As mentioned above, the rotor of IMs is provided with single- or double-cage windings (Figure 2.12), besides typical three-phase windings on wound rotors.

The cage bars and end rings are made of die-cast aluminium for low and medium power and from brass or copper for large powers. For medium and high powers, the bars are silver rings – welded to end to provide low resistance contact.

For double cages, we may use brass (higher resistivity) for the upper cage and copper for the lower cage. In this case, each cage has its own end ring, mainly due to thermal expansion constraints.

For high-efficiency IMs, copper tends to be preferred due to higher conductivity, larger allowable current density, and working temperatures.

As die-cast copper cage manufacturing is maturing, even for small motors (in home appliances), the copper cage will be used more and more, besides today's welded copper-cage IM's hot water pump of home furnaces.

The die casting of aluminium at rather low temperatures results in low rotor mass production costs for low power IMs.

The debate over aluminium or copper is not decided yet, and both materials are likely to be used depending on the application and power (torque) level.

Although some construction parts such as frames, cooling systems, shafts, bearings, and terminal boxes have not been described yet here, we will not dwell on them at this time as they will "surface" again in subsequent chapters. Instead, Figure 2.13 presents a rather complete cutaway view of a fairly modern induction motor. It has a single-stack magnetic core; thus, axial ventilation is used by a fan located on the shaft beyond the bearings. The heat evacuation area is increased by the finned stator frame. This technology has proved practical up to 2 MW in low-voltage IMs.

The IM in Figure 2.13 has a single-cage rotor winding. The stator winding is built in two layers out of round magnetic wire. The coils are random wound. The stator and rotor slots are of the semiclosed type. Configuration in Figure 2.13 is dubbed as totally enclosed fan cooled (TEFC), as the ventilator is placed outside bearings on the shaft.

It is a low-voltage IM (below 690 V RMS – line voltage).

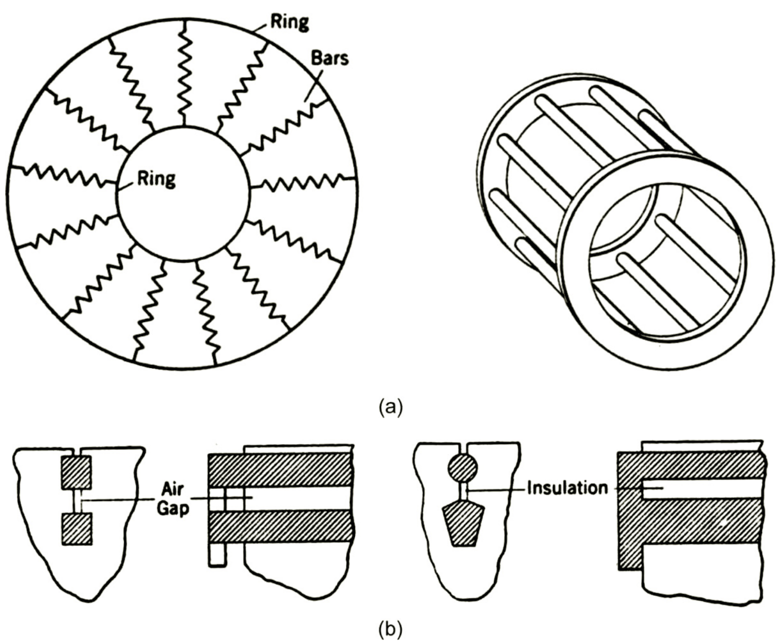


**FIGURE 2.12** Cage rotor windings: (a) single cage and (b) double cage.

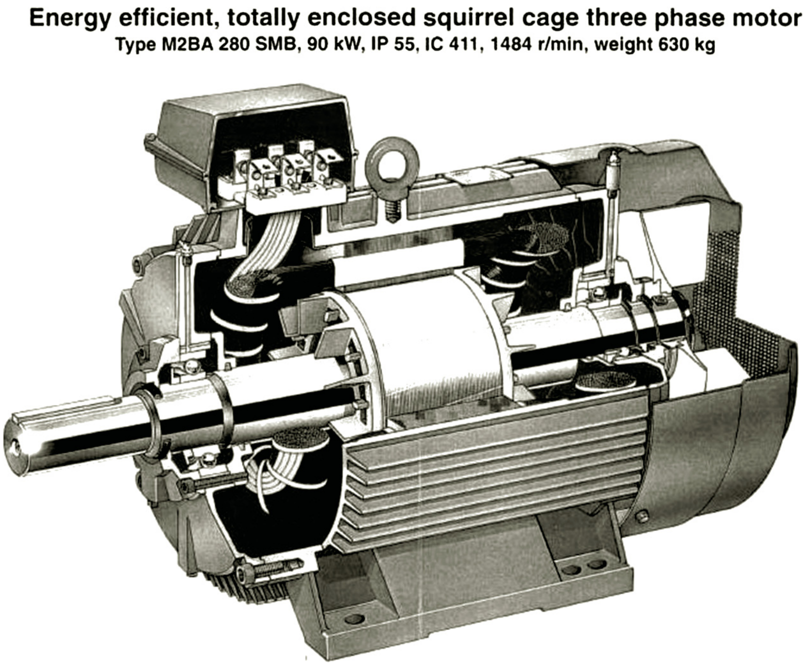


**FIGURE 2.13** Cutaway view of a modern induction motor.

## 2.2 CONSTRUCTION ASPECTS OF LINEAR INDUCTION MOTORS

In principle, for each rotary IM, there is a linear motion counterpart. The imaginary process of cutting and unrolling the rotary machine to obtain the linear induction motor (LIM) is by now classic (Figure 2.14) [1].

The primary may now be shorter or larger than the secondary. The shorter component will be the mover. In Figure 2.14, the short primary is the mover. The primary may be double- (Figure 2.14d) or single-sided (Figure 2.14c and e).

The secondary material is copper or aluminium for the double-sided LIM, and it may be aluminium (copper) on solid iron for the single-sided LIM. Alternatively, a ladder conductor secondary placed in the slots of a laminated core may be used, as for cage rotor rotary IMs (Figure 2.14c). This latter case is typical for short travel (up to a few metres), low-speed (below 3 m/s) applications.

Finally, the secondary solid material may be replaced by a conducting fluid (liquid metal), when a double-sided linear induction pump is obtained [2].

All configurations shown in Figure 2.14 may be dubbed as flat ones. The primary winding produces an airgap field with a strong travelling component at the linear speed $u_s$, for the pole pitch $\tau$ and frequency $f_1$

$$u_s = \tau \cdot \frac{\omega_1}{\pi} = 2\tau f_1 \tag{2.5}$$

The number of pole pairs does not influence the ideal no-load linear speed $u_s$. Incidentally, the peripheral ideal no-load speed in rotary IMs has the same formula (2.5) where $\tau$ is also the pole pitch (the spatial semiperiod of the travelling field).

In contrast to rotary IMs, the LIM has an open magnetic structure along the direction of motion. Additional phenomena called longitudinal effects occur due to this. They tend to increase with speed,

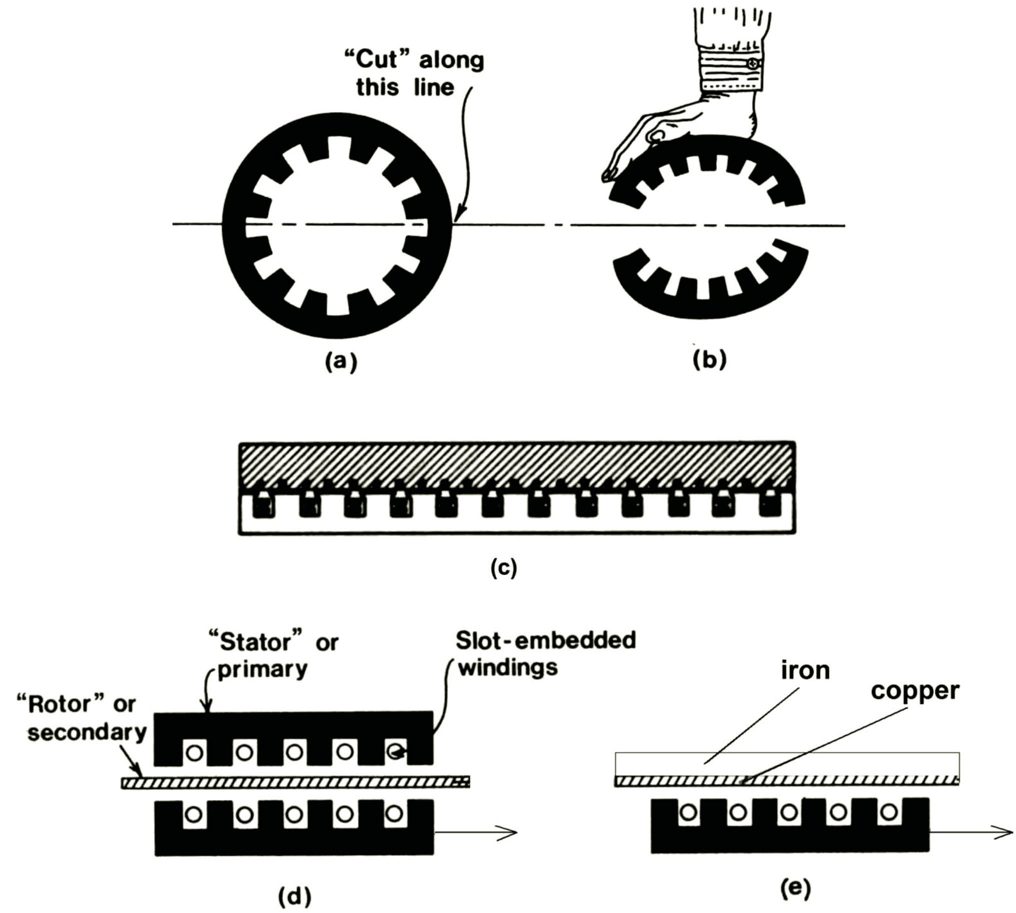


**FIGURE 2.14** Cutting and unrolling process to obtain an LIM.

deteriorating the thrust, efficiency, and power factor performance. Also, above 3–5 m/s speed, the airgap has to be large (due to mechanical clearance constraints): in general, 3–12 mm. This leads to high magnetisation currents and, thus, lower power factor than in rotary IMs.

However, the LIM produces electromagnetic thrust directly and, thus, eliminates any mechanical transmission in linear motion applications (transportation).

Apart from flat LIM, tubular LIMs may be obtained by rerolling the flat LIM around the direction of motion (Figure 2.15).

The coils of primary winding are now of circular shape. The rotor may be an aluminium cylinder on solid iron. Alternatively, a secondary cage may be built. In this case, the cage is made of ring-shaped bars. Transverse laminations of disc shape may be used to make the magnetic circuit easy to manufacture, but care must be exercised to reduce the core losses in the primary. The blessing of circularity renders this LIM more compact and proper for short travels (1 m or less).

In general, LIMs are characterised by a continuous thrust density (N/cm$^2$ of primary) of up to 2 (2.5) N/cm$^2$ without forced cooling. The large values correspond to larger LIMs. The current LIM used for a few urban transportation systems in North America, Middle East, and East Asia has proved that they are rugged and almost maintenance free. More on LIMs are presented in Chapter 12 (Volume 2).

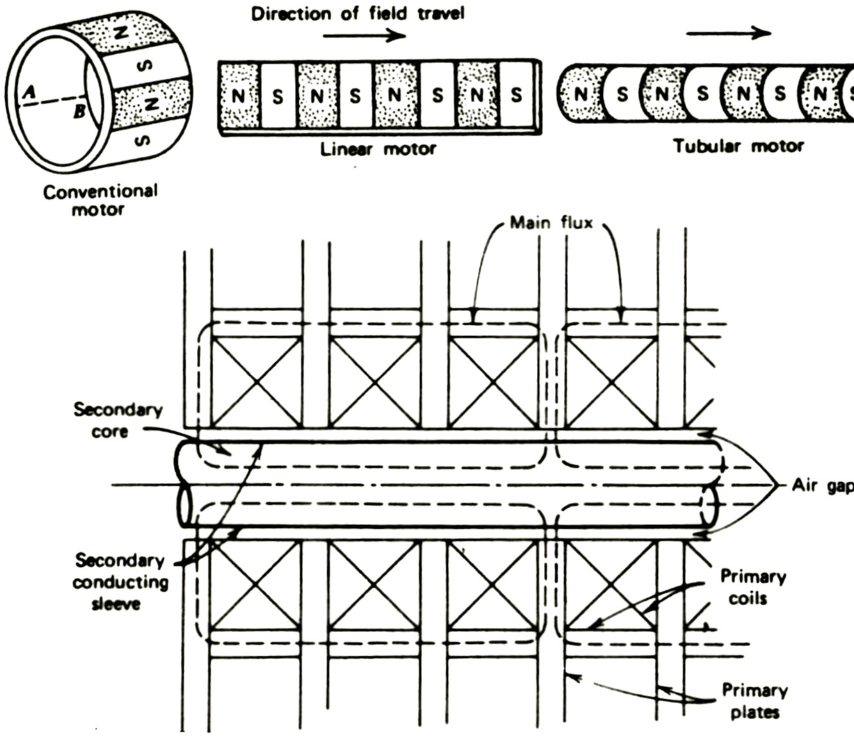


**FIGURE 2.15** The tubular LIM.

## 2.3 OPERATION PRINCIPLES OF IMS

The operation principles are basically related to torque (for rotary IMs) and, respectively, thrust (for LIMs) production. In other words, it is about forces in travelling electromagnetic fields. Or even simpler, why the IM spins and the LIM moves linearly. Basically the torque (force) production in IMs and LIMs may be approached via

- Forces on conductors in a travelling field
- The Maxwell stress tensor [3]
- The energy (coenergy) derivative
- Variational principles (Lagrange equations) [4].

The electromagnetic travelling field produced by the stator currents exists in the airgap and crosses the rotor teeth to embrace the rotor winding (say, rotor cage) – Figure 2.16. Only a small fraction of it traverses radially the top of the rotor slot which contains conductor material.

It is thus evident that, with rotor and stator conductors in slots, there are no main forces experienced by the conductors themselves. Therefore, the method of forces experienced by conductors in fields does not apply directly to rotary IMs with conductors in slots.

The current occurs in the rotor cage (in slots) because the magnetic travelling flux produced by the stator in any rotor cage loop varies in time even at zero speed (Figure 2.17). If the cage rotor rotates at speed n (in rps), the stator-produced travelling flux density in the airgap (2.2) moves with respect to the rotor with the relative speed $n_{sr}$.

$$n_{sr} = \frac{f_1}{p_1} - n = S \cdot \frac{f_1}{p_1} \tag{2.6}$$

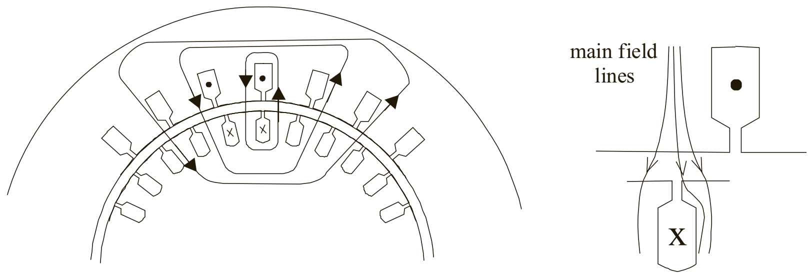


**FIGURE 2.16** Flux paths in IMs.

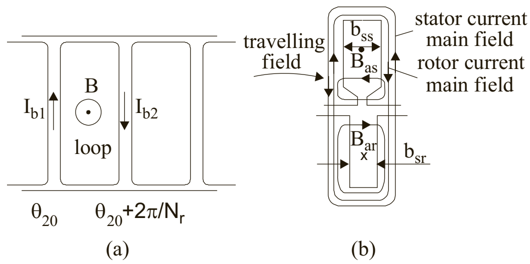


**FIGURE 2.17** Travelling flux crossing the rotor cage loops (a), leakage and main fields (b).

S is called IM slip.

So in rotor coordinates, (2.2) may be written as

$$B(\theta_r,t) = B_m \cos\left(p_1\theta_2 - S\omega_1 t\right) \tag{2.7}$$

Consequently, with the cage bars in slots, according to electromagnetic induction law, a voltage is induced in loop 1 of the rotor cage, and thus, a current occurs in it such that its reaction flux opposes the initial flux (visible in Figure 2.17).

The current which occurs in the rotor cage, at rotor slip frequency $Sf_1$ (see Equation (2.7)), produces a reaction field that crosses the airgap. This is the main reaction field. Thus, the resultant airgap field is the "product" of both stator and rotor currents. As the two currents tend to be shifted more than $2\pi/3$, the resultant (magnetisation) current is reasonably low; in fact, it is 25%–80% of the rated current, depending on the machine airgap g to pole pitch $\tau$ ratio. The higher the ratio $\tau/g$, the smaller the magnetisation current in p.u. (per unit or relative values).

The stator and rotor currents also produce leakage flux paths crossing the slots: $B_{as}$ and $B_{ar}$ (Figure 2.17).

According to the Maxwell stress tensor theory, at the surface border between mediums with different magnetic materials and permeabilities ($\mu_0$ in air, $\mu \neq \mu_0$ in the core), the magnetic field produces forces. The interaction force component perpendicular to the rotor slot wall is [3]

$$F_{tn} = \frac{B_{ar}(\theta_r,t)B_{tr}(\theta_r,t)}{\mu_0}\bar{n}_{tooth} \tag{2.8}$$

The magnetic field has a radial ($B_{tr}$) and a tangential ($B_{ar}$) component only.

Now, for the rotor slot, $B_{ar}(\theta_r)$ – tangential flux density – is the slot leakage flux density.

$$B_{ar}(\theta_r) = \frac{\mu_0 I_b(\theta_r,t)}{b_{sr}} \tag{2.9}$$

The radial flux density that counts in the torque production is that produced by the stator currents, $B_{tr}(\theta_r)$, in the rotor tooth.

$$B_{tr}(\theta_r, t) = B(\theta_r, t) \cdot \frac{b_{tr} + b_{sr}}{b_{sr}} \tag{2.10}$$

In (2.10), $b_{tr}$ is the mean rotor tooth width while $B(\theta_r,t)$ is the airgap flux density produced by the stator currents in the airgap.

When we add the specific Maxwell stress tensors [1] on the left- and right-side walls of the rotor slot, we should note that the normal direction changes sign on the two surfaces. Thus, the addition becomes a subtraction.

$$f_{tooth}\left(N/m^2\right) = -\left(\frac{B_{ar}(\theta_r + \Delta\theta, t) B_{tr}(\theta_r + \Delta\theta, t)}{\mu_0} - \frac{B_{ar}(\theta_r, t) B_{tr}(\theta_r, t)}{\mu_0}\right) \tag{2.11}$$

Essentially, the slot leakage field $B_{ar}$ does not change with $\Delta\theta$ – the radial angle that corresponds to a slot width.

$$f_{tooth}\left(N/m^2\right) = -\frac{B_{ar}(\theta_r, t)}{\mu_0}\left(B_{tr}(\theta_r + \Delta\theta, t) - B_{tr}(\theta_r, t)\right) \tag{2.12}$$

The approximate difference may be replaced by a differential when the number of slots is large. Also from (2.9):

$$f_{tooth}\left(N/m^2\right) = -\frac{-I_b(\theta_r, t)}{b_{sr}} \cdot \frac{\Delta B(\theta_r, t)}{\Delta\theta_{slot}} \cdot \frac{(b_{tr} + b_{sr})}{b_{sr}} \cdot \Delta\theta_{slot} \tag{2.13}$$

Therefore, it is the change of stator-produced field with $\theta_r$, the travelling field existence, which produces the tangential force experienced by the walls of each slot. The total force for one slot may be obtained by multiplying the specific force in (2.13) by the rotor slot height and the stack length.

It may be demonstrated that with a pure travelling field and rotor current travelling wave $I_b(\theta_r,t)$, the tangential forces on each slot pair of walls add up to produce finally a smooth torque. Not so if the field is not purely travelling.

Based on the same rationale, the opposite direction tangential force on stator slot walls may be calculated. It is produced by the interaction of stator leakage field with rotor main reaction field. This is to be expected as action equals reaction according to Newton's third law. So the tangential forces that produce the torque occur on the tooth radial walls. Despite this reality, the principle of IM is traditionally explained by forces on currents in a magnetic field.

It may be demonstrated that, mathematically, it is correct to "move" the rotor currents from rotor slots, eliminate the slots, and place them in an infinitely thin conductor sheet on the rotor surface to replace the actual slot-cage rotor configuration (Figure 2.18). This way the tangential force will be exerted directly on the "rotor" conductors. Let us use this concept to further explain the operation modes of IM.

The relative speed between rotor conductors and stator travelling field is $\overline{U} - \overline{U}_s$, so the induced electrical field in the rotor conductors is

$$\overline{E} = \left(\overline{U} - \overline{U}_s\right) \times \overline{B} \tag{2.14}$$

As the rotor cage is short-circuited, no external electric field is applied to it, so the current density in the rotor conductor $\overline{J}$ is

$$\overline{J} = \sigma_{Al}\overline{E} \tag{2.15}$$

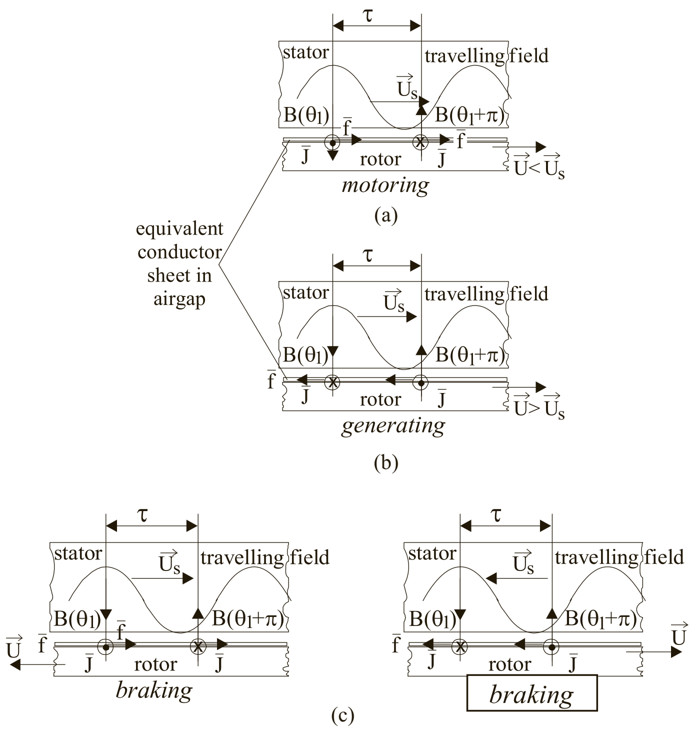


**FIGURE 2.18** Operation modes of IMs: (a) motoring: $\vec{U} < \vec{U}_s$ both in the same direction, (b) generating: $\vec{U} > \vec{U}_s$; both in the same direction, (c) braking: $\vec{U}$ opposite to $\vec{U}_s$; either $\vec{U}$ or $\vec{U}_s$ changes direction.

Finally, the force (per unit volume) exerted on the rotor conductor by the travelling field, $f_t$, is

$$f_t = \bar{J} \times \bar{B} \tag{2.16}$$

Applying these fundamental equations for rotor speed $\bar{U}$ and field speed $\bar{U}_s$ in the same direction, we obtain the motoring mode for $\vec{U} < \vec{U}_s$, and, respectively, the generating mode for $\vec{U} > \vec{U}_s$, as shown in Figure 2.17a and b. In the motoring mode, the force on rotor conductors acts along the direction of motion, while, in the generating mode, it acts against it. At the same time, the electromagnetic (airgap) power $P_e$ is negative.

$$\begin{aligned} P_e &= \bar{f}_t \cdot \bar{U}_s > 0; \text{ for motoring } (ft > 0, U > 0) \\ P_e &= \bar{f}_t \cdot \bar{U}_s < 0; \text{ for generating } (ft < 0, U > 0) \end{aligned} \tag{2.17}$$

This simply means that in the generating mode, the active power travels from rotor to stator to be sent back to the grid after losses are covered. In the braking mode ($U < 0$ and $U_s > 0$ or $U > 0$ and $U_s < 0$), as seen in Figure 2.18c, the torque acts against motion again but the electromagnetic power $P_e$ remains positive ($\bar{U}_s > 0$ and $\bar{f}_t > 0$ or $\bar{U}_s < 0$ and $\bar{f}_t < 0$). Consequently, active power is drawn from the power source. It is also drawn from the shaft. The summation of the two is converted into IM losses.

The braking mode is, thus, energy-intensive and should be used only at low frequencies and speeds (low $U_s$ and U), in variable speed drives, to "lock" the variable speed drive at standstill under load.

The LIM operation principles and operation modes are quite similar to those presented for rotary IMs.

In wound rotor IMs, the rotor may be fed from a separate source at slip frequency $f_2 = S \cdot f_1$, variable with speed. The principle is, however, the same as for the cage rotor IM (interaction between stator field and rotor currents (or their leakage field)).

Recently, permanent magnets and (or) magnetic saliency have been added on the IM cage rotor to enhance their efficiency in constant speed drives, while dual stator windings with nested cage rotors have been introduced for variable speed generators with fractional kVA pulse width modulation (PWM) converters. They will be dedicated special paragraphs in this book (see the Contents).

## 2.4 SUMMARY

- The IM is an A.C. machine. It may be energised directly from a three- or single-phase A.C. power grids. Alternatively, it may be energised through a PWM converter at variable voltage (V) and frequency (f).
- The IM is essentially a travelling field machine. It has an ideal no-load speed $n_1 = f_1/p_1$; $p_1$ is the number of travelling field periods per one revolution.
- The main parts of IM are the stator and rotor slotted magnetic cores and windings. The magnetic cores are, in general, made of thin silicon steel sheets (laminations) to reduce the core losses to values such as 2–4 W/Kg at 60 Hz and 1 T.
- Three- or two-phase windings are placed in the primary (stator) slots. Windings are coil systems connected to produce a travelling mmf (ampere-turns) in the airgap between the stator and the rotor cores.
- The slot geometry depends on power (torque) level and performance constraints.
- Starting torque and current, breakdown torque, rated efficiency, and power factor are typical constraints (specifications) for power grid directly energised IMs.
- Two-phase windings are used for capacitor IMs energised from a single-phase A.C. supply to produce travelling field. Single-phase A.C. supply is typical for home appliances.
- Cage windings made of solid bars (of aluminum, brass or copper [5]) in slots with end rings are used on most IM rotors.
- The rotor bar cross section is tightly related to all starting and running performance. Deep-bar or double-cage windings are used for high starting torque, low starting current IMs fed from the power grid (constant V and f).
- LIMs are obtained from rotary IMs by the cut-and-unroll process. Flat and tubular configurations are feasible with single- or double-sided primary. Either primary or secondary may be the mover in LIMs. Ladder or aluminium sheet or iron are typical for single-sided LIM secondaries. Continuous thrust densities up to 2–2.5 N/cm$^2$ are feasible with air cooling LIMs.
- In general, the airgap g per pole pitch $\tau$ ratio is larger than for rotary IM, and thus, the power factor and efficiency are lower. However, the absence of mechanical transmission in linear motion applications leads to virtually maintenance-free propulsion systems. Urban transportation systems with LIM propulsion are now in use in a few cities from three continents.
- The principle of operation of IMs is related to torque production. By using the Maxwell stress tensor concept it has been shown that, with windings in slots, the torque (due to tangential forces) is exerted mainly on slot walls and not on the conductors themselves.
- Stress analysis during severe transients should illustrate this reality. It may be demonstrated that the rotor winding in slots can be "mathematically" moved in the airgap and transformed into an equivalent infinitely thin current sheet. The same torque is now exerted directly on the rotor conductors in the airgap. The LIM with conductor sheet on iron resembles this situation naturally.

- Based on the $\bar{J} \times \bar{B}$ force principle, three operation modes of IM are easily identified (with $U_s$ – ideal no-load speed, U – mover speed):
  - Motoring: $|U| < |U_s|$; U and $U_s$ either positive or negative
  - Generating: $|U| > |U_s|$; U and $U_s$ either positive or negative
  - Braking: ($U > 0$ & $U_s < 0$) or ($U < 0$ & $U_s > 0$).
- For the motoring mode, the torque acts along the direction of motion, while, for the generator mode, it acts against it as it does during braking mode.
- However, during generating, the IM returns some power to the grid, after covering the losses, while for braking, it draws active power also from the power grid.
- Generating is energy conversion advantageous while braking is energy-intensive. Braking is recommended only at low frequency and speed, with variable V/f PWM converter supply, to stall the IM drive on load (like in overhead cranes). The energy consumption is moderate in such cases anyway (as the frequency is small).

## REFERENCES


1. I. Boldea, S. A. Nasar, *Linear Motion Electric Machines*, Wiley Interscience, New York, 1976.
2. I. Boldea, S. A. Nasar, *Linear Motion Electromagnetic Systems*, Wiley Interscience, New York, 1985, Chapter 5.
3. M. Schwartz, *Principles of Electrodynamics*, Dover Publications Inc., New York, 1972, pp.180.
4. D. C. White, H. H. Woodson, *Electromechanical Energy Conversion*, John Wiley & Sons Inc. London, 1959.
5. R. Kimmich, M. Doppelbauer, D. T. Peters, J. G. Cowie, E. F. Brush, Jr., *Die-cast Copper Rotor Motor Via Simple Substitution and Motor Redesign for Copper*, Record of ICEM-2006, Ref. No. 358.

Taylor & Francis
Taylor & Francis Group
http://taylorandfrancis.com

# 3 Magnetic, Electric, and Insulation Materials for IM

## 3.1 INTRODUCTION

Induction machines (IMs) contain magnetic circuits travelled by A.C. and travelling magnetic fields and electric circuits flowed by alternative currents. The electric circuits are insulated from the magnetic circuits (cores). The insulation system comprises the conductor insulation, slot, and interphase insulation.

Magnetic, electrical, and insulation materials are characterised by their characteristics (B–H curve, electrical resistivity, dielectric constant, and breakdown electric field (V/m)) and their losses.

At frequencies encountered in IMs (up to tens of kHz, when pulse width modulation (PWM) inverter fed), the insulation losses are neglected. Soft magnetic materials are used in IM as the magnetic field is currently produced. The flux density (B)/magnetic field (H) curve and cycle depend on the soft material composition and fabrication process. Their losses in W/kg depend on the B–H hysteresis cycle, frequency, electrical resistivity, and the A.C. (or) travelling field penetration into the soft magnetic material.

Silicon steel sheets are standard soft magnetic materials for IMs. Amorphous soft powder materials have been introduced recently with some potential for high-frequency (high-speed) IMs. The pure copper is the favourite material for the stator electric circuit (windings), while aluminium or brass is used mainly for rotor squirrel-cage windings.

Insulation materials are getting thinner and better and are ranked into a few classes: A (105°C), B (130°C), F (155°C), and H (180°C).

## 3.2 SOFT MAGNETIC MATERIALS

In free space, the flux density B and the magnetic field H are related by the permeability of free space $\mu_0 = 4\pi 10^{-7}$ H/m (S.I.)

$$B\left[\frac{Wb}{m^2}\right] = \mu_0\left[\frac{H}{m}\right]\cdot H\left[\frac{A}{m}\right] \tag{3.1}$$

Within a certain material, a different magnetisation process occurs.

$$B = \mu\cdot H;\quad \mu = \mu_0\,\mu_R \tag{3.2}$$

In (3.2), $\mu$ is termed as permeability and $\mu_R$ as relative permeability (non-dimensional).

Permeability is defined for homogenous (uniform quality) and isotropic (same properties in all directions) materials. In non-homogeneous or (and) non-isotropic materials, $\mu$ becomes a tensor. Most common materials are non-linear: $\mu$ varies with B.

A material is classified according to the value of its relative permeability, $\mu_R$, which is related to its atomic structure.

Most non-magnetic materials are either paramagnetic – with $\mu_R$ slightly greater than 1.0 – or diamagnetic with $\mu_R$ slightly less than 1.0. Superconductors are perfect diamagnetic materials. In such materials when $B \to 0$, $\mu_R \to 0$.

Magnetic properties are related to the existence of permanent magnetic dipoles within the matter.

There are quite a few classes of more magnetic materials ($\mu_R \gg 1$). Amongst them, we will deal here with soft ferromagnetic materials. Soft magnetic materials include alloys made of iron, nickel, cobalt, and one rare earth element and/or soft steels with silicon.

There is also a class of magnetic materials made of powdered iron particles (or other magnetic material) suspended in an epoxy or plastic (non-ferrous) matrix. These soft powder magnetic materials are formed by compression or injection, moulding, or other techniques.

There are a number of properties of interest in a soft magnetic material such as permeability versus B, saturation flux density, H(B), temperature variation of permeability, hysteresis characteristics, electric conductivity, Curie temperature, and loss coefficients.

The graphical representation of non-linear B(H) curve (besides the pertinent table) is of high interest (Figure 3.1). Also of high interest is the hysteresis loop (Figure 3.2).

There are quite a few standard laboratory methods to obtain these two characteristics. The B–H curve can be obtained in two ways: the virgin (initial) B–H curve, obtained from a totally demagnetised sample; and the normal (average) B–H curve, obtained as the tips of hysteresis loops of increasing magnitude. There is only a small difference between the two methods.

The B–H curve is the result of domain changes within the magnetic material. The domains of soft magnetic materials are $10^{-4}$–$10^{-7}$ m in size. When completely demagnetised, these domains have random magnetisation with zero flux in all finite samples.

When an external magnetic field H is applied, the domains aligned to H tend to grow when B is increased (region I on Figure 3.1). In region II, H is further increased and the domain walls move rapidly until each crystal of the material becomes a single domain. In region III, the domains rotate towards alignment with H. This results in magnetic saturation $B_s$. Beyond this condition, the small increase in B is basically due to the increase in the space occupied by the material for $B = \mu_0 H_{r0}$.

This "free-space" flux density may be subtracted to obtain the intrinsic magnetisation curve. The non-linear character of B–H curve (Figure 3.1) leads to two different definitions of relative permeability:

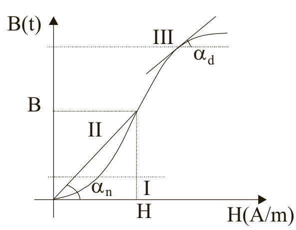


**FIGURE 3.1** Typical B–H curve.

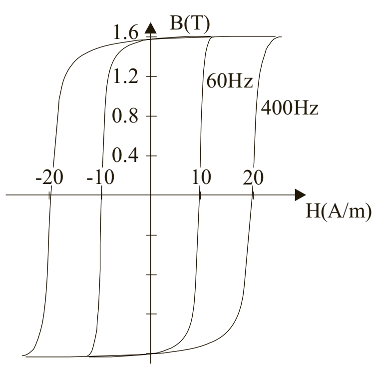


**FIGURE 3.2** Deltamax tape-wound core 0.5 mm strip hysteresis loop.

- The normal permeability $\mu_{Rn}$:

$$\mu_{Rn} = \frac{B}{\mu_0 H} = \frac{\tan\alpha_n}{\mu_0} \tag{3.3}$$

- The differential relative permeability $\mu_{Rd}$:

$$\mu_{Rd} = \frac{dB}{\mu_0 dH} = \frac{\tan\alpha_d}{\mu_0} \tag{3.4}$$

Only in region II, $\mu_{Rn} = \mu_{Rd}$. In regions I and III, in general, $\mu_{Rn} > \mu_{Rd}$ (Figure 3.3). The permeability is maximum in region II. For M19 silicon steel sheets, $B_s = 2$ T, $H_s = 40{,}000$ A/m, and $\mu_{Rmax} = 10{,}000$).

So the minimum relative permeability is

$$(\mu_{Rn})_{B_s=2.0\,T} = \frac{2.0}{4\pi 10^{-7} \cdot 40{,}000} = 39.8! \tag{3.5}$$

The second graphical characteristic of interest is the hysteresis loop (Figure 3.2). This is a symmetrical hysteresis loop obtained after a number of reversals of magnetic field (force) between $\pm H_c$. The area within the loop is related to the energy required to reverse the magnetic domain walls as H is reversed. This nonreversible energy is called hysteresis loss and varies with temperature and frequency of H reversals in a given material (Figure 3.2). A typical magnetisation curve B–H for silicon steel nonoriented grain is given in Table 3.1.

It has been shown experimentally that the magnetisation curve varies with frequency as shown in Table 3.2. This time the magnetic field is kept in original data (1Oe = 79.5 A/m) [1].

In essence for the same flux density B, the magnetic field increases with frequency. It is recommended to reduce the design flux density when the frequency increases above 200 Hz as the core losses grow markedly with frequency.

Special materials such as Hiperco 50 show saturation flux densities $B_s = 2.3–2.4$ T at $H_s < 10{,}000$ A/m, which allows for higher airgap flux density in IMs and, thus, lower weight designs (Tables 3.3 and 3.4).

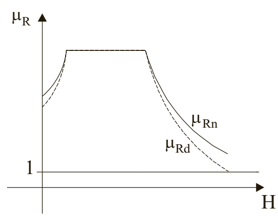


**FIGURE 3.3** Relative permeability versus H.

**TABLE 3.1**
**B–H Curve for Silicon (3.5%) Steel (0.5 mm thick) at 50 Hz**

| | | | | | | | | | | |
|---|---|---|---|---|---|---|---|---|---|---|
| B (T) | 0.05 | 0.1 | 0.15 | 0.2 | 0.25 | 0.3 | 0.35 | 0.4 | 0.45 | 0.5 |
| H (A/m) | 22.8 | 35 | 45 | 49 | 57 | 65 | 70 | 76 | 83 | 90 |
| B (T) | 0.55 | 0.6 | 0.65 | 0.7 | 0.75 | 0.8 | 0.85 | 0.9 | 0.95 | 1 |
| H (A/m) | 98 | 106 | 115 | 124 | 135 | 148 | 162 | 177 | 198 | 220 |
| B (T) | 1.05 | 1.1 | 1.15 | 1.2 | 1.25 | 1.3 | 1.35 | 1.4 | 1.45 | 1.5 |
| H (A/m) | 237 | 273 | 310 | 356 | 417 | 482 | 585 | 760 | 1050 | 1340 |
| B (T) | 1.55 | 1.6 | 1.65 | 1.7 | 1.75 | 1.8 | 1.85 | 1.9 | 1.95 | 2.0 |
| H (A/m) | 1760 | 2460 | 3460 | 4800 | 6160 | 8270 | 11,170 | 15,220 | 22,000 | 34,000 |

**TABLE 3.2**
**1Oe = 79.5 A/m**

| Induction | Typical D.C. and Derived A.C. Magnetising Force (Oe) of As-Sheared 29-Cage M19 Fully Processed Cold Rolled Nonoriented (CRNO) at Various Frequencies | | | | | | | | | | |
|---|---|---|---|---|---|---|---|---|---|---|---|
| **(kG)** | **D.C.** | **50 Hz** | **60 Hz** | **100 Hz** | **150 Hz** | **200 Hz** | **300 Hz** | **400 Hz** | **600 Hz** | **1000 Hz** | **1500 Hz** | **2000 Hz** |
| 1.0 | | 0.333 | 0.334 | 0.341 | 0.349 | 0.356 | 0.372 | 0.385 | 0.412 | 0.485 | 0.564 | 0.642 |
| 2.0 | 0.401 | 0.475 | 0.480 | 0.495 | 0.513 | 0.533 | 0.567 | 0.599 | 0.661 | 0.808 | 0.955 | 1.092 |
| 4.0 | 0.564 | 0.659 | 0.669 | 0.700 | 0.39 | 0.777 | 0.846 | 0.911 | 1.040 | 1.298 | 1.557 | 1.800 |
| 7.0 | 0.845 | 0.904 | 0.916 | 0.968 | 1.030 | 1.094 | 1.211 | 1.325 | 1.553 | 2.000 | 2.483 | 2.954 |
| 10.0 | 1.335 | 1.248 | 1.263 | 1.324 | 1.403 | 1.481 | 1.648 | 1.822 | 2.169 | 2.867 | 3.697 | 4.534 |
| 12.0 | 2.058 | 1.705 | 1.718 | 1.777 | 1.859 | 1.942 | 2.129 | 2.326 | 2.736 | 3.657 | 4.769 | 5.889 |
| 13.0 | 2.951 | 2.211 | 2.223 | 2.273 | 2.342 | 2.424 | 2.609 | 2.815 | 3.244 | 4.268 | 5.499 | |
| 14.0 | 5.470 | 3.508 | 3.510 | 3.571 | 3.633 | 3.691 | 3.855 | 4.132 | | | | |
| 15.0 | 13.928 | 8.276 | 8.313 | 8.366 | 8.366 | 8.478 | 8.651 | 9.737 | | | | |
| 15.5 | 22.784 | 13.615 | 13.587 | 13.754 | 13.725 | 13.776 | 14.102 | 16.496 | | | | |
| 16.0 | 35.201 | 21.589 | 21.715 | 21.800 | 21.842 | 21.884 | | | | | | |
| 16.5 | 50.940 | 32.383 | 32.506 | 32.629 | 32.547 | 32.588 | | | | | | |
| 17.0 | 70.260 | 46.115 | 46.234 | 46.392 | 46.644 | 46.630 | | | | | | |
| 18.0 | 122.01 | | | | | | | | | | | |
| 19.0 | 201.58 | | | | | | | | | | | |
| 20.0 | 393.50 | | | | | | | | | | | |
| 21.0 | 1111.84 | | | | | | | | | | | |

## 3.3 CORE (MAGNETIC) LOSSES

Energy loss in the magnetic material itself is a very significant characteristic in the energy efficiency of IMs. This loss is termed core loss or magnetic loss.

Traditionally, core loss has been divided into two components: hysteresis loss and eddy current loss. The hysteresis loss is equal to the product between the hysteresis loop area and the frequency of the magnetic field in sinusoidal systems.

$$P_h \approx k_h f B_m^2 \,[W/kg]; \quad B_m \text{ - maximum flux density} \tag{3.6}$$

Hysteresis losses are 10%–30% higher in travelling fields than in A.C. fields for $B_m < 1.5(1.6)$ T. However, in a travelling field, they have a maximum, in general, between 1.5 and 1.6 T and then decrease to low values for B > 2.0 T. The computation of hysteresis losses is still an open issue due to the hysteresis cycle's complex shape, its dependence on frequency and on the character of the magnetic field (travelling or A.C.) [2].

Preisach modelling of hysteresis cycle is very popular [3], but neural network models have proved much less computation time consuming [4].

Eddy current losses are caused by induced electric currents in the magnetic material by an external A.C. or travelling magnetic field.

**TABLE 3.3**
**Hiperco 50 Magnetisation Curve B/H – T/(A/m)**

| | | | | | | | | | | | | |
|---|---|---|---|---|---|---|---|---|---|---|---|---|
| B (T) | 0.017 | 0.7 | 1.5 | 1.9 | 2 | 2.1 | 2.15 | 2.2 | 2.25 | 2.267 | 2.275 | 2.283 |
| H (A/m) | 0 | 39.75 | 79.5 | 159 | 318 | 477 | 715.5 | 1431 | 3975 | 7950 | 11,925 | 15,900 |

**TABLE 3.4**
**Hiperco 50 Losses W/Kg**

| | | | | | | | | | | | |
|---|---|---|---|---|---|---|---|---|---|---|---|
| **f = 60 Hz** | | | | | | | | | | | |
| Core loss (W/Kg) | 0.8866 | 1.0087 | 1.2317 | 1.3946 | 1.5671 | 1.7589 | 1.9410 | 2.1614 | 2.4202 | 2.6215 | 2.8612 |
| B (T) | 1 | 1.1 | 1.2 | 1.3 | 1.4 | 1.5 | 1.6 | 1.7 | 1.8 | 1.9 | 2 |
| **f = 400 Hz** | | | | | | | | | | | |
| Core loss (W/Kg) | 8.5429 | 10.196 | 11.849 | 13.734 | 15.432 | 17.636 | 19.290 | 21.770 | 23.975 | 25.904 | 27.282 |
| B (T) | 1 | 1.1 | 1.2 | 1.3 | 1.4 | 1.5 | 1.6 | 1.7 | 1.8 | 1.9 | 2 |
| **f = 800 Hz** | | | | | | | | | | | |
| Core loss (W/Kg) | 23.589 | 27.282 | 31.416 | 35.274 | 40.786 | 45.072 | 51.768 | 58.137 | 65.485 | 72.671 | 76.917 |
| B (T) | 1 | 1.1 | 1.2 | 1.3 | 1.4 | 1.5 | 1.6 | 1.7 | 1.8 | 1.9 | 2 |
| **f = 1200 Hz** | | | | | | | | | | | |
| Core loss (W/Kg) | 40.738 | 47.242 | 58.659 | 65.745 | 77.162 | 84.642 | 92.909 | 104.32 | 113.38 | 128.34 | 135.43 |
| B (T) | 1 | 1.1 | 1.2 | 1.3 | 1.4 | 1.5 | 1.6 | 1.7 | 1.8 | 1.9 | 2 |

$$P_e \approx k_e f^2 B_m{}^2 \left[W/kg\right] \tag{3.7}$$

Finite elements are used to determine the magnetic distribution with zero electrical conductivity, and then the core losses may be calculated by some analytical approximations as (3.6) and (3.7) or [5]

$$P_{core} \approx k_h f B_m{}^{\alpha} K(B_m) + \frac{\sigma_{Fe}}{12}\frac{d^2 f}{\gamma_{Fe}} \int_{1/f} \left(\frac{dB}{dt}\right)^2 dt + K_{ex} f \int_{1/f} \left(\frac{dB}{dt}\right)^{1.5} \tag{3.8}$$

where $K = 1 + \frac{0.65}{B_m}\sum^{n} \Delta B_i$

- $B_m$ – maximum flux density
- f – frequency
- $\gamma_{Fe}$ – material density
- d – lamination thickness
- $K_h$ – hysteresis loss constant
- $K_{ex}$ – excess loss constant
- $\Delta B_i$ – change of flux density during a time step
- n – total number of time steps.

Equation (3.8) is a generalisation of Equations (3.6) and (3.7) for nonsinusoidal time-varying magnetic fields as produced in PWM inverter IM drives. Recently, better fits of power losses formula for cold-rolled motor laminations for a wide frequency and magnetisation range have been proposed [6].

For sinusoidal systems, the eddy currents in a thin lamination may be calculated rather easily by assuming the external magnetic field $H_0 e^{j\omega_1 t}$ acting parallel to the lamination plane (Figure 3.4).

Maxwell's equations yield

$$\begin{aligned} &\frac{\partial H_y}{\partial x} = J_z; \quad H_{0y} = H_0 e^{j\omega_1 t} \\ &-\frac{\partial E_z}{\partial x} = -j\omega_1 \mu \left(H_{0y} + H_y\right); \quad \sigma_{Fe} E_z = J_z \end{aligned} \tag{3.9}$$

where J is current density and E is electric field.

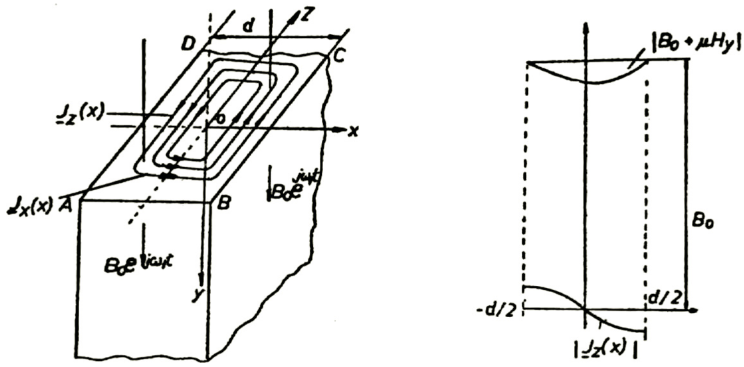


**FIGURE 3.4** Eddy current paths in a soft material lamination.

As the lamination thickness is small in comparison with its length and width, $J_x$ contribution is neglected. Consequently, (3.9) is reduced to

$$\frac{\partial^2 H_y}{\partial x^2} - j\omega_1 \mu \sigma_{Fe} H_y = j\omega_1 \sigma_{Fe} B_0 \tag{3.10}$$

$B_0 = \mu_0 H_0$ is the initial flux density on the lamination surface.

The solution of (3.10) is

$$H_y(x) = A_1 e^{\gamma x} + A_2 e^{-\gamma x} + \frac{B_0}{\mu_0} \tag{3.11}$$

$$\gamma = \beta(1 + j); \quad B = \sqrt{\frac{\omega_1 \mu \sigma_{Fe}}{2}} \tag{3.12}$$

The current density $J_z(x)$ is

$$J_z(x) = \frac{\partial H_y}{\partial x} = \gamma\left(A_1 e^{\gamma x} + A_2 e^{-\gamma x}\right) \tag{3.13}$$

The boundary conditions are

$$H_y\left(\frac{d}{2}\right) = H_y\left(-\frac{d}{2}\right) = 0 \tag{3.14}$$

Finally,

$$A_1 = A_2 = \frac{B_0}{2\mu \cosh\beta \frac{d}{2}(1 + j)} \tag{3.15}$$

$$J_z(x) = -\frac{\beta(1 + j)}{\mu} \frac{B_0 \sinh(1 + j)\beta x}{\cosh\beta \frac{d}{2}(1 + j)} \tag{3.16}$$

The eddy current loss per unit weight $P_e$ is

$$P_e = \frac{2\gamma_{Fe}}{d\sigma_{Fe}} \frac{1}{2} \int_0^{d/2} (J_z(x))^2 \, dx = \frac{\beta \gamma_{Fe} d\omega_1}{\mu} B_0^2 \left[\frac{\sinh(\beta d) - \sin(\beta d)}{\cosh(\beta d) + \cos(\beta d)}\right]\left[\frac{W}{kg}\right] \tag{3.17}$$

The iron permeability has been considered constant within the lamination thickness though the flux density slightly decreases.

For a good utilisation of the material, the flux density reduction along lamination thickness has to be small. In other words, $\beta d \ll 1$. In such conditions, the eddy current losses increase with the lamination thickness.

The electrical conductivity $\sigma_{Fe}$ is also influential, and silicon added to soft steel reduces $\sigma_{Fe}$ to $(2\text{–}2.5) \times 10^6\ (\Omega m)^{-1}$. This is why 0.5–0.6 mm thick laminations are used at 50(60) Hz and, in general, up to 200–300 Hz IMs.

For such laminations, eddy current losses may be approximated to

$$P_e \approx K_w B_m^{\ 2}\left[\frac{W}{kg}\right]; \quad K_w = \frac{\omega_1^{\ 2}\sigma_{Fe} d^2}{24}\gamma_{Fe} \tag{3.18}$$

The above loss formula derivation process is valid for A.C. magnetic field excitation. For pure travelling field, the eddy current losses are twice as much for same laminations, frequency, and peak flux density.

Given the complexity of eddy current and hysteresis losses, it is recommended that tests be run to measure them in conditions very similar to those encountered in the particular IM.

Soft magnetic material producers manufacture laminations for many purposes. They run their own tests and provide data on core losses for practical values of frequency and flux density.

Besides Epstein's traditional method, made with rectangular lamination samples, the wound toroidal cores method has also been introduced [7] for A.C. field losses. For travelling field loss measurement, a rotational loss tester may be used [8].

Typical core loss data for M15 – 3% silicon 0.5 mm thick lamination material – used in small IMs, is given in Figure 3.5a [9].

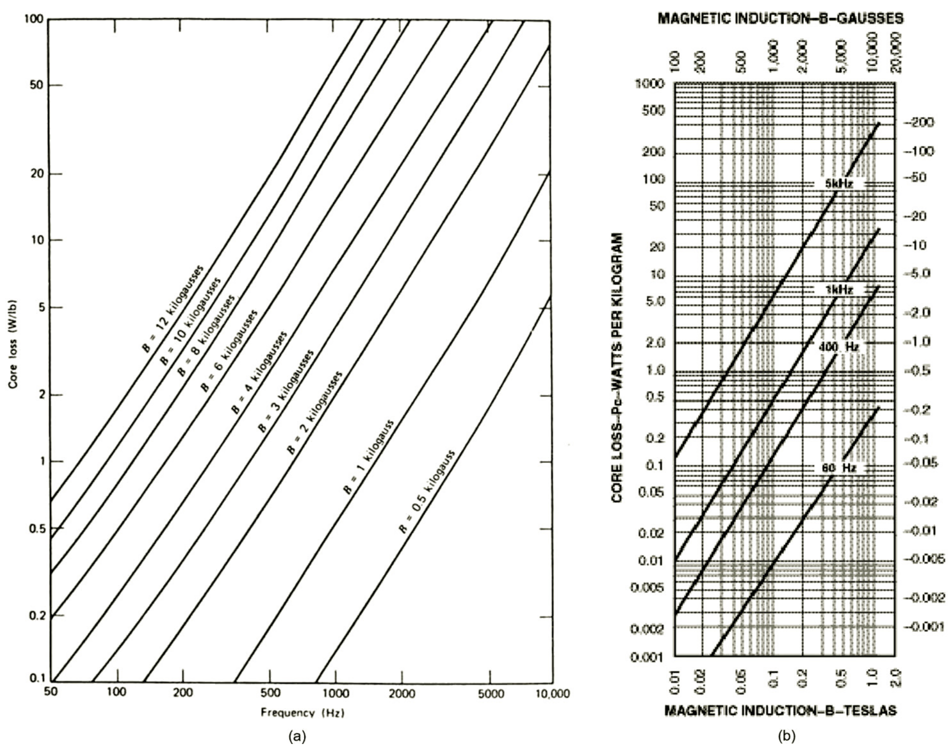


**FIGURE 3.5** Core losses for M15 – 3% silicon 0.5 mm thick laminations [9], (a) and 0.1 mm thick, 3% silicon Metglass (AMM) core losses, (b).

**TABLE 3.5**
**Typical Core Loss (W/lb) As-Sheared 29 Cage M19 Fully Processed CRNO at Various Frequencies [1]**

| Induction (kG) | 50 Hz | 60 Hz | 100 Hz | 150 Hz | 200 Hz | 300 Hz | 400 Hz | 600 Hz | 1000 Hz | 1500 Hz | 2000 Hz |
|---|---|---|---|---|---|---|---|---|---|---|---|
| 1.0 | 0.008 | 0.009 | 0.017 | 0.029 | 0.042 | 0.074 | 0.112 | 0.205 | 0.465 | 0.900 | 1.451 |
| 2.0 | 0.031 | 0.039 | 0.072 | 0.0119 | 0.173 | 0.300 | 0.451 | 0.812 | 1.786 | 3.370 | 5.318 |
| 4.0 | 0.109 | 0.134 | 0.252 | 0.424 | 0.621 | 1.085 | 1.635 | 2.960 | 6.340 | 11.834 | 18.523 |
| 7.0 | 0.273 | 0.340 | 0.647 | 1.106 | 1.640 | 2.920 | 4.450 | 8.180 | 17.753 | 33.720 | 53.971 |
| 10.0 | 0.494 | 0.617 | 1.182 | 2.040 | 3.060 | 5.530 | 8.590 | 16.180 | 36.303 | 71.529 | 116.702 |
| 12.0 | 0.687 | 0.858 | 1.648 | 2.860 | 4.290 | 7.830 | 12.203 | 23.500 | 54.258 | 108.995 | 179.321 |
| 13.0 | 0.812 | 1.014 | 1.942 | 3.360 | 5.060 | 9.230 | 14.409 | 27.810 | 65.100 | 131.98 | |
| 14.0 | 0.969 | 1.209 | 2.310 | 4.000 | 6.000 | 10.920 | 17.000 | | | | |
| 15.0 | 1.161 | 1.447 | 2.770 | 4.760 | 7.150 | 13.000 | 20.144 | | | | |
| 15.5 | 1.256 | 1.559 | 2.990 | 5.150 | 7.710 | 13.942 | 21.619 | | | | |
| 16.0 | 1.342 | 1.667 | 3.179 | 5.466 | 8.189 | | | | | | |
| 16.5 | 1.420 | 1.763 | 3.375 | 5.788 | 8.674 | | | | | | |
| 17.0 | 1.492 | 1.852 | 3.540 | 6.089 | 9.129 | | | | | | |

As expected, core losses increase with frequency and flux density. A similar situation occurs, with a superior but still common material: steel M19 FP (0.4 mm) 29 gauge (Table 3.5) [1].

A rather complete up-to-date data source on soft magnetic materials' characteristics and losses may be found in Ref. [1].

Core loss represents 25%–35% of all losses in low-power 50 (60) Hz IMs and slightly more in medium- and large-power IMs at 50(60) Hz. The development of high-speed IMs, up to more than 45,000 rpm at 20 kW [10], has caused a new momentum in the research for better magnetic materials as core losses are even larger than winding losses in such applications.

Thinner (0.35 mm or less) laminations of special materials (3.25% silicon) with special thermal treatment are used to strike a better compromise between low 60 Hz and moderate 800/1000 Hz core losses (1.2 W/kg at 60 Hz, 1 T; 28 W/kg at 800 Hz, 1 T).

6.5% silicon steel nonoriented steel laminations for low-power IMs at 60 Hz have shown capable of a 40% reduction in core losses [11]. The noise level has also been reduced this way [11]. Similar improvements have been reported with 0.35 mm thick oriented grain laminations by alternating laminations with perpendicular magnetisation orientation or crossed magnetic structure (CMS) [12].

**Recent Progress on Core Loss Assessment**

As the fundamental frequency in electric machine tends to increase (for high-speed variable speed drives) formulae as (3.8), with constant coefficients do not fit experimental results.

Also, high-temperature annealing core laminations have been proven to reduce the hysteresis losses but increase the eddy current losses.

Finally, the magnetic core properties degrade due to manufacturing process (punching, pressing, welding, packaging), and variability due to manufacturing has to be observed. To treat the above problems and thus provide reliable data on hysteresis cycle and losses and on eddy current losses, recent R & D effort concentrated on the following:

- Proving that the variation of hysteresis cycle with frequency is due to skin effect in the lamination especially when the frequency increases [13].
- Investigating experimentally, by a modified electromagnetic Halbach core test rig, the rotational core losses as they tend to have a maximum of around 1.5–1.6 T monotonously with flux density [14].

- Measuring the stator core loss degradation by the manufacturing process by a stator toroidal model that uses the stator core and investigates mainly the stator back core losses [15,16].

Soft magnetic composites (SMCs) have been produced by powder metallurgy technologies. The magnetic powder particles are coated by insulation layers and a binder which are compressed such that to provide

- Large enough magnetic permeability
- Low-enough core losses
- Densities above 7.1 g/cm$^3$ (for high-enough permeability).

The eddy current loss tends to be constant with frequency, while hysteresis loss increases almost linearly with frequency (up to 1 kHz or so).

At 400–500 Hz and above, the losses in SMC become smaller than for 0.5 mm thick silicon steels. However, the relative permeability is still low: 100–200. Only for recent materials, fabricated by cold compression, the relative permeability has been increased above 500 for flux densities in the 1 T range [17,18]. On the other hand, amorphous magnetic materials with plastic fill between magnetic particles, such as Metglass (Figure 3.5b), show not only lower losses at 300–500 Hz but also allow for higher flux densities.

Added advantages such as more freedom in choosing the stator core geometry and the increase of slot-filling factor by coil in slot magnetic compression-embedded windings [19] may lead to wide use of SMCs in induction motors. The electric loading may thus be increased. The heat transmissivity also increases [17].

In the near future, better silicon 0.5 mm (0.35 mm) thick steel laminations with nonoriented grain seem to remain the basic soft magnetic materials for IM fabrication. For high speed (frequency above 300 Hz), thinner laminations are to be used. The insulation coating layer of each lamination is getting thinner and thinner to retain a good stacking factor (above 85%).

## 3.4 ELECTRICAL CONDUCTORS

Electrical copper conductors are used to produce the stator three (two)-phase windings. The same is true for wound-rotor windings.

The electrical copper has a high purity and is fabricated by involved electrolysis process. The purity is well above 99%. The cross section of copper conductors (wires) to be introduced in stator slots is either circular or rectangular (Figure 3.6). The electrical resistivity of magnetic wire (electric conductor) $\rho_{Co} = (1.65–1.8) \times 10^{-8}\ \Omega m$ at 20°C and varies with temperature as

$$\rho_{Co}(T) = (\rho_{Co})_{20^\circ}\left[1 + (T - 20)/273\right] \tag{3.19}$$

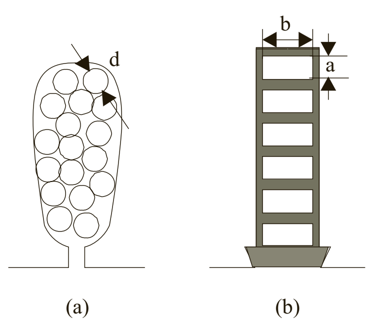


**FIGURE 3.6** Stator slot with round (a) and rectangular (b) conductors.

Round magnetic wires come into standardised gauges up to a bare copper diameter of about 2.5 mm (3 mm) (or 0.12 inch), in general (Tables 3.6 and 3.7).

The total cross section $A_{con}$ of the coil conductor depends on the rated phase current $I_{1n}$ and the design current density $J_{con}$:

$$A_{con} = I_{1n} / J_{con} \tag{3.20}$$

**TABLE 3.6**
**Round Magnetic Wire Gauges in Inches**

| | Bare Wire Diameter | Film Additions (inches) | | Overall Diameter (inches) | | | Weight at 20°C–68°F | | Resistance at 20°C–68°F | | | |
|---|---|---|---|---|---|---|---|---|---|---|---|---|
| Awg Size | Nominal (inches) | Min. | Max. | Min. | Nom. | Max. | Lbs./M Ft. Nom. | Ft./Lb. Nom. | Ohms./M Ft. Nom. | Ohms./ Lb. Nom. | Wires/ In. Nom. | Awg Size |
| 8 | 0.1285 | 0.0016 | 0.0026 | 0.1288 | 0.1306 | 0.1324 | 50.20 | 19.92 | 0.6281 | 0.01251 | 7.66 | 8 |
| 9 | 0.1144 | 0.0016 | 0.0026 | 0.1149 | 0.1165 | 0.1181 | 39.81 | 25.12 | 0.7925 | 0.01991 | 8.58 | 9 |
| 10 | 0.1019 | 0.0015 | 0.0025 | 0.1024 | 0.1039 | 0.1054 | 31.59 | 31.66 | 0.9988 | 0.03162 | 9.62 | 10 |
| 11 | 0.0907 | 0.0015 | 0.0025 | 0.0913 | 0.0927 | 0.0941 | 25.04 | 39.94 | 1.26 | 0.05032 | 10.8 | 11 |
| 12 | 0.0808 | 0.0014 | 0.0024 | 0.0814 | 0.0827 | 0.0840 | 19.92 | 50.20 | 1.59 | 0.07982 | 12.1 | 12 |
| 13 | 0.0720 | 0.0014 | 0.0023 | 0.0727 | 0.0738 | 0.0750 | 15.81 | 63.25 | 2.00 | 0.1265 | 13.5 | 13 |
| 14 | 0.0641 | 0.0014 | 0.0023 | 0.0649 | 0.0659 | 0.0659 | 12.49 | 80.06 | 2.52 | 0.2018 | 15.2 | 14 |
| 15 | 0.0571 | 0.0013 | 0.0022 | 0.0578 | 0.0588 | 0.0599 | 9.948 | 100.5 | 3.18 | 0.3196 | 17.0 | 15 |
| 16 | 0.0508 | 0.0012 | 0.0021 | 0.0515 | 0.0525 | 0.0534 | 7.880 | 126.9 | 4.02 | 0.5101 | 19.0 | 16 |
| 17 | 0.0453 | 0.0012 | 0.0020 | 0.0460 | 0.0469 | 0.0478 | 6.269 | 159.5 | 5.05 | 0.8055 | 21.3 | 17 |
| 18 | 0.0403 | 0.0011 | 0.0019 | 0.0410 | 0.0418 | 0.0426 | 4.970 | 201.2 | 6.39 | 1.286 | 23.9 | 18 |
| 19 | 0.0359 | 0.0011 | 0.0019 | 0.0366 | 0.0374 | 0.0382 | 3.943 | 253.6 | 8.05 | 2.041 | 26.7 | 19 |
| 20 | 0.0320 | 0.0010 | 0.0018 | 0.0327 | 0.0334 | 0.0341 | 3.138 | 318.7 | 10.1 | 3.219 | 29.9 | 20 |
| 21 | 0.0285 | 0.0010 | 0.0018 | 0.0292 | 0.0299 | 0.0306 | 2.492 | 401.2 | 12.8 | 5.135 | 33.4 | 21 |
| 22 | 0.0253 | 0.0010 | 0.0017 | 0.0260 | 0.0267 | 0.0273 | 1.969 | 507.9 | 16.2 | 8.228 | 37.5 | 22 |
| 23 | 0.0226 | 0.0009 | 0.0016 | 0.0233 | 0.0238 | 0.0244 | 1.572 | 636.1 | 20.3 | 12.91 | 42.0 | 23 |
| 24 | 0.0201 | 0.0009 | 0.0015 | 0.0208 | 0.0213 | 0.0218 | 1.240 | 806.5 | 25.7 | 20.73 | 46.9 | 24 |
| 25 | 0.0179 | 0.0009 | 0.0014 | 0.0186 | 0.0191 | 0.0195 | 988 | 1012 | 32.4 | 32.79 | 52.4 | 25 |
| 26 | 0.0159 | 0.0008 | 0.0013 | 0.0165 | 0.0169 | 0.0174 | 779 | 1284 | 41.0 | 52.64 | 59.2 | 26 |
| 27 | 0.0142 | 0.0008 | 0.0013 | 0.0149 | 0.0153 | 0.0156 | 0.623 | 1605 | 51.4 | 82.50 | 65.4 | 27 |
| 28 | 0.0126 | 0.0007 | 0.0012 | 0.0132 | 0.0136 | 0.0139 | 0.491 | 2037 | 65.3 | 133.0 | 73.5 | 28 |
| 29 | 0.0113 | 0.0007 | 0.0012 | 0.0119 | 0.0122 | 0.0126 | 0.395 | 2532 | 81.2 | 205.6 | 82.0 | 29 |
| 30 | 0.0100 | 0.0006 | 0.0011 | 0.0105 | 0.0109 | 0.112 | 0.310 | 3226 | 104 | 335.5 | 91.7 | 30 |
| 31 | 0.0089 | 0.0006 | 0.0011 | 0.0094 | 0.0097 | 0.0100 | 0.246 | 4065 | 131 | 532.5 | 103 | 31 |
| 32 | 0.0080 | 0.0006 | 0.0010 | 0.0085 | 0.0088 | 0.0091 | 0.199 | 5025 | 162 | 814.1 | 114 | 32 |
| 33 | 0.0071 | 0.0005 | 0.0009 | 0.0075 | 0.0078 | 0.0081 | 0.157 | 6394 | 206 | 1317 | 128 | 33 |
| 34 | 0.0063 | 0.0005 | 0.0008 | 0.0067 | 0.0070 | 0.0072 | 0.123 | 8130 | 261 | 2122 | 143 | 34 |
| 35 | 0.0056 | 0.0004 | 0.0007 | 0.0059 | 0.0062 | 0.0064 | 0.0977 | 10,235 | 331 | 3388 | 161 | 35 |
| 36 | 0.0050 | 0.0004 | 0.0007 | 0.0053 | 0.0056 | 0.0058 | 0.0783 | 12,771 | 415 | 5300 | 179 | 36 |
| 37 | 0.0045 | 0.0003 | 0.0006 | 0.0047 | 0.0050 | 0.0052 | 0.0632 | 15,823 | 512 | 8101 | 200 | 37 |
| 38 | 0.0040 | 0.0003 | 0.0006 | 0.0042 | 0.0045 | 0.0047 | 0.0501 | 19,960 | 648 | 12,934 | 222 | 38 |
| 39 | 0.0035 | 0.0002 | 0.0005 | 0.0036 | 0.0039 | 0.0041 | 0.0383 | 26,110 | 847 | 22,115 | 256 | 39 |
| 40 | 0.0031 | 0.0002 | 0.0005 | 0.0032 | 0.0035 | 0.0037 | 0.0301 | 33,222 | 1080 | 35,880 | 286 | 40 |
| 41 | 0.0028 | 0.0002 | 0.0004 | 0.0029 | 0.0031 | 0.0033 | 0.0244 | 40,984 | 1320 | 54,099 | 323 | 41 |
| 42 | 0.0025 | 0.0002 | 0.0004 | 0.0026 | 0.0028 | 0.0030 | 0.0195 | 51,282 | 1660 | 85,128 | 357 | 42 |
| 43 | 0.0022 | 0.0002 | 0.0003 | 0.0023 | 0.0025 | 0.0026 | 0.0153 | 65,360 | 2140 | 139,870 | 400 | 43 |
| 44 | 0.0020 | 0.0001 | 0.0003 | 0.0020 | 0.0022 | 0.0024 | 0.0124 | 80,645 | 2590 | 208,870 | 455 | 44 |

**TABLE 3.7**
**Typical Round Magnetic Wire Gauges in mm**

| Rated Diameter (mm) | Insulated Wire Diameter (mm) | Rated Diameter (mm) | Insulated Wire Diameter (mm) |
|---|---|---|---|
| 0.3 | 0.327 | 0.75 | 0.7949 |
| 0.32 | 0.348 | 0.80 | 0.8455 |
| 0.33 | 0.359 | 0.85 | 0.897 |
| 0.35 | 0.3795 | 0.90 | 0.948 |
| 0.38 | 0.4105 | 0.95 | 1.0 |
| 0.40 | 0.4315 | 1.00 | 1.051 |
| 0.42 | 0.4625 | 1.05 | 1.102 |
| 0.45 | 0.4835 | 1.10 | 1.153 |
| 0.48 | 0.515 | 1.12 | 1.173 |
| 0.50 | 0.536 | 1.15 | 1.2035 |
| 0.53 | 0.567 | 1.18 | 1.2345 |
| 0.55 | 0.5875 | 1.20 | 1.305 |
| 0.58 | 0.6185 | 1.25 | 1.325 |
| 0.60 | 0.639 | 1.30 | 1.356 |
| 0.63 | 0.6705 | 1.32 | 1.3765 |
| 0.65 | 0.691 | 1.35 | 1.407 |
| 0.67 | 0.7145 | 1.40 | 1.4575 |
| 0.70 | 0.742 | 1.45 | 1.508 |
| 0.71 | 0.7525 | 1.50 | 1.559 |

The design current density varies between 3.5 and 15 A/mm$^2$ depending on the cooling system, service duty cycle, and the targeted efficiency of the IM. High-efficiency IMs are characterised by lower current density (3.5–6 A/mm$^2$). If the $A_{con}$ in (3.19) is larger than the cross section of the largest round wire gauge available, a few conductors of lower diameter are connected in parallel and wound together. Up to 6–8 elementary conductors may be connected together.

If $A_{con}$ is larger than 30–40 mm$^2$ (that is, 6–8, 2.5 mm diameter wires in parallel), rectangular conductors are recommended.

In many countries, rectangular conductor cross sections are also standardised. In some cases, small cross sections such as (0.8–2)·2 mm × mm or (0.8–6) × 6 mm × mm are used for rectangular conductors.

In general, the rectangular conductor height a is kept low (a < 3.55 mm) to reduce the skin effect; that is, to keep the A.C. resistance low. A large cross-section area of 3.55 × 50 mm × mm would be typical for large-power IMs.

The rotor cage is in general made of aluminium: die-casted aluminium in low-power IMs (up to 300 kW or so) or of aluminium bars attached through brazing or welding processes to end rings.

Fabricated rotor cages are made of aluminium or copper alloys and of brass (the upper cage of a double cage) for powers above 300 kW, in general. The casting process of aluminium uses the rotor lamination stack as a partial mould because the melting point of silicon steel is much higher than that of aluminium. The electrical resistivity of aluminium $\rho_{Al} \cong (2.7\text{–}3.0) \times 10^{-8}$ Ωm and varies with temperature as shown in (3.19).

Though the rotor cage bars are in general uninsulated from the magnetic core, most of the current flow through the cage bars as their resistivity is more than 20–30 times smaller than that of the laminated core.

Insulated cage bars would be ideal, but this would severely limit the rotor temperature unless a special high-temperature (high-cost) insulation coating is used.

## 3.5 INSULATION MATERIALS

The primary purpose of stator insulation is to withstand turn-to-turn, phase-to-phase, and phase-to-ground voltage such that to direct the stator phase currents through the desired paths of stator windings.

Insulation serves a similar purpose in phase-wound rotors whose phase leads are connected to insulated copper rings and then through brushes to stationary devices (resistances or/and special power electronic converters). Insulation is required to withstand voltages associated to: brush rigging (if any), winding connections, winding leads, auxiliaries such as temperature probes, and bearings (especially for PWM inverter drives).

The stator laminations are insulated from each other by special coatings (0.013 mm thick) to reduce eddy current core losses.

In standard IMs, the rotor (slip) frequency is rather small, and thus, inter-lamination insulation may not be necessary, unless the IM is to work for prolonged intervals at large slip values.

For all wound-rotor motors, the rotor laminations are insulated from each other. The bearing sitting is insulated from the stator to reduce the bearing (shaft) voltage (current), especially for large-power IMs whose stator laminations are made of a few segments, thus allowing a notable A.C. axial flux linkage. This way, premature bearing damage may be prevented and even more so in PWM inverter-fed IMs, where additional common voltage mode superhigh frequency capacitor currents through the bearings occur.

Stator winding insulation systems may be divided into two types, related to power and voltage levels.

- Random-wound conductor IMs with small and round conductors
- Form-wound conductor IMs with relatively large area rectangular conductors.

Insulation systems for IMs are characterised by voltage and temperature requirements. The IM insulation has to withstand the expected operating voltages between conductors, conductors (phase) and ground, and phase to phase.

The American National Standards Institute (ANSI) specifies that the insulation test voltage shall be twice the rated voltage plus 1000 V applied to the stator winding for 1 minute.

The heat produced by the winding currents and the core losses causes hot-spot temperatures that have to be limited in accordance with the thermal capability of the organic (resin) insulation used in the machine and to its chemical stability and capability to prevent conductor-to-conductor and conductor-to-ground short-circuits during IM operation.

There is continuous, but slow deterioration of the organic (resin) insulation by internal chemical reaction, contamination, and chemical interactions. Thermal degradation develops cracks in the enamel, varnish, or resin, reducing the dielectric strength of insulation.

Insulation materials for electric machines have been organised in stable temperature classes at which they can perform satisfactorily for the expected service lifetime.

The temperature classes are (again):

| | |
|---|---|
| class A: 105°C | class F: 155°C |
| class B: 130°C | class G: 180°C |

The main insulation components for the random-wound coil windings are the enamel insulation on the wire, the insulation between coils and ground/slot walls, and slot liner insulation and between phases (Figure 3.7).

The connections between the coils of a phase and the leads to terminal box have to be insulated. Also, the binding cord used to tie down end windings to reduce their vibration is made of insulation materials.

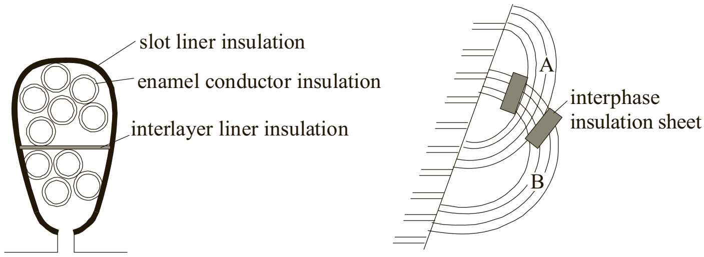


**FIGURE 3.7** Random-wound coils insulation.

Random-wound IMs are built for voltages below 1 kV. The moderate currents involved can be handled by wound conductors (eventually a few in parallel) where enamel insulation is the critical component. To apply the enamel, the wire is passed through a solution of polymerisable resin and into the high-curing temperature tower where it turns into a thin, solid, and flexible coating.

### 3.5.1 Random-Wound IM Insulation

Several passes are required for the desired thickness (0.025 mm thick or so). There are dedicated standards that mention the tests on enamel conductors (ASTMD-1676); American Society for Testing and Materials (ASTM) standards part 39 for electric insulation test methods: solids and solidifying liquids should be considered for the scope.

Enamel wire, stretched and scraped when the coils are introduced in slots, should survive this operation without notable damage to the enamel. Some insulation varnish is applied over the enamel wire after the stator winding is completed. The varnish provides additional enamel protection against moisture, dirt, and chemical contamination and also provides mechanical support for the windings.

Slot and phase-to-phase insulation for class A temperatures is a somewhat flexible sheet material (such as cellulose paper), 0.125–0.25 mm thick, or a polyester film. In some cases, fused resin coatings are applied to stator slot walls by electrostatic attraction of polymerisable resin powder. The stator is heated to fuse and cure the resin to a smooth coating.

For high-temperature IMs (class F, H), glass cloth mica paper or asbestos treated with special varnishes are used for slot and phase-to-phase insulation. Varnishes may interact with the enamel to reduce thermal stability. Enamels and varnishes are tested separately according to ASTM (D2307, D1973, and D3145) or International Electrotechnical Commission (IEC) standards.

Model motor insulation systems (motorettes) are tested according to Institute of Electrical and Electronics Engineers (IEEE) standards for small motors.

All these insulation-accelerated life tests involve the ageing of insulation test specimens until they fail at temperatures higher than the operating temperature of the respective motor. The logarithms of the accelerated ageing times are then graphed against their reciprocal Kelvin test temperatures (Arrhenius graph). The graph is then extrapolated to the planed (reduced) temperature to predict the actual lifetime of insulation.

### 3.5.2 Form-Wound Windings

Form-wound windings are employed in high-power IMs. The slots are rectangular and so are the conductors. The slot filling factor increases due to this combination.

The insulation of the coil conductors (turns) is applied before inserting the coils in slots. The coils are also vacuum impregnated outside the machine. The slot insulation is made of resin-bonded mica applied as a wrapper or tape with a fibrous sheet for support (in high-voltage IMs above 1–2 kV).

Vacuum impregnation is done with polymerisable resins which are then cured to solids by heating. During the cure, the conductors may be constraint to size to enter the slot as the epoxy-type resins are sufficiently elastic for the scope.

Voltage, through partial discharges, may cause insulation failure in higher voltage IMs. Incorporating mica in the major insulation schemes solves this problem to a large degree.

A conducting paint may be applied over the slot portion of the coils to fill the space between the insulated preformed coil and slot wall, to avoid partial discharges. Lower and medium voltage coil insulation is measured in accelerated higher temperature tests (IEEE standard 275) by using the model system called formette. Formette testing is similar to motorette testing for random-wound IMs [20].

Diagnostic non-destructive tests to check the integrity and capability of large IM insulation are also standardised [20–23].

## 3.6 SUMMARY

- The three main materials used to build IMs are of magnetic, electric, and insulation type.
- As IM is an A.C. machine, reducing eddy current losses in its magnetic core is paramount.
- It is shown that these losses increase with the soft magnetic sheet thickness parallel to the external A.C. field.
- Soft magnetic materials (silicon steel) used in thin laminations (0.5 mm thick up to 200 Hz) have low hysteresis and eddy current losses (about or less 2 W/kg at 1 T and 60 Hz).
- Besides losses, the B–H (magnetisation) curve characterises a soft magnetic material [13].
- The magnetic permeability $\mu = B/H$ varies from (5000–8000) $\mu_0$ at 1 T to (40–60) $\mu_0$ at 2.0 T in modern silicon steel laminations. High permeability is essential to low magnetisation (no load) current and losses.
- High-speed IMs require frequencies above 300 Hz (and up to 800 Hz and more). Thinner silicon lamination steels with special thermal treatments are required to secure core losses in the order of 30–50 W/kg at 800 Hz and 1 T.
- 6.5% silicon steel lamination for small IMs have been proved adequate to reduce core losses by as much as 40% at 50 (60) Hz.
- Also, interspersing oriented grain (transformer) laminations (0.35 mm thick) with orthogonal orientation laminations has been shown to produce a 30%–40% reduction in core losses at 50 (60) Hz and 1 T in comparison with 0.5 mm thick nonoriented grain silicon steel used in most IMs.
- SMCs have been introduced and shown to produce lower losses than silicon steel laminations only above 300 Hz but at the expense of lower permeability ((100–200) $\mu_0$ in general). Cold compression methods are expected to increase slot filling factor notably and thus increase the current loading. Size reduction is obtained also due to the increase of heat transmissivity through SMCs. Amorphous magnetic materials (Metglass) have been recently introduced for lower losses and high permeability (0.1 mm thick), 400 Hz, 1.6 T: 50% of core losses of silicon steel at 0.1 mm thickness.
- Electric conductors for stator windings and wound rotors are made of pure (electrical) copper.
- Cast aluminium is used for rotor cage windings up to 300 kW.
- Fabricated aluminium or copper bars and rings are used for higher power IM cage rotors. Die-cast methods for copper cage have been proposed recently [24]. Lightly ferromagnetic aluminium rotor bars have also been proposed to increase starting torque at lower starting current, while preserving rated speed performance [25].
- The rotor cage bars are not, in general, insulated from the rotor lamination core. Interbar currents may thus occur.
- The windings are made out of random-wound coils with round wire and form-wound coils for large IMs with rectangular wire.

- The windings are insulated from the magnetic core through insulation materials. Also, the conductors are enamelled to insulate one conductor from another.
- Insulation systems are classified according to temperature limits in four classes: Class A-105°C, Class B-130°C, Class F-155°C, and Class G-180°C.
- Insulation testing is thoroughly standardised as the insulation breakdown diminishes the operation life of an IM through short-circuit.
- Thinner and better insulation materials keep "surfacing" as they are crucial to better performance IMs fed from the power grid and PWM inverters.
- Better finite element (FE) and analytical methods and test procedures to appraise existing and novel materials for IMs are being proposed.

## REFERENCES


1. S. Sprague, D. Jones, Using the new lamination steels database in motor design, *Proceedings of SMMA-2000 Fall Conference in Chicago*, pp. 1–12.
2. M. Birkfeld, K. A. Hempel, Calculation of the magnetic behaviour of electrical steel sheet under two dimensional excitation by means of the reluctance tensor, *IEEE Transactions on Magnetics*, Vol. MAG-33, No. 5, 1997, pp. 3757–3759.
3. I. D. Mayergoyz, *Mathematical Models for Hysteresis*, Springer Verlag, New York, 1991.
4. H. H. Saliah, D. A. Lowther, B. Forghani, A neural network model of magnetic hysteresis for computational magnetics, *IEEE Transactions on Magnetics*, Vol. MAG-33, No. 5, 1997, pp. 4146–4148.
5. M. A. Mueller et al., Calculation of iron losses from time – Stepped finite element models of cage induction machines, *Seventh International Conference on EMD*, IEE Conference Publication No. 412, Durham, UK.
6. M. Popescu, D. M. Ionel, A best-fit model of power losses in cold rolled motor lamination steel operating in a wide range of frequency and magnetisation, *IEEE Transactions on Magnetics*, Vol. MAG-43, No. 4, 2007, pp. 1753–1756.
7. A. J. Moses, N. Tutkun, Investigation of power losses in wound toroidal cores under PWM excitation, *IEEE Transactions on Magnetics*, Vol. MAG-33, No. 5, 1997, pp. 3763–3765.
8. M. Enokizono, T. Tanabe, Studies on a new simplified rotational loss tester, *IEEE Transactions on Magnetics*, Vol. 33, No. 5, 1997, pp. 4020–4022.
9. S. A. Nasar, *Handbook of Electrical Machines*, Chapter 2, p. 211, McGraw Hill Inc., New York, 1987.
10. W. L. Soong, G. B. Kliman, R. N. Johnson, R. White, J. Miller, Novel high speed induction motor for a commercial centrifugal compressor, *IEEE Transactions on Industry Applications*, Vol. IA-36, No. 3, 2000, pp. 706–713.
11. M. Machizuki, S. Hibino, F. Ishibashi, Application of 6.5% silicon steel sheet to induction motor and to magnetic properties, *EMPS*, Vol. 22, No. 1, 1994, pp. 17–29.
12. A. Boglietti, P. Ferraris, M. Lazzari, F. Profumo, Preliminary consideration about the adoption of unconventional magnetic materials and structures for motors, *IBID*, Vol. 21, No. 4, 1993, pp. 427–436.
13. M. Ibrahim, P. Pillay, Advanced testing and modelling of magnetic materials including a new method of core loss separation for electrical machines, *IEEE Transactions on Industry Applications*, Vol. IA-48, no. 5, 2012, pp. 1507–1515.
14. N. Alatawneh, P. Pillay, Design of a novel test fixture to measure rotational core losses in machine laminations, *IEEE Transactions on Industry Applications*, Vol. IA-48, no. 5, 2012, pp. 1467–1477.
15. A. J. Clerc, A. Muetze, Measurement of stator core magnetic degradation during the manufacturing process, *IEEE Transactions on Industry Applications*, Vol. IA-48, no. 4, 2012, pp. 1344–1352.
16. M. Enokizono, S. Takahashi, A. Ikariga, A measurement system for two-dimensional D.C. biased magnetic property, *KIEE Transactions on ENECS*, Vol. 2-B, No. 4, 2002, pp. 143–148.
17. D. Gay, Composite iron powder for A.C. electromagnetic applications: History and use, *Record of SMMA-2000 Fall Conference*, Chicago, Oct. 4–6, 2000.
18. M. Persson, P. Jansson, A. G. Jack, B. C. Mecrow, Soft magnetic materials–Use for electric machines, *IEEE 7th International Conference on EMD*, 1995, pp. 242–246.
19. E. A. Knoth, Motors for the 21st century, *Record of SMMA-2000 Fall Conference Chicago*, Oct. 4–6, 2000.
20. T. W. Dakin, Electric machine insulations, Chapter 13 in *Electric Machine Handbook*, Edited by S.A. Nasar, McGraw-Hill, New York, 1987.

21. P. L. Cochran, *Polyphase Induction Motors*, CRC Press, Boca Raton, FL, 1989, Chapter 11.
22. R. M. Engelmann, W. H. Middendorf (Eds.), *Handbook of Electric Machines*, Marcel Dekker Inc., New York, 1995.
23. R. Morin, R. Bartnikas, P. Menard, A three phase multistress accelerated electrical aging test facility for stator bars, *IEEE Transactions on Energy Conversion*, Vol. EC-15, No. 2, 2000, pp. 149–156.
24. R. Kimmich, M. Doppelbauer, D. T. Pefers, J. G. Cowie, E. F. Bruvn Jr., Die cast copper rotor motors via simple substitution and motor redesign for copper, *Record of ICEM-2006*, Ref. No. 358.
25. M. R. Khan, M. F. Momen, Lightly ferromagnetic rotor bars for three phase squirrel-cage induction machines, *IEEE Transactions on Industry Applications*, Vol. IA-40, No. 6, 2004, pp. 1536–1540.

# 4 Induction Machine Windings and Their mmfs

## 4.1 INTRODUCTION

As shown in Chapter 2, the slots of the stator and rotor cores of induction machines (IMs) are filled with electric conductors, insulated (in the stator) from cores, and connected in a certain way. This ensemble constitutes the windings. The primary (or the stator) slots contain a polyphase (three- or two-phase) A.C. winding. The rotor may have either a three- or two-phase winding or a squirrel cage. Here we will discuss the polyphase windings.

Designing A.C. windings means, in fact, assigning coils in the slots to various phases, establishing the direction of currents in coil sides and coil connections per phase and between phases, and finally calculating the number of turns for various coils and the conductor sizing.

We start with single pole number three-phase windings as they are most commonly used in induction motors. Then pole-changing windings are also treated in some detail. Such windings are used in wind generators or in doubly fed variable speed configurations. Two-phase windings are given then special attention. Finally, squirrel cage winding magnetomotive forces (mmfs) are analysed.

Keeping in mind that A.C. windings are a complex subject having books dedicated to it [1,2], we will treat here first its basics. Then we introduce new topics such as "pole amplitude modulation", "polyphase symmetrisation" [3,4], "intersperse windings" [5], "simulated annealing" [6], and "the three equation principle" [7] for pole changing. These are new ways to produce A.C. windings for special applications (for pole changing or mmf chosen harmonics elimination). Finally, fractional multilayer three-phase windings with reduced harmonics content are treated in some detail [8,9]. The present chapter is structured to cover both the theory and case studies of A.C. winding design, classifications, and mmf harmonic analysis.

## 4.2 THE IDEAL TRAVELLING MMF OF A.C. WINDINGS

The primary (A.C. fed) winding is formed by interconnecting various conductors in slots around the circumferential periphery of the machine. As shown in Chapter 2, we may have a polyphase winding on the so-called wound rotor. Otherwise the rotor may have a squirrel cage in its slots. The objective with polyphase A.C. windings is to produce a pure travelling mmf, through proper feeding of various phases with sinusoidal symmetrical currents. And all this mmf ($F_{s1}$ (x, t)) in order to produce constant (rippleless) torque under steady state is

$$F_{s1}(x,t) = F_{s1m}\cos\left(\frac{\pi}{\tau}x - \omega_1 t - \theta_0\right) \tag{4.1}$$

where

- x – coordinate along stator bore periphery
- $\tau$ – spatial half period of mmf ideal wave
- $\omega_1$ – angular frequency of phase currents
- $\theta_0$ – angular position at t = 0

We may decompose (4.1) into two terms

$$F_{s1}(x,t) = F_{s1m}\left[\cos\left(\frac{\pi}{\tau}x - \theta_0\right)\cos\omega_1 t + \sin\left(\frac{\pi}{\tau}x - \theta_0\right)\sin\omega_1 t\right] \tag{4.2}$$

Equation (4.2) has a special physical meaning. In essence, there are now two mmfs at standstill (fixed) with sinusoidal spatial distribution and sinusoidal currents. The space angle lag and the time angle between the two mmfs is π/2. This suggests that a pure travelling mmf may be produced with two symmetrical windings π/2 shifted in time (Figure 4.1a). This is how the two-phase IM evolved.

Similarly, we may decompose (4.1) into three terms

$$F_{s1}(x,t) = \frac{2}{3}F_{s1m}\left[\cos\left(\frac{\pi}{\tau}x - \theta_0\right)\cos\omega_1 t + \cos\left(\frac{\pi}{\tau}x - \theta_0 - \frac{2\pi}{3}\right)\cos\left(\omega_1 t - \frac{2\pi}{3}\right)\right.$$
$$\left. + \cos\left(\frac{\pi}{\tau}x - \theta_0 + \frac{2\pi}{3}\right)\cos\left(\omega_1 t + \frac{2\pi}{3}\right)\right] \tag{4.3}$$

Consequently, three mmfs (single-phase windings) at standstill (fixed) with sinusoidal spatial (x) distribution and departured in space by 2π/m radians, with sinusoidal symmetrical currents – equal amplitude, 2π/3 radians time lag angle – are also able to produce a travelling mmf (Figure 4.1b).

In general, m phases with a phase lag (in time and space) of 2π/m can produce a travelling wave. Six phases (m = 6) would be a rather practical case besides m = 3 phases. Recently, five and seven phases have been introduced for fault-tolerant IM drives. The number of mmf electrical periods per one revolution is called the number of pole pairs $p_1$.

$$p_1 = \frac{\pi D}{2\tau}; \quad 2p_1 = 2,4,6,8,... \tag{4.4}$$

where D is the stator bore diameter.

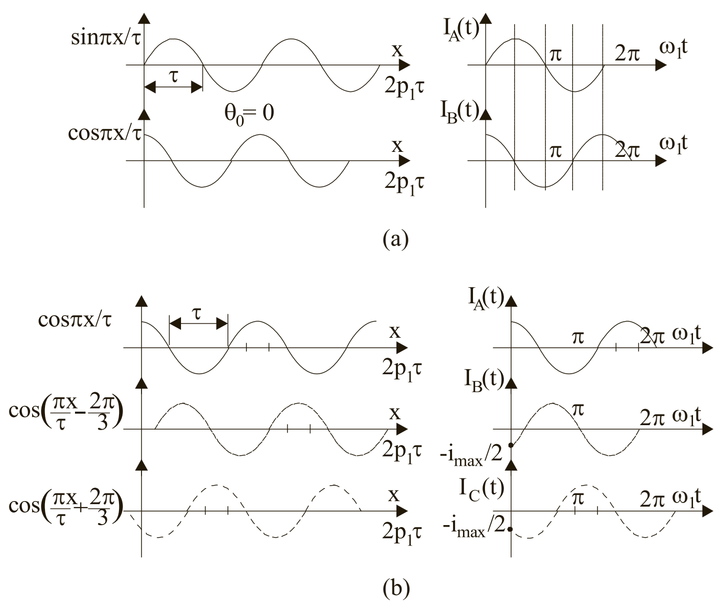


**FIGURE 4.1** Ideal multiphase mmfs: (a) two-phase and (b) three-phase machines.

It should be noted that, for $p_1 > 1$, according to (4.4), the electrical angle $\alpha_e$ is $p_1$ times larger than the mechanical angle $\alpha_g$

$$\alpha_e = p_1\alpha_g \tag{4.5}$$

A sinusoidal distribution of mmfs (ampere-turns) would be feasible only with the slotless machine and windings placed in the airgap. Such a solution is hardly practical for IMs because the magnetisation of a large total airgap would mean very large magnetisation mmf and, consequently, low power factor and efficiency. It would also mean problems with severe mechanical stress acting directly on the electrical conductors of the windings.

In practical IMs, the coils of the windings are always placed in slots of various shapes (Chapter 2).

The total number of slots per stator $N_s$ should be divisible to the number of phases m so that

$$N_s/m = \text{integer} \tag{4.6}$$

A parameter of great importance is the number of slots per pole per phase q:

$$q = \frac{N_s}{2p_1m} \tag{4.7}$$

The number of slots/pole/phase q may be an integer (q = 1, 2, …12) or fraction.

In most IMs, q is an integer to provide complete (pole to pole) symmetry for the winding.

The windings are made of coils. Lap and wave coils are used for IMs (Figure 4.2).

The coils may be placed in slots in one (Figure 4.3a) or two layers (Figure 4.3b).

Single-layer windings imply full pitch ($y = \tau$) coils to produce an mmf fundamental with pole pitch $\tau$.

Double-layer windings also allow chorded (or fractional pitch) coils ($y < \tau$) such that the end connections of coils are shortened, and thus, copper loss is reduced. Moreover, as shown later in this chapter, the space harmonics content of mmf may be reduced by chorded coils. Unfortunately, so is the fundamental mmf.

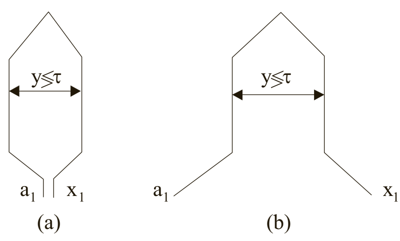


**FIGURE 4.2** Lap (a) and wave (b) single turn (bar) coils.

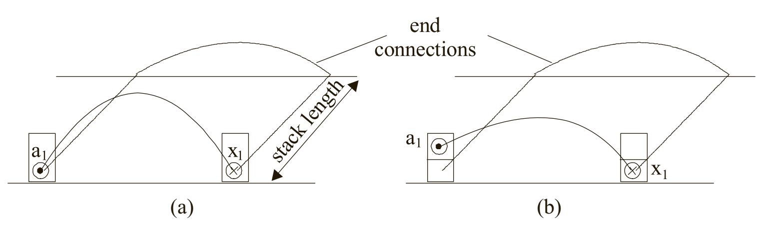


**FIGURE 4.3** Single-layer (a) and double-layer (b) coils (windings).

## 4.3 A PRIMITIVE SINGLE-LAYER WINDING

Let us design a four-pole ($2p_1 = 4$) three-phase single-layer winding with q = 1 slots/pole/phase. $N_s = 2p_1qm = 2{\cdot}2{\cdot}1{\cdot}3 = 12$ slots in all.

From the previous paragraph, we infer that for each phase, we have to produce an mmf with $2p_1 = 4$ poles (semiperiods). To do so, for a single-layer winding, the coil pitch $y = \tau = N_s/2p_1 = 12/4 = 3$ slot pitches.

For 12 slots, there are 6 coils in all. That is, two coils per phase to produce four poles. It is now obvious that the four-phase A slots are $y = \tau = 3$ slot pitches apart. We may start in slot 1 and continue with slots 4, 7, and 10 for phase A (Figure 4.4a).

Phases B and C are placed in slots by moving 2/3 of a pole pitch (two-slot pitches in our case) to the right. All coils/phases may be connected in series to form one current path (a = 1) or they may be connected in parallel to form two current paths in parallel (a = 2). The number of current paths a is obtained in general by connecting part of coils in series and then the current paths in parallel such that all the current paths are symmetric. Current paths in parallel serve to reduce wire gauge (for given output phase current) and, as shown later, to reduce uncompensated magnetic pull between rotor and stator in the presence of rotor eccentricity.

If the slot is considered infinitely thin (or the slot opening $b_{os} \approx 0$), the mmf (ampere-turns) jumps up, as expected, by $n_{cs}{\cdot}i_{A,B,C}$, along the middle of each slot.

For the time being, let us consider $b_{os} = 0$ (a virtual closed slot).

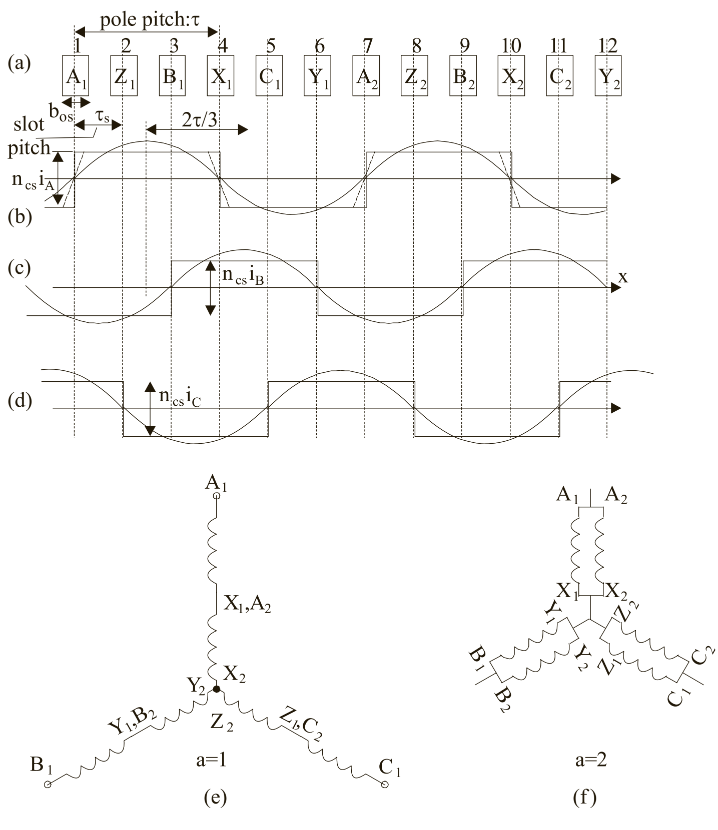


**FIGURE 4.4** Single-layer three-phase winding for $2p_1 = 4$ poles and q = 1 slots/pole/phase: (a) slot/phase allocation; (b–d) ideal mmf distribution for the three phases when their currents are maximum; (e) star series connection of coils/phase; (f) parallel connection of coils/phase.

The rectangular mmf distribution may be decomposed into harmonics for each phase. For phase A, we simply obtain

$$F_{A1}(x,t) = \frac{2}{\pi} \cdot \frac{n_{cs} I\sqrt{2}\cos\omega_1 t}{\nu} \cos\frac{\nu\pi x}{\tau} \tag{4.8}$$

For the fundamental, $\nu = 1$, we obtain the maximum amplitude. The higher the order of the harmonic, the lower its amplitude in (4.8).

While in principle such a primitive machine works, the harmonics content is too rich.

It is only intuitive that if the number of steps in the rectangular ideal distribution would be increased, the harmonics content would be reduced. This goal could be met by increasing q or (and) via chording the coils in a two-layer winding. Let us then present such a case.

## 4.4 A PRIMITIVE TWO-LAYER CHORDED WINDING

Let us still consider $2p_1 = 4$ poles, $m = 3$ phases but increase q from 1 to 2. Thus, the total number of slots $N_s = 2p_1qm = 2{\cdot}2{\cdot}2{\cdot}3 = 24$.

The pole pitch $\tau$ measured in slot pitches is $\tau = N_s/2p_1 = 24/4 = 6$. Let us reduce the coil throw (span) y such that $y = 5\tau/6$.

We still have to produce four poles. Let us proceed as in the previous paragraph but only for one layer, disregarding the coil throw.

In a two-layer winding, the total number of coils is equal to the number of slots. So in our case, there are $N_s/m = 24/3$ coils per phase. Also, there are eight slots occupied by one phase in each layer, four with inward and four with outward current direction. With each layer, each phase has to produce four poles in our case. So slots 1,2; 7′,8′; 13,14; 19′,20′ in layer one belong to phase A. The superscript prime refers to outward current direction in the coils. The distance between neighbouring slot groups of each phase in one layer is always equal to the pole pitch to preserve the mmf distribution half period (Figure 4.5).

Notice that in Figure 4.5, for each phase, the second layer is displaced to the left by $\tau - y = 6 - 5 = 1$ slot pitch with respect to the first layer. Also, after two poles, the situation repeats itself. This is typical for a fully symmetrical winding.

Each coil has one side in one layer, say in slot 1, and the second one in slot $y + 1 = 5 + 1 = 6$. In this case, all coils are identical, and thus, the end connections occupy less axial room and are shorter due to chording. Such a winding is typical with random wound coils made of round magnetic wire.

For this case, we explore the mmf ideal resultant distribution for the situation when the current in phase A is maximum ($i_A = i_{max}$). For symmetrical currents, $i_B = i_C = -i_{max}/2$ (Figure 4.1b).

Each coil has $n_c$ conductors and, with zero slot opening, the mmf jumps up at every slot location by the total number of ampere-turns. Notice that half the slots have coils of same phase while the other half accommodate coils of different phases.

The mmf of phase A, for maximum current value (Figure 4.5b), has two steps per polarity as $q = 2$. It had only one step for $q = 1$ (Figure 4.4). Also, the resultant mmf has three unequal steps per polarity ($q + \tau - y = 2 + 6 - 5 = 3$). It is indeed closer to a sinusoidal distribution. Increasing q and using chorded coils reduces the space harmonics content of the mmf.

Also shown in Figure 4.5 is the movement by $2\tau/3$ (or $2\pi/3$ electrical radians) of the mmf maximum when the time advances with $2\pi/3$ electrical (time) radians or T/3 (T is the time period of sinusoidal currents).

## 4.5 THE MMF HARMONICS FOR INTEGER q

Using the geometrical representation in Figure 4.5, it becomes fairly easy to decompose the resultant mmf in space harmonics noticing the step form of the distributions.

Proceeding with phase A, we obtain (by some extrapolation for integer q),

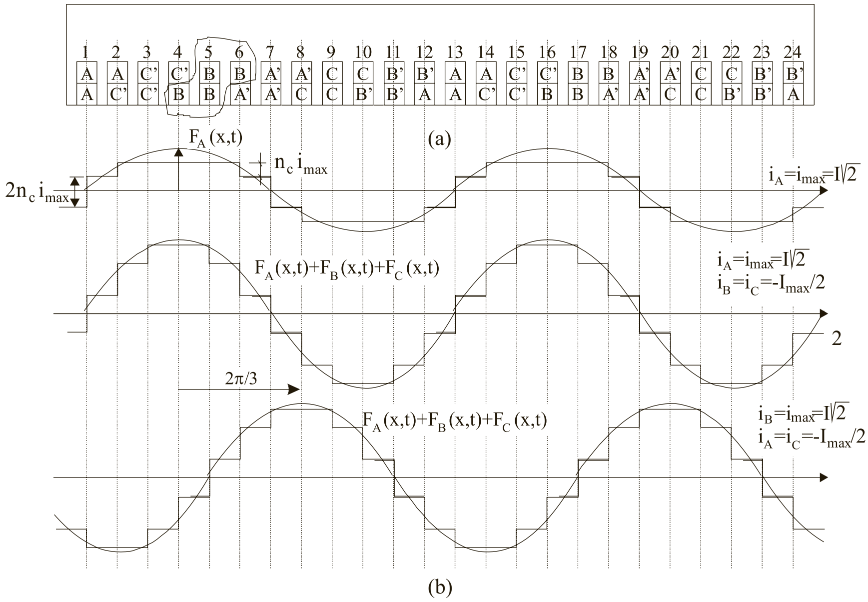


**FIGURE 4.5** Two-layer winding for Ns = 24 slots, 2 $p_1$ = 4 poles, $y/\tau = 5/6$ (a) slot/phase allocation and (b) mmfs distribution.

$$F_{A1}(x,t) = \frac{2}{\pi} n_c q I\sqrt{2} K_{q1} K_{y1} \cos\frac{\pi}{\tau} x \cos\omega_1 t \tag{4.9}$$

with

$$K_{q1} = \sin\pi/6/\left(q\sin\pi/6q\right) \le 1; \quad K_{y1} = \sin\frac{\pi}{2} y/\tau \le 1 \tag{4.10}$$

$K_{q1}$ is known as the zone (or spread) factor and $K_{y1}$ the chording factor. For q = 1, $K_{q1}$ = 1, and for full pitch coils, $y/\tau = 1$, $K_{y1}$ = 1, as expected.

To keep the winding fully symmetric, $y/\tau \ge 2/3$. This way all poles have similar slot/phase allocation.

Assuming now that all coils per phase are in series, the number of turns per phase $W_1$ is

$$W_1 = 2p_1 q n_c \tag{4.11}$$

With (4.11), Equation (4.9) becomes

$$F_{A1}(x,t) = \frac{2}{\pi P_1} W_1 I\sqrt{2} K_{q1} K_{y1} \cos\frac{\pi}{\tau} x \cos\omega_1 t \tag{4.12}$$

For three phases, we obtain

$$F_1(x,t) = F_{1m}\cos\left(\frac{\pi}{\tau}x - \omega_1 t\right) \tag{4.13}$$

with

$$F_{1m} = \frac{3W_1 I\sqrt{2}K_{q1}K_{y1}}{\pi p_1} \quad \text{(amperturns per pole)} \tag{4.14}$$

The derivative of pole mmf with respect to position x is called linear current density (or current sheet) A (in A/m)

$$A_1(x,t) = \frac{\partial F_1(x,t)}{\partial x} = A_{1m}\sin\left(-\frac{\pi}{\tau}x + \omega_1 t\right) \tag{4.15}$$

$$A_{1m} = \frac{3\sqrt{2}W_1 I\sqrt{2}K_{q1}K_{y1}}{P_1\tau} = \frac{\pi}{\tau}F_{1m} \tag{4.16}$$

$A_{1m}$ is the maximum value of the current sheet and is also identified as current loading. The current loading is a design parameter (constant) $A_{1m} \approx 5000$–$50{,}000$ A/m, in general, for IMs in the power range of kilowatts to megawatts. It is limited by the temperature rise mainly and increases with machine torque (size).

The harmonics content of the mmf is treated in a similar manner to obtain

$$F(x,t) = \frac{3W_1 I\sqrt{2}K_{q\nu}K_{y\nu}}{\pi p_1 \nu}\cdot$$

$$\cdot\left[K_{BI}\cos\left(\frac{\nu\pi}{\tau}x - \omega_1 t - (\nu-1)\frac{2\pi}{3}\right) - K_{BII}\cos\left(\frac{\nu\pi}{\tau}x + \omega_1 t - (\nu+1)\frac{2\pi}{3}\right)\right] \tag{4.17}$$

with

$$K_{q\nu} = \frac{\sin \nu\pi/6}{q\sin \nu\pi/6q}; \quad K_{y\nu} = \sin\left(\frac{\nu\pi y}{2\tau}\right) \tag{4.18}$$

$$K_{BI} = \frac{\sin(\nu-1)\pi}{3\sin(\nu-1)\pi/3}; \quad K_{BII} = \frac{\sin(\nu+1)\pi}{3\sin(\nu+1)\pi/3} \tag{4.19}$$

Due to mmf full symmetry (with q = integer), only odd harmonics occur. For three-phase star connection, 3K harmonics may not occur as the current sum is zero and their phase shift angle is $3K\cdot 2\pi/3 = 2\pi K$.

We are left with harmonics $\nu = 3K \pm 1$; that is, $\nu = 5, 7, 11, 13, 17, \ldots$

We should notice in (4.19) that for $\nu_d = 3K + 1$, $K_{BI} = 1$ and $K_{BII} = 0$. The first term in (4.17) represents, however, a direct (forward) travelling wave as, for a constant argument under cosines, we do obtain

$$\left(\frac{dx}{dt}\right) = \frac{\omega_1\tau}{\pi\nu} = \frac{2\tau f_1}{\nu}; \quad \omega_1 = 2\pi f_1 \tag{4.20}$$

On the contrary, for $\nu = 3K - 1$, $K_{BI} = 0$ and $K_{BII} = 1$. The second term in (4.17) represents a backward travelling wave. For a constant argument under cosine, after a time derivative, we have

$$\left(\frac{dx}{dt}\right)_{\nu=3K-1} = \frac{-\omega_1\tau}{\pi\nu} = \frac{-2\tau f_1}{\nu} \tag{4.21}$$

We should also notice that the travelling speed of mmf space harmonics, due to the placement of conductors in slots, is ν times smaller than that of the fundamental (ν = 1).

The space harmonics of the mmf just investigated are due both to the placement of conductors in slots and to the placement of various phases as phase belts under each pole. In our case, the phase belt spread is π/3 (or one-third of a pole). There are also two-layer windings with 2π/3 phase belts, but the π/3 (60°) phase belt windings are more practical.

So far, the slot opening influences on the mmf stepwise distribution have not been considered. It will be done later in this chapter.

Notice that the product of zone (spread or distribution) factor $K_{q\nu}$ and the chording factor $K_{y\nu}$ is called the stator winding factor $K_{w\nu}$.

$$K_{w\nu} = K_{q\nu}K_{y\nu} \tag{4.22}$$

As in most cases, only the mmf fundamental (ν = 1) is useful, reducing most harmonics and cancelling some is a good design attribute. Chording the coils to cancel $K_{y\nu}$ leads to

$$\sin\left(\frac{\nu\pi y}{2\tau}\right) = 0; \quad \frac{\nu\pi y}{2\tau} = n\pi; \quad \frac{y}{\tau} > \frac{2}{3} \tag{4.23}$$

As the mmf harmonic amplitude (4.17) is inversely proportional to the harmonic order, it is almost standard to reduce (cancel) the fifth harmonic (ν = 5) by making n = 2 in (4.23).

$$\frac{y}{\tau} = \frac{4}{5} \tag{4.23a}$$

In reality, this ratio may not be realised with an integer q (q = 2) and thus y/τ = 5/6 or 7/9 is the practical solution which keeps the fifth mmf harmonic low. Chording the coils also reduces $K_{y1}$. For y/τ = 5/6, $\sin\frac{\pi}{2}\frac{5}{6} = 0.966 < 1.0$, but a 4% reduction in the mmf fundamental is worth the advantages of reducing the coil end-connection length (lower copper losses) and a drastic reduction of fifth mmf harmonic.

As will be shown later in the book, mmf harmonics produce parasitic torques, radial forces, additional core and winding losses, noise, and vibration.

### Example 4.1

Let us consider an IM with the following data: stator core diameter D = 0.15 m, number of stator slots $N_s = 24$, number of poles $2p_1 = 4$, y/τ = 5/6, two-layer winding; slot area $A_{slot} = 100\,mm^2$, total slot fill factor $K_{fill} = 0.5$, current density $j_{Co} = 5\ A/mm^2$, number of turns per coil $n_c = 25$. Let us calculate

a. The rated current (RMS value), wire gauge
b. The pole pitch τ
c. $K_{q1}$ and $K_{y1}$, $K_{w1}$
d. The amplitude of the mmf $F_{1m}$ and current sheet $A_{1m}$
e. $K_{q7}$, $K_{y7}$, and $F_{7m}$ (ν = 7)

### *Solution*

Part of the slot is filled with insulation (conductor insulation, slot wall insulation, and layer insulation) while there is some room between round wires. The total filling factor of slot takes care of all these aspects. The mmf per slot is

$$2n_cI = A_{slot} \cdot K_{fill} \cdot J_{Co} = 100 \cdot 0.5 \cdot 5 = 250 \text{ Aturns}$$

As nc = 25; I = 250/(2·25) = 5A (rms).

The wire gauge $d_{Co}$ is

$$d_{Co} = \sqrt{\frac{4}{\pi}\frac{I}{J_{Co}}} = \sqrt{\frac{4}{\pi}\frac{5}{5}} = 1.128\,\text{mm}$$

The pole pitch $\tau$ is

$$\tau = \frac{\pi D}{2p_1} = \frac{\pi \cdot 0.15}{2 \cdot 2} = 0.11775\text{ m}$$

From (4.10),

$$K_{q1} = \frac{\sin\frac{\pi}{6}}{2\sin\frac{\pi}{6\cdot 2}} = 0.9659$$

$$K_{y1} = \sin\frac{\pi}{2}\cdot\frac{5}{6} = 0.966; \quad K_{w1} = K_{q1}K_{y1} = 0.9659 \cdot 0.966 = 0.933$$

The mmf fundamental amplitude, (from 4.14), is

$$W_1 = 2P_1qn_c = 2\cdot 2\cdot 2\cdot 25 = 200\,\text{turns/phase}$$

$$F_{1m} = \frac{3W_1I\sqrt{2}K_{w1}}{\pi p} = \frac{3\cdot 200\cdot 5\sqrt{2}\cdot 0.933}{\pi\cdot 2} = 628\,\text{turns/pole}$$

From (4.16), the current sheet (loading) $A_{1m}$ is

$$A_{1m} = F_{1m}\frac{\pi}{\tau} = 628\cdot\frac{\pi}{0.15} = 13155.3\,\text{Aturns/m}$$

From (4.18),

$$K_{q7} = \frac{\sin(7\pi/6)}{2\sin(7\pi/6\cdot 2)} = -0.2588; \qquad K_{y7} = \sin\frac{7\pi}{2}\cdot\frac{5}{6} = 0.2588$$

$$K_{w7} = -0.2588\cdot 0.2588 = -0.066987$$

From (4.18),

$$F_{7m} = \frac{3W_1I\sqrt{2}K_{q7}K_{y7}}{\pi p_1 7} = \frac{3\cdot 200\cdot 5\sqrt{2}\cdot 0.066987}{\pi\cdot 2\cdot 7} = 6.445\,\text{Aturns/pole}$$

This is less than 1% of the fundamental $F_{1m}$ = 628 Aturns/pole.

*Note*. It may be shown that for 120° phase belts [10], the distribution (spread) factor $K_{q\nu}$ is

$$K_{q\nu} = \frac{\sin \nu(\pi/3)}{q \sin(\nu\pi/3 \cdot q)} \tag{4.24}$$

For some cases, q = 2 and ν = 1, we find $K_{q1} = \sin \pi/3 = 0.867$.

This is much smaller than 0.9659, the value obtained for the 60° phase belt, which explains in part why the latter case is preferred in practice.

Now that we introduced ourselves to A.C. windings through two case studies, let us proceed and develop general rules to design practical A.C. windings.

## 4.6 RULES FOR DESIGNING PRACTICAL A.C. WINDINGS

The A.C. windings for induction motors are usually built in one or two layers.

The basic structural element is represented by coils. We already pointed out (Figure 4.2) that there may be lap and wave coils. This is the case for single turn (bar) coils. Such coils are made of continuous bars (Figure 4.6a) for open slots or from semibars bent and welded together after insertion in semiclosed slots (Figure 4.6b).

These are preformed coils generally suitable for large machines.

Continuous bar coils may also be made from a few elementary conductors in parallel to reduce the skin effect to acceptable levels.

On the other hand, round-wire, mechanically flexible coils forced "wire by wire" into semiclosed slots are typical for low-power IMs.

Such coils may have various shapes as shown in Figure 4.7.

A few remarks are in order.

- Wire coils for single-layer windings, typical for low-power induction motors (kW range and $2p_1 = 2$ pole), have in general wave shape
- Coils for single-layer windings are always full pitch as an average
- The coils may be concentrated or identical
- The main concern should be to produce equal resistance and leakage inductance per phase
- From this point of view, rounded concentrated or chain-shape identical coils are to be preferred for single-layer windings.

Double-layer winding coils for low-power IMs are trapezoidal and round-shaped wire types (Figure 4.8a and b).

For large power motors, preformed multibar (rectangular wire) (Figure 4.8c) or unibar coils (Figure 4.6) are used.

Now, to return to the basic rules for A.C. winding design, let us first remember that they may be integer q or fractional q (q = a + b/c) windings with the total number of slots $N_s = 2p_1qm$. The number

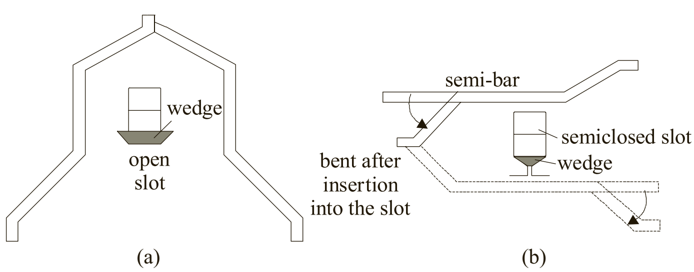


**FIGURE 4.6** Bar coils: (a) continuous bar and (b) semibar.

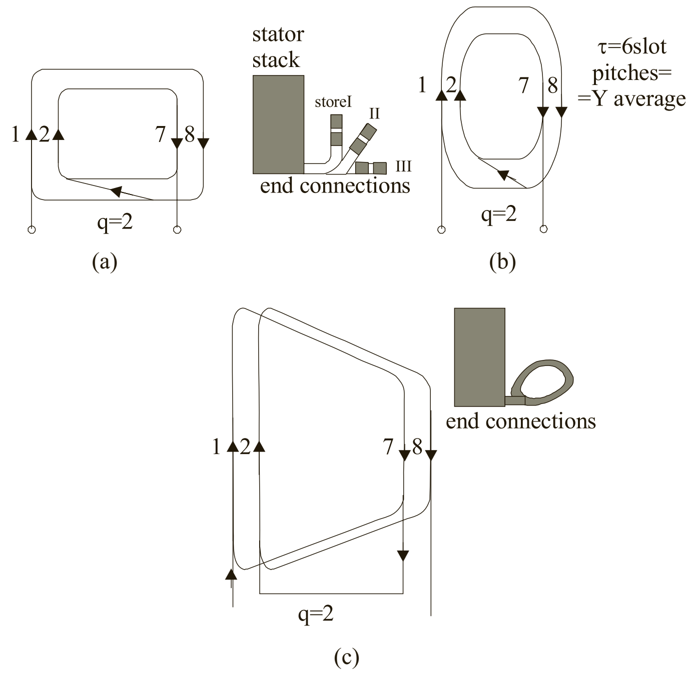


**FIGURE 4.7** Full pitch coil groups/phase/pole – for q = 2 – for single-layer A.C. windings: (a) with concentrated rectangular shape coils and 2 (3) store end connections; (b) with concentrated rounded coils; and (c) with chain shape coils.

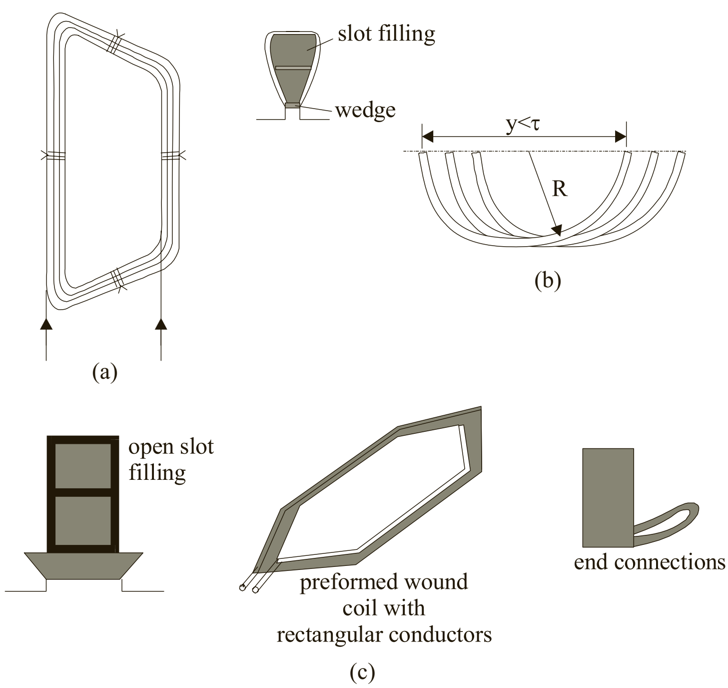


**FIGURE 4.8** Typical coils for two-layer A.C. windings: (a) trapezoidal flexible coil (round wire); (b) rounded flexible coil (rounded wire); and (c) preformed wound coil (of rectangular wire) for open slots.

of slots per pole could be only an integer. Consequently, for a fractional q, the latter is different and integer for a phase under different poles. Only the average q is fractional. Single-layer windings are built only with an integer q.

As one coil sides occupy 2 slots, it means that $N_s/2m$ = an integer (m – number of phases; m = 3 in our case) for single-layer windings. The number of inward current coil sides is evidently equal to the number of outward current coil sides.

For two-layer windings, the allocation of slots per phase is performed in one (say upper) layer. The second layer is occupied "automatically" by observing the coil pitch whose first side is in one layer and the second one in the second layer. In this case, it is sufficient to have $N_s/m$ = an integer.

A pure travelling stator mmf (4.13), with an open rotor winding and a constant airgap (slot opening effects are neglected), when the stator and iron core permeability is infinite, will produce a no-load ideal flux density in the airgap as

$$B_{g10}(x,t) = \frac{\mu_0 F_{1m}}{g}\cos\left(\frac{\pi}{\tau}x - \omega_1 t\right) \tag{4.25}$$

according to Biot–Savart law.

This flux density will self-induce sinusoidal emfs in the stator windings.

The emfs induced in coil sides placed in neighbouring slots are thus phase shifted by $\alpha_{es}$

$$\alpha_{es} = \frac{2\pi P_1}{N_s} \tag{4.26}$$

The number of slots with emfs in phase, t, is

$$t = \text{greatest common divisor}\ (N_s, p_1) = \text{g.c.d.}\ (N_s, p_1) \le p_1 \tag{4.27}$$

Thus, the number of slots with emfs of distinct phase is $N_s/t$. Finally, the phase shift between neighbouring distinct slot emfs $\alpha_{et}$ is

$$\alpha_{et} = \frac{2\pi t}{N_s} \tag{4.28}$$

If $\alpha_{es} = \alpha_{et}$, that is $t = p_1$, the counting of slots in the emf phasor star diagram is the real one in the machine.

Now let us reconsider the case of a single-layer winding with $N_s = 24$, $2p_1 = 4$. In this situation,

$$\alpha_{es} = \frac{2\pi P_1}{N_s} = \frac{2\pi\cdot 2}{24} = \frac{\pi}{6} \tag{4.29}$$

$$t = \text{g.c.d.}\ (N_s, p_1) = \text{g.c.d.}(24,2) = 2 = p_1 \tag{4.30}$$

So the number of distinct emfs in slots is $N_s/t = 24/2 = 12$ and their phase shift $\alpha_{et} = \alpha_{es} = \pi/6$. So their counting (order) is the natural one (Figure 4.9).

The allocation of slots to phases to produce a symmetric winding is to be done as follows for

- Single-layer windings
  - Build up the slot emf phasor star based on calculating $\alpha_{et}$, $\alpha_{es}$, and $N_s/t$ distinct arrows counting them in natural order after $\alpha_{es}$.

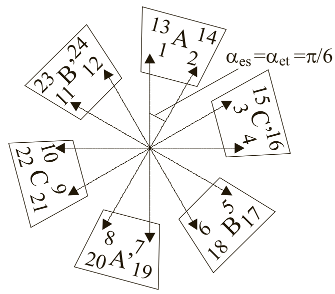


**FIGURE 4.9** The star of slot emf phasors for a single-layer winding with $q = 2$, $2p_1 = 3$, $m = 3$, and $N_s = 24$ slots.

   - Choose randomly $N_s/2m$ successive arrows to make up the inward current slots of phase A (Figure 4.9).
   - The outward current arrows of phase A are phase shifted by π radians with respect to the inward current ones.
   - By skipping $N_s/2m$ slots from phase A, we find the slots of phase B.
   - Skipping further $N_s/2m$ slots from phase B, we find the slots of phase C.
- Double-layer windings
   - Build up the slot emf phasor star as for single-layer windings.
   - For each phase choose $N_s/m$ arrows and divide them into two groups (one for inward and one for outward current sides) such that they are as opposite as possible.
   - The same routine is repeated for the other phases providing a phase shift of $2\pi/3$ radians between phases.

It is well understood that the above rules are also valid for the case of fractional q. Fractional q windings are built only in two layers and small q to reduce the order of first-slot harmonic.

- Placing the coils in slots

For single-layer full-pitch windings, the inward and outward side coils occupy entirely the allocated slots from left to right for each phase. There will be $N_s/2m$ coils/phase.

The chorded coils of double-layer windings, with a pitch y ($2\tau/3 \le y < \tau$ for integer q and single-pole count windings), are placed from left to right for each phase, with one side in one layer and the other side in the second layer. They are connected observing the inward (A, B, C) and outward (A′, B′, C′) directions of currents on their sides.

- Connecting the coils per phase

The $N_s/2m$ coils per phase for single-layer windings and the $N_s/m$ coils per phase for double-layer windings are connected in series (or series/parallel) such that for the first layer, the inward/outward directions are observed. With all coils/phase in series, we obtain a single current path ($a = 1$). We may obtain "a" current paths if the coils from $2p_1/a$ poles are connected in series and, then, the "a " chains in parallel.

### Example 4.2

Let us design a single-layer winding with $2p_1 = 2$ poles, $q = 4$, $m = 3$ phases

### *Solution*

The angle $\alpha_{es}$ (4.26), t (4.27), and $\alpha_{et}$ (4.28) are

$$N_s = 2p_1qm = 24; \quad \alpha_{es} = \frac{2\pi p_1}{N_s} = \frac{2\pi \cdot 1}{24} = \frac{\pi}{12}$$

$t = g.c.d.(N_s,p_1) = g.c.d.(24,1) = 1$

$$\alpha_{et} = \frac{2\pi t}{N_s} = \frac{2\pi \cdot 1}{24} = \frac{\pi}{12}$$

Also the count of distinct arrows of slot emf star $N_s/t = 24/1 = 24$.

Consequently, the number of arrows in the slot emf star is 24 and their order is the real (geometrical) one (1, 2, …, 24) – Figure 4.10.

Making use of Figure 4.10, we may, thus, allocate the slots to phases as shown in Figure 4.11.

## Example 4.3

Let us consider a double-layer three-phase winding with $q = 3, 2p_1 = 4, m = 3, \left(N_s = 2p_1qm = 36\,\text{slots}\right)$, chorded coils $y/\tau = 7/9$ with $a = 2$ current paths

### *Solution*

Proceeding as explained above, we may calculate $\alpha_{es}$, t, and $\alpha_{et}$

$$\alpha_{es} = \frac{2\pi p_1}{N_s} = \frac{2\pi \cdot 2}{36} = \frac{\pi}{9}$$

$t = g.c.d.(36, 2) = 2$

$$\alpha_{et} = \frac{2\pi t}{N_s} = \frac{2\pi \cdot 2}{36} = \frac{\pi}{9} = \alpha_{es} \quad N_s/t = 36/2 = 18$$

There are 18 distinct arrows in the slot emf star as shown in Figure 4.12.

The winding layout is shown in Figure 4.13. We should notice that the second-layer slot allocation is lagging by $\tau - y = 9 - 7 = 2$ slots from the first-layer allocation.

Phase A produces four fully symmetric poles. Also, the current paths are fully symmetric. Equipotential points of two current paths U – U′, V – V′, and W – W′ could be connected to each other to handle circulating currents due to, say, rotor eccentricity.

Having two current paths, the current in the coils is half the current at the terminals. Consequently, the wire gauge of conductors in the coils is smaller, and thus, the coils are more flexible and easier to handle.

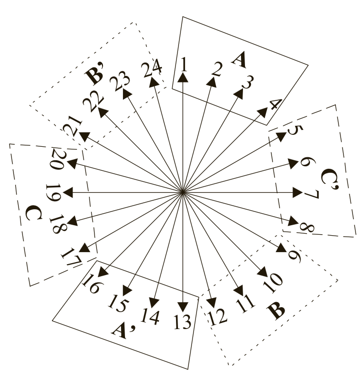


**FIGURE 4.10** The star of slot emf phasors for a single-layer winding: $q = 1$, $2p_1 = 2$, $m = 3$, and $N_s = 24$.

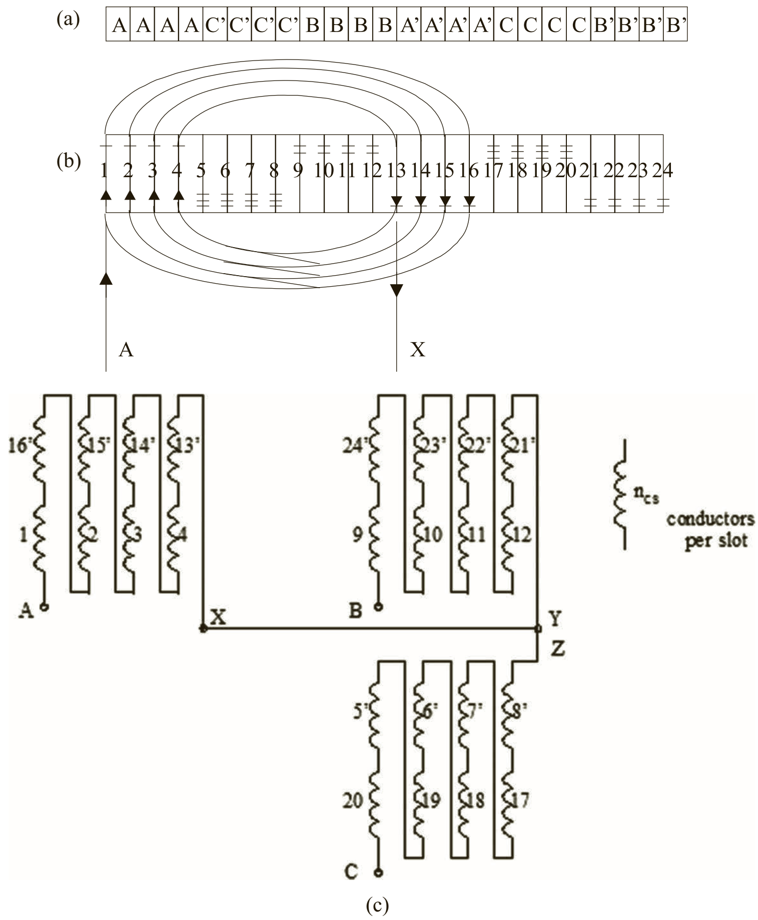


**FIGURE 4.11** Single-layer winding layout: (a) slot/phase allocation; (b) rounded coils of phase A; and (c) coils per phase.

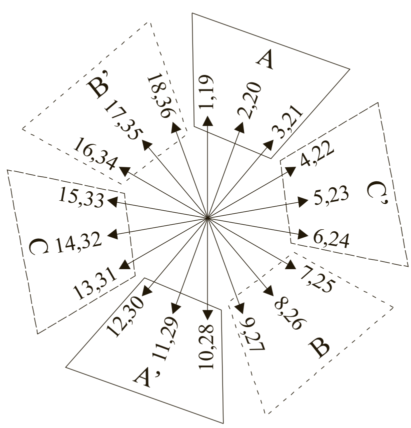


**FIGURE 4.12** The star of slot emf phasors for a double-layer winding (one layer shown) with $2p_1 = 4$ poles, $q = 3$ slots/pole/phase, $m = 3$, $N_s = 36$.

| | 1 | 2 | 3 | 4 | 5 | 6 | 7 | 8 | 9 | 10 | 11 | 12 | 13 | 14 | 15 | 16 | 17 | 18 | 19 | 20 | 21 | 22 | 23 | 24 | 25 | 26 | 27 | 28 | 29 | 30 | 31 | 32 | 33 | 34 | 35 | 36 |
|---|---|---|---|---|---|---|---|---|---|---|---|---|---|---|---|---|---|---|---|---|---|---|---|---|---|---|---|---|---|---|---|---|---|---|---|---|
| layer1 | A | A | A | C' | C' | C' | B | B | B | A' | A' | A' | C | C | C | B' | B' | B' | A | A | A | C' | C' | C' | B | B | B | A' | A' | A' | C | C | C | B' | B' | B' |
| layer2 | A | C' | C' | C' | B | B | B | A' | A' | A' | C | C | C | B' | B' | B' | A | A | A | C' | C' | C' | B | B | B | A' | A' | A' | C | C | C | B' | B' | B' | A | A |

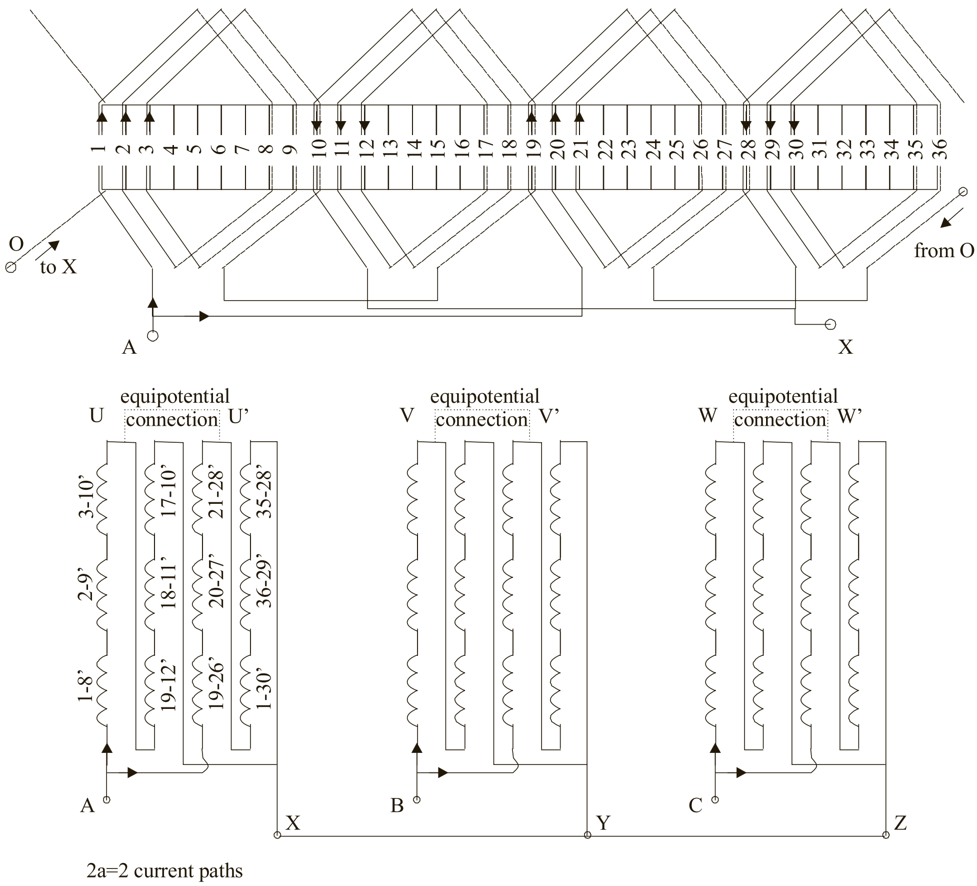


**FIGURE 4.13** Double-layer winding: $2p_1 = 4$ poles, $q = 3$, $y/\tau = 7/9$, $N_s = 36$ slots, $a = 2$ current paths.

Note that using wave coils is justified in single-bar coils to reduce the external leads (to one) by which the coils are connected to each other in series. Copper, labour, and space savings are the advantages of this solution.

## 4.7 BASIC FRACTIONAL q THREE-PHASE A.C. WINDINGS

Fractional q A.C. windings are not typical for induction motors due to their inherent pole asymmetry as slot/phase allocation under adjacent poles is not the same in contrast to integer q three-phase windings. However, with a small q ($q \le 3$) to reduce the harmonics content of airgap flux density, by increasing the order of the first-slot harmonic from $6q \pm 1$ for integer q to $6(ac + b) \pm 1$ for $q = (ca + b)/c$ = fractional, two-layer such windings are favoured to single-layer versions. To set the rules to design such a standard winding – with identical coils – we may proceed with an example.

Let us consider a small induction motor with $2p_1 = 8$ and $q = 3/2$, $m = 3$. The total number of slots $N_s = 2p_1qm = 2{\cdot}4{\cdot}3/2{\cdot}3 = 36$. The coil span y is

$$y = \text{integer}\left(N_s/2p_1\right) = \text{integer}(36/8) = 4 \text{ slot pitches} \tag{4.31}$$

The parameters t, $\alpha_{es}$, $\alpha_{et}$ are

$$t = \text{g.c.d.}\left(N_s, p_1\right) = \text{g.c.d.}(36, 4) = 4 = p_1 \tag{4.32}$$

$$\alpha_{es} = \frac{2\pi p_1}{N_s} = \frac{\pi \cdot 8}{36} = \frac{2\pi}{9} = \alpha_{et} \tag{4.33}$$

The count of distinct arrows in the star of slot emf phasors is $N_s/t = 36/4 = 9$. This shows that the slot/phase allocation repeats itself after each pole pair (for an integer q it repeats after each pole). Thus, mmf subharmonics, or fractional space harmonics, are still absent in this case of fractional q. This property holds for any $q = (2l + 1)/2$ for two-layer configurations.

The star of slot emf phasors has q arrows and the counting of them is the natural one ($\alpha_{es} = \alpha_{et}$) (Figure 4.14a).

A few remarks are in order:

- The actual value of q for each phase under neighbouring poles is 2 and 1, respectively, to give an average of 3/2
- Due to the periodicity of two poles ($2\tau$), the mmf distribution does not show fractional harmonics ($\nu < 1$)
- There are both odd and even harmonics as the positive and negative polarities of mmf (Figure 4.14c) are not fully symmetric
- Due to a two-pole periodicity, we may have a = 1 (Figure 4.14d) or a = 2, 4
- The chording and distribution (spread) factors ($K_{y1}$, $K_{q1}$) for the fundamental may be determined from Figure 4.14e using simple phasor composition operations.

$$K_{y1} = \sin\left[\frac{\pi p_1}{N_s}\text{integer}\left(N_s/2p_1\right)\right] \tag{4.34}$$

$$K_{q1} = \frac{1 + 2\cos\left(\frac{\pi t}{N_s}\right)}{3} \tag{4.35}$$

(a)

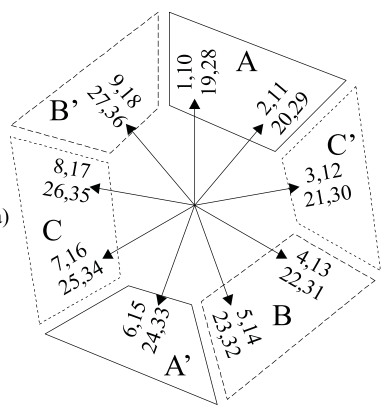


**FIGURE 4.14** Fractionary q (q = 3/2, $2p_1 = 8$, m = 3, $N_s = 36$) winding: (a) emf star; (b) slot/phase allocation; (c) mmf; (d) coils of phase A; and (e) chording and spread factors.

(*Continued*)

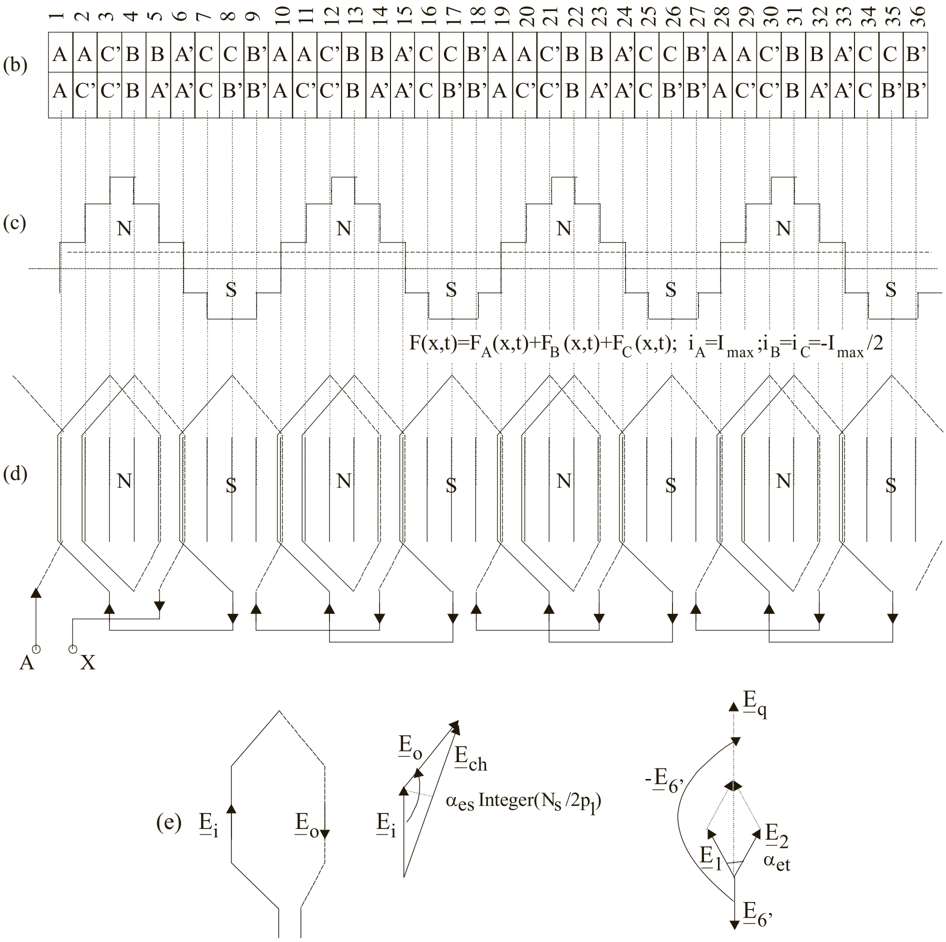


**FIGURE 4.14 (CONTINUED)** Fractionary q ($q = 3/2$, $2p_1 = 8$, $m = 3$, $N_s = 36$) winding: (a) emf star; (b) slot/phase allocation; (c) mmf; (d) coils of phase A; and (e) chording and spread factors.

This is a kind of general method valid both for integer and fractional q.

Extracting the fundamental and the space harmonics of the mmf distribution (Figure 4.14c) takes care implicitly of these factors both for the fundamental and for the harmonics.

## 4.8 BASIC POLE-CHANGING THREE-PHASE A.C. WINDINGS

From (4.20), the speed of the mmf fundamental dx/dt is

$$\left(\frac{dx}{dt}\right)_{\nu=1} = 2\tau f_1 \tag{4.36}$$

The corresponding angular speed is

$$\Omega_1 = \frac{dx}{dt}\frac{\pi}{D} = \frac{2\pi f_1}{p_1}; \quad n_1 = \frac{f_1}{p_1} \tag{4.37}$$

The mmf fundamental wave travels at a speed $n_1 = f_1/p_1$. This is the ideal speed of the motor with cage rotor.

Changing the speed may be accomplished either by changing the frequency (through a static power converter) or by changing the number of poles.

Changing the number of poles to produce a two-speed motor is a traditional method. Its appeal is still strong today due to low hardware costs where continuous speed variation is not required. In any case, the rotor should have a squirrel cage to accommodate both pole pitches. Even in variable speed drives with variable frequency static converters, when a very large constant power speed range (over 2(3) to 1) is required, such a solution is to be considered to avoid a notable increase in motor weight (and cost).

Two-speed induction generators are also used for wind energy conversion to allow for a notable speed variation in order to extract more energy from the wind speed.

There are two possibilities to produce a two-speed motor. The most obvious one is to place two distinct windings in the slots. The number of poles would be $2p_1 > 2p_2$. However, the machine becomes very large and costly, while for the winding placed on the bottom of the slots, the slot leakage inductance will be very large with all due consequences.

Using a pole-changing winding seems thus a more practical solution. However, standard pole-changing windings have been produced mainly for $2p_1/2p_2 = 1/2$ or $2p_1/2p_2 = 1/3$.

The most acclaimed winding has been invented by Dahlander and bears his name.

In essence, the current direction (polarity) in half of a $2p_2$ pole winding is changed to produce only $2p_1 = 2p_2/2$ poles. The two halves may be reconnected in series or parallel and Y or Δ connections of phases are applied. Thus, for a given line voltage and frequency supply, with various such connections, constant power or torque or a certain ratio of powers for the two speeds may be obtained.

Let us now proceed with an example and consider a two-layer three-phase winding with q = 2, $2p_2 = 4$, m = 3, $N_s = 24$ slots, and $y/\tau = 5/6$ and investigate the connection changes to switch it to a two-pole ($2p_1 = 2$) machine.

The design of such a winding is shown in Figure 4.15. The variables are $t = \text{g.c.d}(N_s, p_2) = 2 = p_2$, $\alpha_{es} = \alpha_{et} = 2\pi p_2/N_s = \pi/6$, and $N_s/t = 12$. The star of slot emf phasors is shown in Figure 4.15a.

Figure 4.15c illustrates the fact that only the current direction in the section A2 – X2 of phase A is changed to produce a $2p_1 = 2$ pole winding. A similar operation is done for phases B and C.

A possible connection of phase halves called Δ/2Y is shown in Figure 4.16.

It may be demonstrated that for the Δ ($2p_2 = 4$)/2Y ($2p_1 = 2$) connection, the power obtained for the two speeds is about the same.

We should also notice that with chorded coils for $2p_2 = 4$ ($y/\tau = 5/6$), the mmf distribution for $2p_1 = 2$ has a rather small fundamental and is rich in harmonics.

(a)
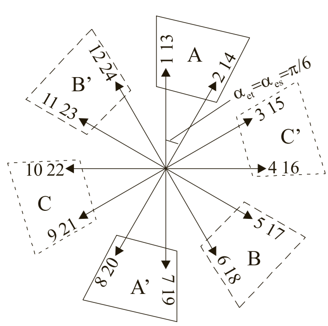


**FIGURE 4.15** Two- or four-pole winding ($N_s = 24$) (a) emf star, (b) slot/phase allocation, (c) coils of phase A, (d), (e) mmf for $2p_2 = 4$ and $2p_1 = 2$.

*(Continued)*

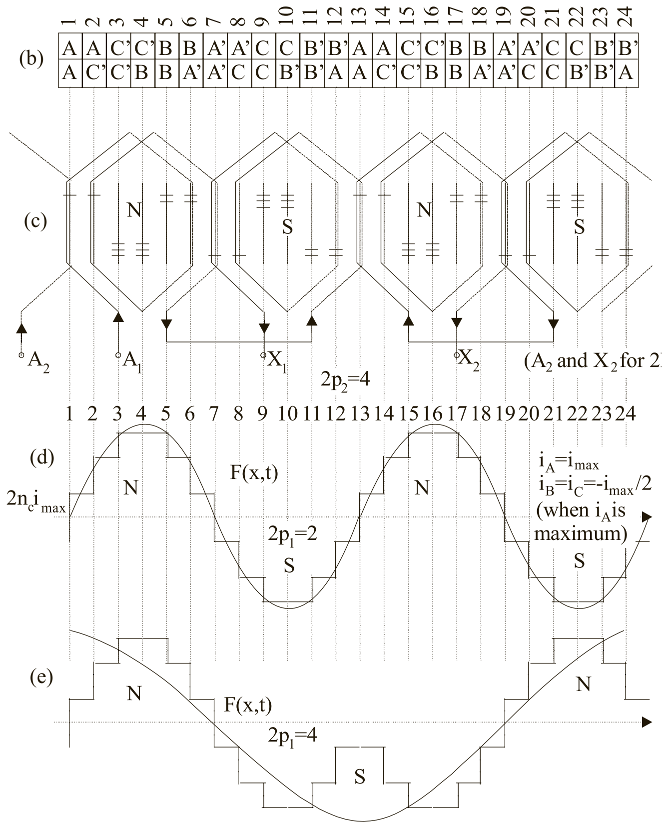


**FIGURE 4.15 (CONTINUED)** Two- or four-pole winding ($N_s$ = 24) (a) emf star, (b) slot/phase allocation, (c) coils of phase A, (d), (e) mmf for $2p_2$ = 4 and $2p_1$ = 2.

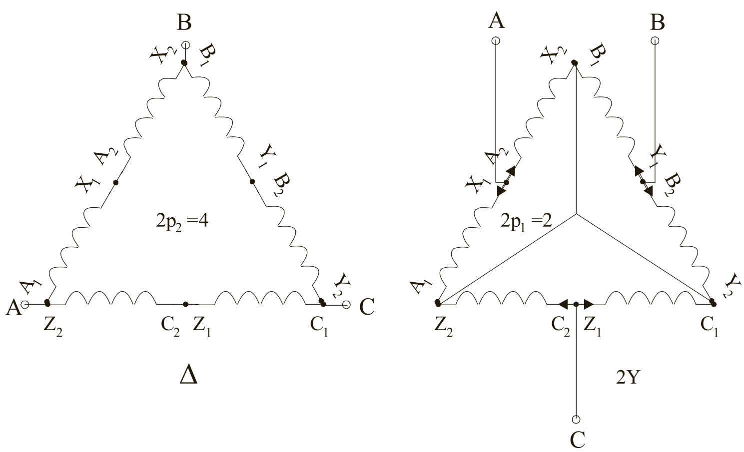


**FIGURE 4.16** 2/4 pole winding connection for constant power.

In order to achieve the same winding factor for both pole numbers, the coil span should be greater than the pole pitch for the large number of poles (y = 7, 8 slot pitches in our case). Even if close to each other, the two winding factors are, in general, below 0.85.

The machine is thus to be larger than usual for the same power, and care must be exercised to maintain an acceptable noise level.

Various connections of phases may produce designs with constant (same rated torque for both speeds) or variable torque. For example, a Y–YY parallel connection for $2p_2/2p_1 = 2/1$ is producing a ratio of power $P_2/P_1 = 0.35 - 0.4$ as needed for fan driving. Also, in general, when switching the pole number, we may need to modify the phase sequence to keep the same direction of rotation.

One may check if this operation is necessary by representing the stator mmf for the two cases at two instants in time. If the positive maximum of the mmfs advances in time in opposite directions, then the phase sequence has to be changed.

## 4.9 TWO-PHASE A.C. WINDINGS

When only a single-phase supply is available, two-phase windings are used. One is called the main winding (M) and the other, connected in series with a capacitor, is called the auxiliary winding (Aux).

The two windings are displaced from each other, as shown earlier in this chapter, by 90° (electrical) and are symmetrised for a certain speed (slip) by choosing the correct value of the capacitance. Symmetrisation for start (slip = 0) with a capacitance $C_{start}$ and again for rated slip with a capacitance $C_{run}$ is typical ($C_{start} >> C_{run}$) (Figure 4.17).

When a single capacitor is used, as a compromise between acceptable starting and running, the two windings may even be shifted in space by more than 90° (105°–110°).

Single capacitor configurations for good start are characterised by the disconnection of the auxiliary winding (and capacitor) after starting. In this case, the machine is called capacitor start and the main winding occupies 66% of stator periphery. On the other hand, if bi-directional motion is required, the two windings should each occupy 50% of the stator periphery and should be identical (Figure 4.17b).

Two-phase windings are used for low power (0.1–2 kW) and thus have rather low efficiency. As these motors are made in large numbers due to their use in home appliances, any improvement in the design may be implemented at competitive costs. For example, to reduce the mmf harmonics content, both phases may be placed in all (most) slots in different proportions. Notice that in two-phase windings, multiple of three harmonics may exist and they may deteriorate performance notably.

Let us first consider the capacitor-start motor windings.

As the main winding (M) occupies 2/3 of all slots (Figure 4.18a and b), its mmf distribution (Figure 4.18c) is notably different from that of the auxiliary winding (Figure 4.18d). Also the distribution factors for the two phases ($K_{q1M}$ and $K_{q1Aux}$) are expected to be different as $q_M = 4$ and $q_{Aux} = 2$.

For $N_s = 16$, $2p_1 = 2$, the above winding could be redesigned for reversible motion where both windings occupy the same number of slots. In that case, the windings look as those shown in Figure 4.19.

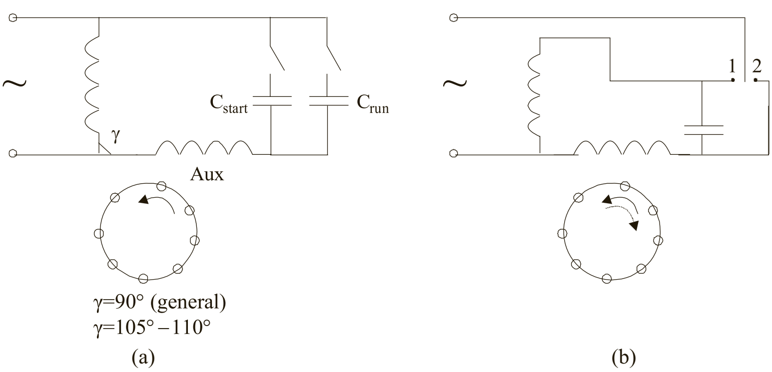


**FIGURE 4.17** Two-phase induction motor for (a) unidirectional motion and (b) bidirectional motion (1 – closed for forward motion; 2 – closed for backward motion).